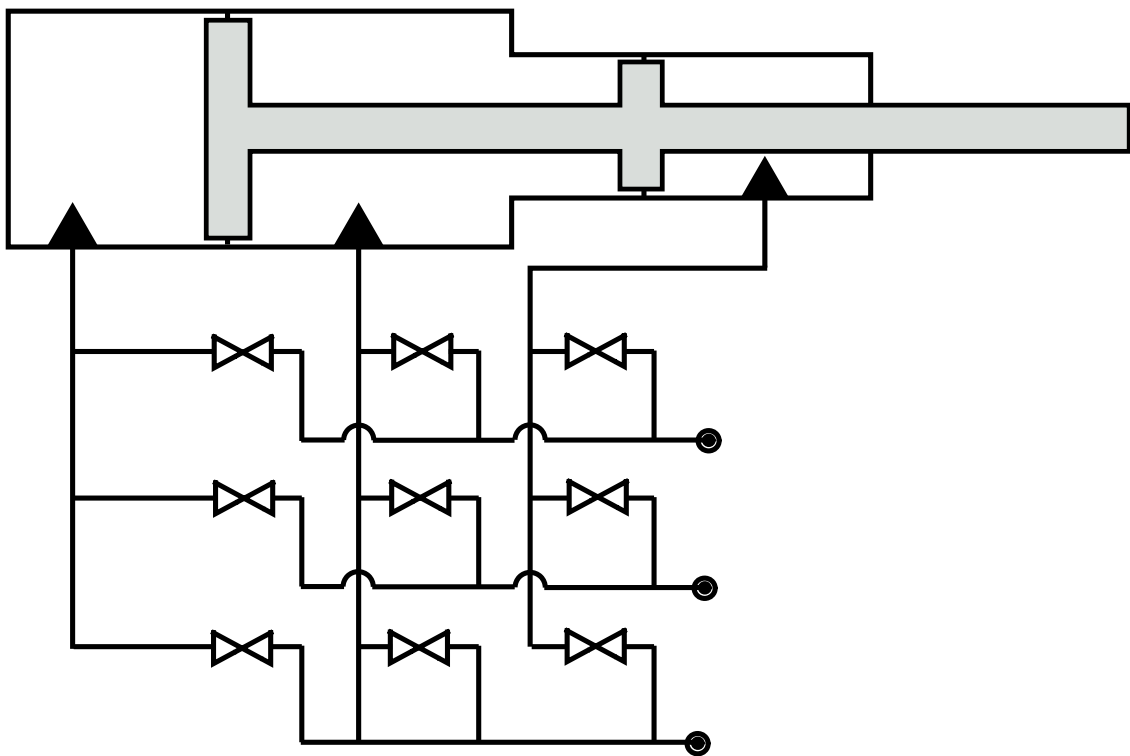


Energy Efficient Control of a Discrete Displacement Multi-Chamber Cylinder



AALBORG UNIVERSITY
STUDENT REPORT

MASTER THESIS
GROUP MCE4-1029
DEPARTMENT OF ENERGY
AALBORG UNIVERSITY
DATE 14/03 - 2023



AALBORG UNIVERSITY
STUDENT REPORT

Second year of Master Studies / Project-Oriented Work

Department of Energy
Pontoppidanstræde 111
9220 Aalborg
www.et.aau.dk/

Title:

Energy Efficient Control of a Discrete Displacement Multi-Chamber Cylinder

Project:

Master Thesis - Spring, 2023

Project Period:

January 2023 - March 2023

Project Group:

MCE4 - 1029

Participants:

Teitur Joensen

Supervisors:

Anders Hedegaard Hansen

Total Pages: 60

Hand in date: 14-03-2022

Synopsis:

The purpose of this project was to model and control the angle of an excavator arm, which would use a discrete displacement multi-chambered cylinder as its actuator, i.e. a hydraulic cylinder which uses digital hydraulic valves rather than proportional valves. A simulink model of the system was created, and three PID controllers were designed to control the angle of the excavator arm. Additionally, since the system uses digital hydraulics, and thus can only use pre-set force configurations, a Force-Shifting Algorithm was developed to control the output of the digital valve setup. The main focus of the project was to investigate ways to increase the energy-efficiency of such a digital hydraulic system. Two methods were investigated: Changing the sampling time of the FSA, which would make it change between configurations less frequently, and implementing a locking mechanism, which would hold the arm in place, to prevent it from oscillating around its reference.

The locking mechanism proved effective at reducing energy consumption, while the slower sampling time was found to actually *increase* the energy consumption of the system.

Preface

This project is based on a mathematical simulation model. The control methods were not tested on any physical setup. Hence, the results of this project are purely theoretical. The parameters of the system were based on a crane setup at Aalborg University.

The programs used in this project includes MATLAB and Simulink for simulation, Maple for derivation of formulas, Inkscape for vector graphics illustrations, and Overleaf for writing.

Sources are listed at the end of the report.

Teitur Joensen

Nomenclature

Symbols		Units
α	Oil-To-Air Proportion	
β	Bulk Modulus	[Pa]
\mathcal{P}	Power	[W]
ω	Rotational velocity	[rad/s]
Φ	Angles in Laplace domain	[rad]
ϕ	Angle	[rad]
ϕ_{tot}	Total angle of arm	[Deg]
τ	Torque	[Nm]
B_{linear}	Linear Damping Coefficient	[Ns/m]
T_s	Sampling Time	[s]
P	Power	[W]
B	Rotational Damping Coefficient	[Ns/rad]
E	Energy	[J]
F	Force	[N]
G	Transfer Function	
g	Gravitational acceleration	[m/s ²]
J	Moment of Inertia	[kgs/m ²]
K	Spring Coefficient	[N/m]
K_v	Valve Coefficient	
L	Length	[m]
M	Mass	[kg]
n	Polytropic Index	
p	Instantaneous Pressure	[Pa]

P_s	Supply Pressure	[Pa]
Q	Flow	[m ³ /s]
V	Volume	[m ³]
x_c	Cylinder Extension	[m]
x_v	Valve Position	[m]

Abbreviations

COM	Center Of Mass
DDC	Discrete Displacement Cylinder
DFCU	Digital Flow Control Unit
FSA	Force Shifting Algorithm
PWM	Pulse Width Modulation

Contents

Preface	v
Nomenclature	vii
1 Introduction, Problem Analysis, System Description	1
1.1 Excavator	2
1.2 Digital Hydraulics	2
1.3 Multi-Chamber Cylinder	3
1.4 System Description	3
2 Project Statement	5
2.1 Objectives	5
2.2 Project limitations and assumptions	5
3 Model	7
3.1 Hydraulic Model	7
3.1.1 Force-Shifting Algorithm	12
3.1.2 Valve Modelling	14
3.1.3 Hydraulic Model Validation	15
3.2 Mechanical Model	17
3.2.1 Trigonometry	17
3.2.2 Noise Model	19
3.2.3 Mechanical Model Validation	20
4 Control	25
4.1 Mechanical Transfer Function And Linearisation	25
4.2 PI Controller	30
4.3 PID Controller Design	31
4.3.1 Lowpass-Filter	33
4.3.2 Anti-Windup	34
4.3.3 PID validation	35
5 Energy Efficiency	39
5.1 Trajectory	39
5.2 FSA Sampling Time Variation Experiment	40
5.2.1 1 ms Sampling Time	40
5.2.2 10 ms Sampling Time	42
5.2.3 100 ms Sampling Time	44

- 5.3 Locking Mechanism 46
 - 5.3.1 Error Margin 46
 - 5.3.2 Stationary Reference 46
 - 5.3.3 Arm Rotational Velocity 47
 - 5.3.4 Test 48
- 6 Conclusion 53**
- 7 Discussion and Future Work 55**
 - 7.1 Energy Efficiency of PI and PID Controllers 55
 - 7.2 Valve Energy Usage 56
 - 7.3 PID Activity During Lock 57
 - 7.4 Alternate Types of Controllers 57
 - 7.5 Improving PID efficiency 57
 - 7.6 Water Hammering 58
 - 7.7 Pulse Width Modulation 59
 - 7.8 Granularity 59
- Bibliography 61**
- A App: Linearisation Points 65**
- B App: Sampling Times 67**

Introduction, Problem Analysis, System Description

1

Due to its high energy density, hydraulics are a popular choice for heavy machinery, such as construction vehicles. One example of this is excavators, which move their arms via hydraulic cylinders.



Figure 1.1. CAT 313 GC Excavator[1]

However, these hydraulic machines are large, and thus require a lot of power, and they were invented in a time where energy efficiency was not a large concern. In a future which is increasingly paying attention to energy efficiency, a lot of energy could be saved by using more efficient methods of control for these large machines.

Digital hydraulics have been proposed as a way of saving energy in hydraulic cylinder systems. Therefore, this project will investigate the application of digital hydraulics on an excavator arm, with a focus on saving energy.

1.1 Excavator

The arm of an excavator is typically divided into three parts: The Boom, The Stick (sometimes called the Arm, but for this project, "Arm" will refer to the entire limb of the excavator), and the Bucket.

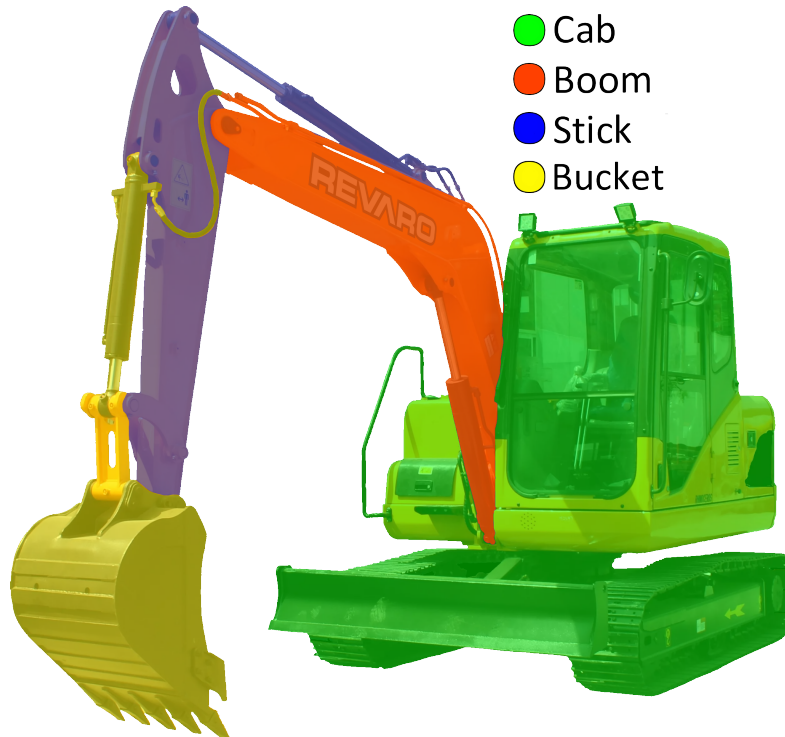


Figure 1.2. The arm of an excavator broken down into its individual links.

For this project, control of the cylinder will only be applied to the first link, highlighted on figure 1.2, which controls the up/down motion of the arm. The stick and bucket will be assumed to remain stationary.

1.2 Digital Hydraulics

The system investigated in this project would use digital hydraulics, i.e. instead of having a proportional valve (which can adjust its position from 0% to 100% open, as needed), it uses several on/off valves (which are always either fully open or fully closed; they can not be partially opened).

This makes it somewhat harder to control the system, since it can not be set to the exact desired value, but instead only has a limited set of positions it can be set to (e.g. a 2x2 set of valves would have 4 positions it can be set to). However, it can also make the system more robust and cost-effective, since these valves are considerably simpler than a proportional valve.

Another advantage of digital hydraulics is that it allows the system to rapidly alter its flow

or force, i.e. it can change *directly* from 0% to 100% flow, rather than slowly increasing it.[2]

For digital hydraulic systems, these on/off valves often come bundled together in a Discrete Flow Control Unit. However, for this project, each valve is a separate component that can be individually controlled.

1.3 Multi-Chamber Cylinder

Typical hydraulic cylinders have two chambers, one for pushing and one for pulling. However, for digital hydraulic systems, it can be advantageous to have more than two chambers, as each new chamber can have a different surface area, thereby producing a different amount of force. This exponentially increases the number of settings the cylinder can be set to, increasing the potential precision of the system. The formula for finding the number of possible configurations for the digital valves is as follows:

$$\text{Configuration Amount} = N^K + 1 \quad (1.1)$$

Where N is the number of valves connected to each chamber, and K is the number of chambers (bearing in mind that each chamber can only be connected to one valve at a time, or else it would cause a hydraulic short-circuit), plus one more configuration where all valves are shut.

1.4 System Description

There is no physical setup for this project; The system in this project will only be a simulation. The parameters are based on a hydraulic crane-setup at Aalborg University. Thus, the usual second link and bucket of the excavator arm is represented by the mass at the end of the crane:

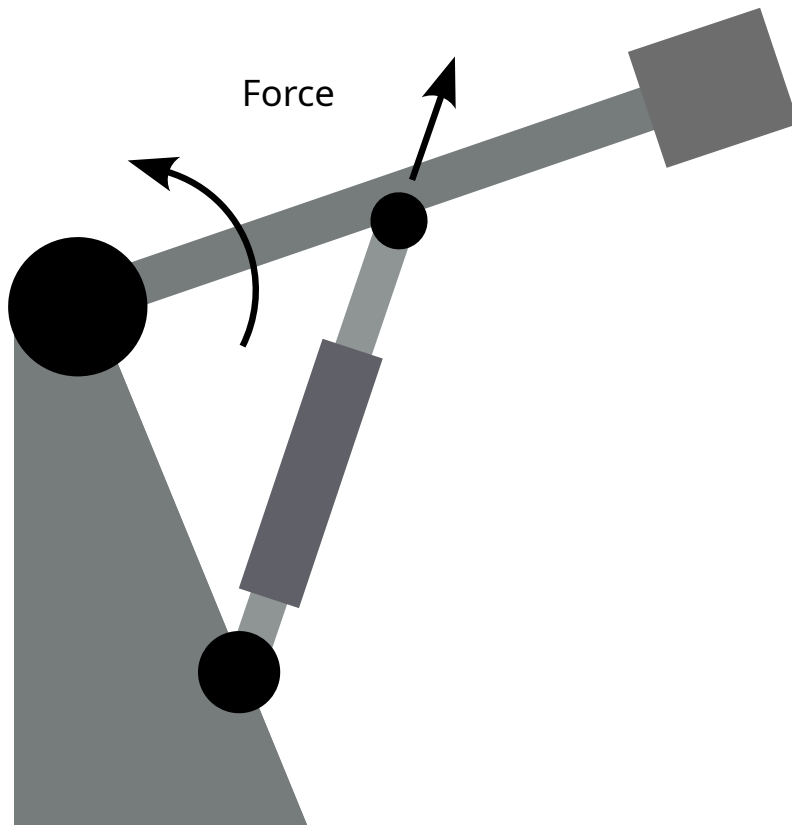


Figure 1.3. The setup of the excavator arm. It is a triangular system, where the cylinder length L_c can extend or contract to move the first link of the arm. The arm is holding a mass at the end of it, which represents the weight of the excavator arm's second link and bucket.

The regular 2-chambered cylinder of the crane would be replaced by a 3-chambered cylinder, controlled via a digital valve setup:

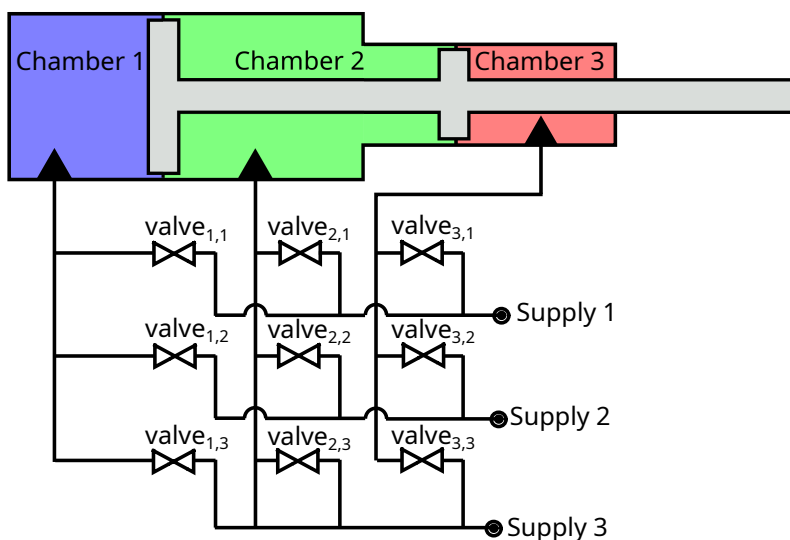


Figure 1.4. The hydraulic cylinder has three chambers, each connected to three valves. Each valve connects to a different supply pressure, 220 bar, 150 bar and 20 bar, respectively.

Project Statement 2

"How can a discrete displacement multi-chamber hydraulic cylinder be controlled to minimize energy consumption, in the context of an excavator arm?"

2.1 Objectives

1. Analyze and model a hydraulic cylinder with 3 chambers, with a digital valve setup, using matlab and simulink to simulate the system.
2. Design a controller for the cylinder, with the angle of the arm as the output, and the force from the cylinder as the input.
3. Program a Force-Shifting Algorithm to control the valves to give the controller the force that it requests.
4. Choose a reference trajectory, and analyze the energy-consumption of the cylinder for that trajectory.
5. Analyze methods to improve the energy-efficiency of the cylinder.

2.2 Project limitations and assumptions

1. The control will only be implemented on a simulation. There will be no physical setup.
2. Only the first link of the excavator is analyzed and controlled. The second link and the bucket is assumed to be a stationary mass attached to the end of the first link.
3. Only the hydraulic energy consumption is taken into account. The energy consumption of the valves and electronics are not included.

Model 3

3.1 Hydraulic Model

The hydraulic system consists of the 3 chambered cylinder, with each chamber connected to 3 supply pressures, for a total of 9 valves.

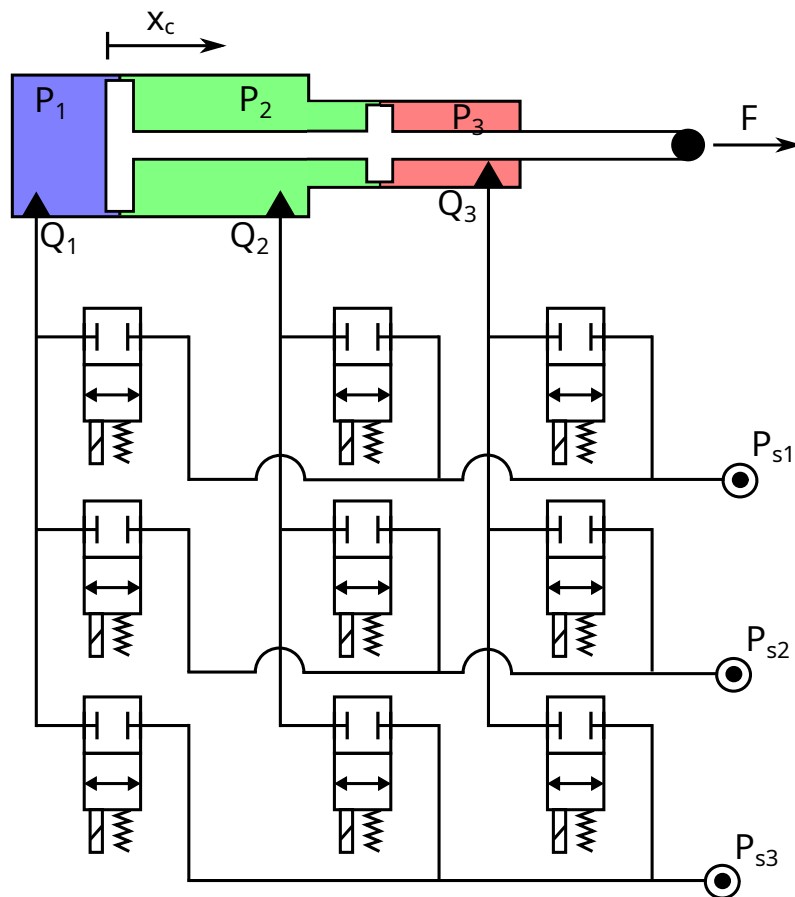


Figure 3.1. The flows and pressures of each chamber.

The flow into each chamber is described with the continuity equation:

$$Q_{in} - Q_{out} = \dot{V} + \frac{V}{\beta} \dot{p} \quad (3.1)$$

Where Q is the flows, V is the volumes, β is the bulk modulus and P is the pressure. Which for each individual chamber would be:

$$Q_1 - Q_{le1} = \dot{x}_c \cdot A_1 + \frac{V_{d1} + x_c \cdot A_1}{\beta_1} \dot{p}_1 \quad (3.2)$$

$$Q_2 + Q_{le1} - Q_{le2} = -\dot{x}_c \cdot A_2 + \frac{V_{2min} + (L - x_c) \cdot A_2}{\beta_2} \dot{p}_2 \quad (3.3)$$

$$Q_3 + Q_{le2} = -\dot{x}_c \cdot A_3 + \frac{V_{d2} + (L - x_c) \cdot A_3}{\beta_3} \dot{p}_3 \quad (3.4)$$

Where x_c is the position of the cylinder, A is the summed effective area of the piston in each chamber (the area of chamber 2 is equal to the area on the right side subtracted from the area on the left-side piston), V_d is the dead volume at each end of the piston (a volume of fluid that is always present in the cylinder), V_{2min} is the minimum volume of fluid in the middle chamber, L is the maximum stroke length of the cylinder, and p is the instantaneous pressure in each chamber.

The chamber flow equations can then be rewritten to describe the changing pressure in each chamber:

$$\dot{p}_1 = \frac{\beta_1}{V_{d1} + x_c \cdot A_1} (Q_1 - Q_{le1} - \dot{x}_c \cdot A_1) \quad (3.5)$$

$$\dot{p}_2 = \frac{\beta_2}{V_{2min} + (L - x_c) \cdot A_2} (Q_2 + Q_{le1} - Q_{le2} + \dot{x}_c \cdot A_2) \quad (3.6)$$

$$\dot{p}_3 = \frac{\beta_3}{V_{d2} + (L - x_c) \cdot A_3} (Q_3 + Q_{le2} + \dot{x}_c \cdot A_3) \quad (3.7)$$

Q_{le} is the leakage through the hydraulic disks, which can be described by the following equation:

$$Q_{le1} = C_{le} \cdot (p_1 - p_2) \quad (3.8)$$

$$Q_{le2} = C_{le} \cdot (p_2 - p_3) \quad (3.9)$$

Where C_{le} is the leakage coefficient. And the bulk modulus is described with the following equation (assuming the bulk modulus is only pressure dependent):

$$\beta = \frac{1}{\frac{1}{\beta_0} + \frac{\epsilon_{air}}{n(p_0 + p)}} \quad (3.10)$$

Where β_0 is the bulk modulus for a completely compressed fluid, ϵ_{air} is the volumetric ratio of air in the oil, n is the polytropic index (which is 1.4 for an adiabatic process), Generally, the less air is in the oil, the closer β will approach to a constant value β_0 .

The flow through a valve can be described by the valve equation:

$$Q = k_v \cdot x_v \cdot \sqrt{|\Delta p|} \cdot \text{sgn}(\Delta p) \quad (3.11)$$

$$k_v = \frac{Q_{nom}}{\sqrt{\frac{\Delta p_{nom}}{2}}} \quad (3.12)$$

Where k_v is the valve coefficient, x_v is the opening of the valve (normally ranging from -1 to +1, but in the case of on/off valves can only be 0 or 1).

The valves are connected to 3 different supply pressures (which are kept at constant values), following the format "*valve_{i,j}*", where i is the cylinder chamber it connects to, and j is the supply pressure it connects to, so the valve equations would be as follows (assuming every valve is of the same type):

$$Q_{1,1} = k_v \cdot x_{v1,1} \cdot \sqrt{|P_{s1} - p_1|} \cdot \text{sgn}(P_{s1} - p_1) \quad (3.13)$$

$$Q_{1,2} = k_v \cdot x_{v1,2} \cdot \sqrt{|P_{s2} - p_1|} \cdot \text{sgn}(P_{s2} - p_1) \quad (3.14)$$

$$Q_{1,3} = k_v \cdot x_{v1,3} \cdot \sqrt{|P_{s3} - p_1|} \cdot \text{sgn}(P_{s3} - p_1) \quad (3.15)$$

$$Q_{2,1} = k_v \cdot x_{v2,1} \cdot \sqrt{|P_{s1} - p_2|} \cdot \text{sgn}(P_{s1} - p_2) \quad (3.16)$$

$$Q_{2,2} = k_v \cdot x_{v2,2} \cdot \sqrt{|P_{s2} - p_2|} \cdot \text{sgn}(P_{s2} - p_2) \quad (3.17)$$

$$Q_{2,3} = k_v \cdot x_{v2,3} \cdot \sqrt{|P_{s3} - p_2|} \cdot \text{sgn}(P_{s3} - p_2) \quad (3.18)$$

$$Q_{3,1} = k_v \cdot x_{v3,1} \cdot \sqrt{|P_{s1} - p_3|} \cdot \text{sgn}(P_{s1} - p_3) \quad (3.19)$$

$$Q_{3,2} = k_v \cdot x_{v3,2} \cdot \sqrt{|P_{s2} - p_3|} \cdot \text{sgn}(P_{s2} - p_3) \quad (3.20)$$

$$Q_{3,3} = k_v \cdot x_{v3,3} \cdot \sqrt{|P_{s3} - p_3|} \cdot \text{sgn}(P_{s3} - p_3) \quad (3.21)$$

$$(3.22)$$

In the case of an on/off valve, x_v equals either 1 or 0.

The flows into each chamber, used in formulas 3.2, 3.3 and 3.4, are a combination of the flows from these individual valves:

$$Q_1 = Q_{1,1} + Q_{1,2} + Q_{1,3} \quad (3.23)$$

$$Q_2 = Q_{2,1} + Q_{2,2} + Q_{2,3} \quad (3.24)$$

$$Q_3 = Q_{3,1} + Q_{3,2} + Q_{3,3} \quad (3.25)$$

$$(3.26)$$

The force exerted by the cylinder is then dependent upon the pressure in each chamber:

$$F_{cyl} = (p_1 \cdot A_1) - (p_2 \cdot A_2) - (p_3 \cdot A_3) \quad (3.27)$$

Given the system's setup with 3x3x3 on/off valves, where each chamber can only have one valve open at a time, there are 27 discrete forces that the cylinder can exert upon the load in steady-state (plus one 28th setting where all the valves are closed). Using the hydraulic parameters of the system, as seen in table 3.2, these discrete forces can be calculated:

Left total piston area	A_1	0.0033	m^2
Middle total piston area	A_2	0.0017	m^2
Right total piston area	A_3	0.0008	m^2
Left dead volume	V_{d1}	$1.7241 \cdot 10^{-3}$	m^3
Right dead volume	V_{d2}	$2.2167 \cdot 10^{-3}$	m^3
Minimum piston length	L_{cmin}	0.772	m
Total stroke length	L	0.386	m
Supply pressure 1	P_{s1}	220	bar
Supply pressure 2	P_{s2}	150	bar
Supply pressure 3	P_{s3}	20	bar
Leakage coefficient	C_{le}	$2.49 \cdot 10^{-13}$	$m^3/(s \cdot Pa)$
Bulk Modulus without air	β_0	16000	bar
Polytropic index	n	1.4	
Oil air proportion	α	0.015	
Nominal flow	Q_{nom}	100	L/min
Nominal pressure	P_{nom}	5	bar
Valve coefficient	K_v	$2.357 \cdot 10^{-6}$	

Table 3.2. Hydraulic system parameters, based on the parameters of a crane-setup at Aalborg University.

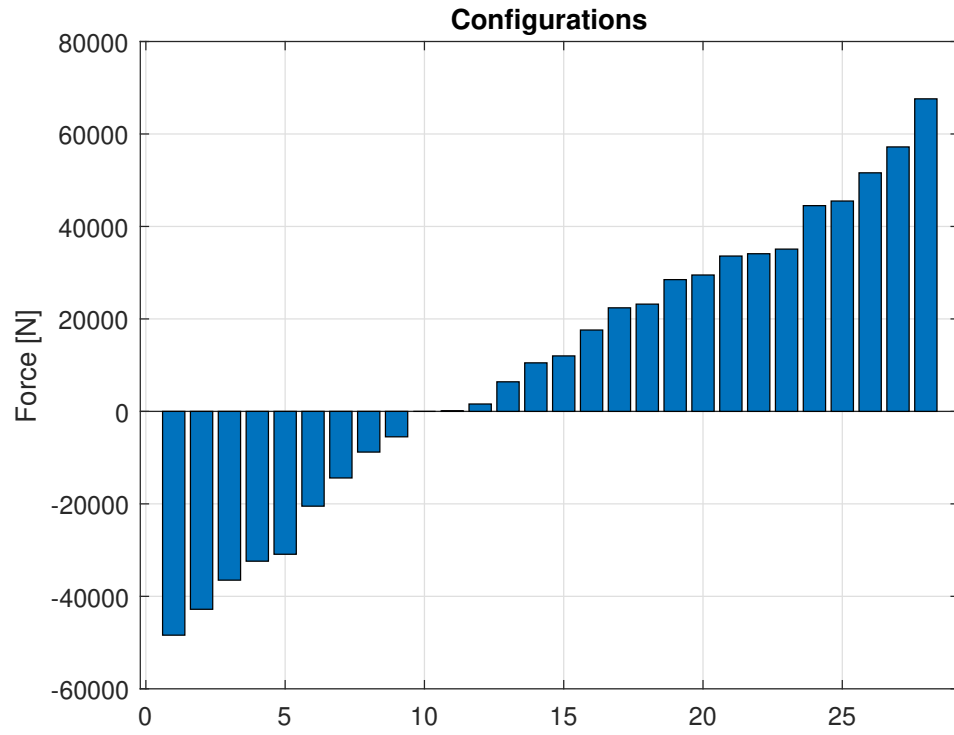


Figure 3.2. Graph of the discrete pressures that the cylinder is able to exert.

Configuration	Force [N]
Configuration 1	-48400
Configuration 2	-42800
Configuration 3	-36500
Configuration 4	-32400
Configuration 5	-30900
Configuration 6	-20500
Configuration 7	-14400
Configuration 8	-8800
Configuration 9	-5500
Configuration 10	0
Configuration 11	100
Configuration 12	1600
Configuration 13	6400
Configuration 14	10500
Configuration 15	12000
Configuration 16	17600
Configuration 17	22400
Configuration 18	23200
Configuration 19	28500
Configuration 20	29500
Configuration 21	33600
Configuration 22	34100
Configuration 23	35100
Configuration 24	44500
Configuration 25	45500
Configuration 26	51600
Configuration 27	57200
Configuration 28	67600

Table 3.3. The 28 discrete forces that the cylinder is able to output.

3.1.1 Force-Shifting Algorithm

In order to select the force-configuration that is closest to the requested reference-value, the program will compile a secondary force-vector, composed of 27 forces that make up the boundaries between the discrete force values.

$$ConfigurationBorder(i) = \frac{Config(i) + Config(i + 1)}{2} \quad (3.28)$$

For example, Configuration 15 has a value of 12000 N, while Configuration 16 has a value of 17600 N, so Configuration Border 15 would be

$$ConfigurationBorder(15) = \frac{Config(15) + Config(16)}{2} = \frac{12000 + 17600}{2} = 14800N \quad (3.29)$$

Which means when the force-reference crosses above 14800 N, the system should switch from Configuration 15 to Configuration 16.

The system does this by checking the reference value, and then counting how many ConfigurationBorder values are *below* this value, and then sets the system to a configuration equal to this number plus 1. For example, if the force-reference is 15000 N, there are 15 ConfigurationBorder values below it, so it will set the system to Configuration 16.

ConfigurationBorder	Force [N]
ConfigurationBorder 1	-45600
ConfigurationBorder 2	-39650
ConfigurationBorder 3	-34450
ConfigurationBorder 4	-31650
ConfigurationBorder 5	-25700
ConfigurationBorder 6	-17450
ConfigurationBorder 7	-11600
ConfigurationBorder 8	-7150
ConfigurationBorder 9	-2750
ConfigurationBorder 10	50
ConfigurationBorder 11	850
ConfigurationBorder 12	4000
ConfigurationBorder 13	8450
ConfigurationBorder 14	11250
ConfigurationBorder 15	14800
ConfigurationBorder 16	20000
ConfigurationBorder 17	22800
ConfigurationBorder 18	25850
ConfigurationBorder 19	29000
ConfigurationBorder 20	31550
ConfigurationBorder 21	33850
ConfigurationBorder 22	34600
ConfigurationBorder 23	39800
ConfigurationBorder 24	45000
ConfigurationBorder 25	48550
ConfigurationBorder 26	54400
ConfigurationBorder 27	62400

Table 3.4. The 27 borders that dictate which configuration the system should be set to.

Each configuration is associated with a vector with 3 numbers in it, based on which valves should be open for each cylinder chamber to achieve the desired force for each configuration (each valve leading to a different pressure source). For example, Configuration 20 has the vector [3 1 2], which means chamber 1 should be connected to P_{s3} (20 bar), chamber 2 should be connected to P_{s1} (220 bar), and chamber 3 should be connected to P_{s2} (150 bar).

It should be noted that Configuration 10 behaves differently from the other configurations, as it is the one with *all* the valves closed. Due to this, while configuration 10 is active,

channels must be opened up to allow flow between the cylinder chambers, or the cylinder would be frozen in place.

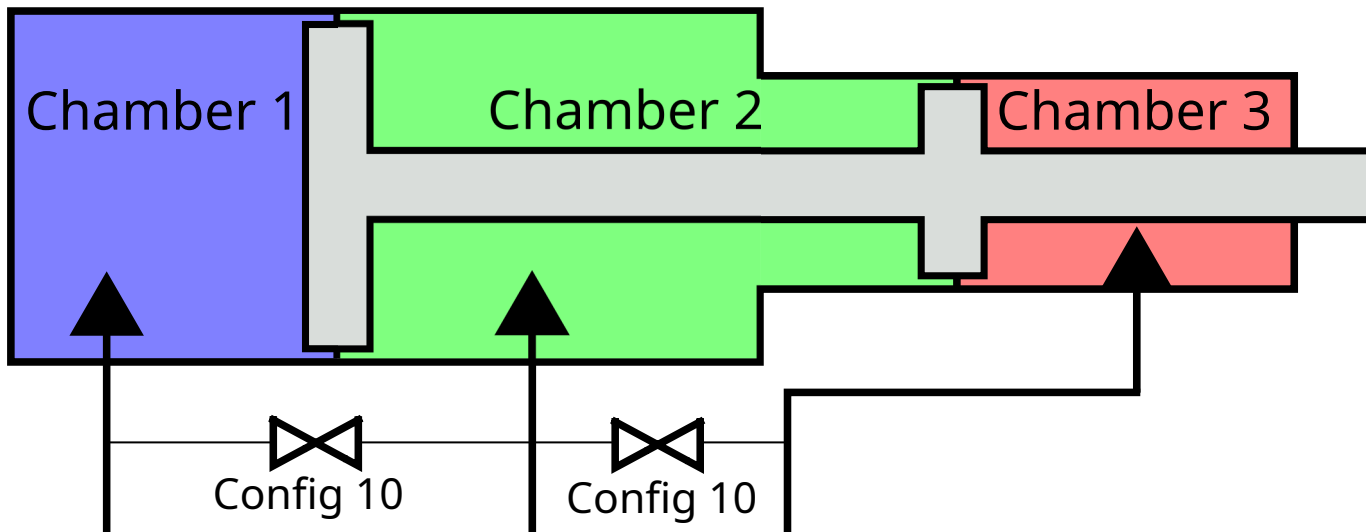


Figure 3.3. Channels between the chambers, which are opened while configuration 10 is active.

3.1.2 Valve Modelling

In order to simulate the valves as a component of the system, the movement of each valve was modelled as a 1st Order Response:

$$G_v(s) = \frac{1}{\tau s + 1} \quad (3.30)$$

Where τ (only in this section) is the time constant, the time it takes to reach 63% of the input reference. The settling time, T_s (only in this section), is defined as 4τ .

The typical response time of an on/off valve is 8 ms - 12 ms for typical digital-valve-systems[2]. Therefore, the time constant of the valve is set as 2 ms:

$$G_v(s) = \frac{1}{0.002s + 1} \quad (3.31)$$

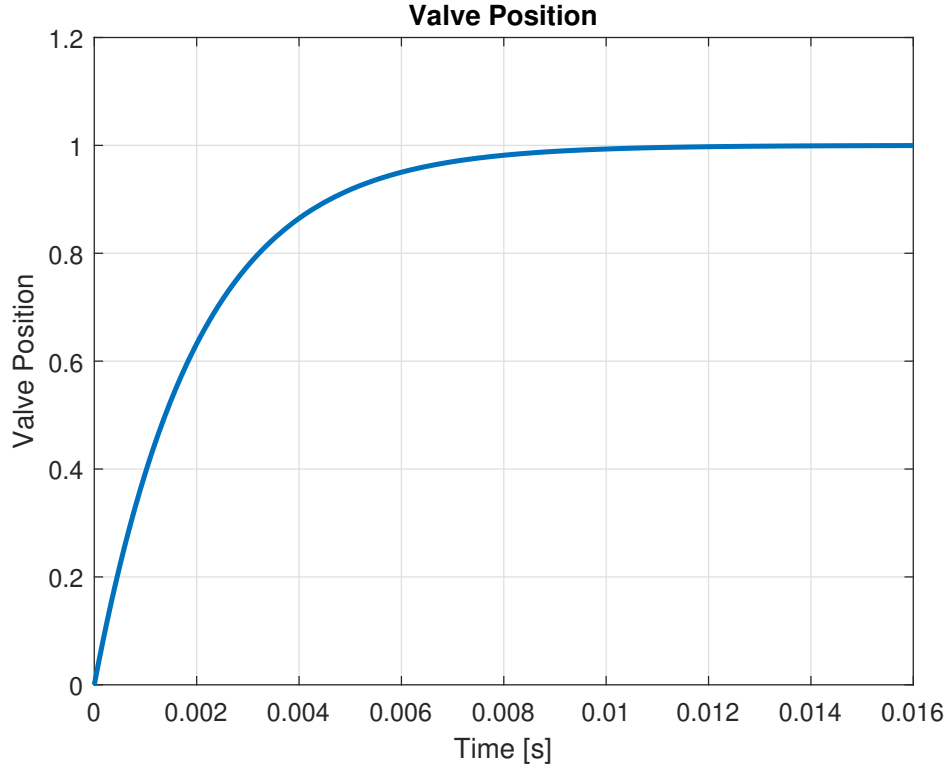


Figure 3.4. Plot of the 1st Order Response of the valve model.

On top of this, valves have a 2 ms input delay[2], so a 2 ms time delay is also added to the valves, for a total response time of 10 ms (with settling time = 4τ).

3.1.3 Hydraulic Model Validation

The simulation model was then tested, to see if the piston was producing the correct forces according to its reference. Three configurations were selected out of the 28 possible configurations: Configurations 3, 14 and 26, which correspond to -36500, 10500 and 51600 N.

A constant reference of these forces was input into the Force Shifting Algorithm, and a mass-spring-damper system was attached as a load, with the following parameters:

Mass	M	402	[kg]
Damping	B	4000	[Ns/m]
Spring	K	1000000	[N/m]
Resting Position	x_{c0}	0.193	[m]

The addition of a spring means the system will reach an equilibrium at a point where the spring force equals the output force of the cylinder. This equilibrium position is equal to the force divided by the spring constant (1 million N/m).

Configuration	Force	Expected Displacement	Expected Position	Actual Position
Resting	0 N	0 m	0.1930 m	0.1930 m
3	-36500 N	-0.0365 m	0.1565 m	0.1565 m
14	10500 N	+0.0105 m	0.2035 m	0.2035 m
26	51600 N	+0.0516 m	0.2446 m	0.2446 m

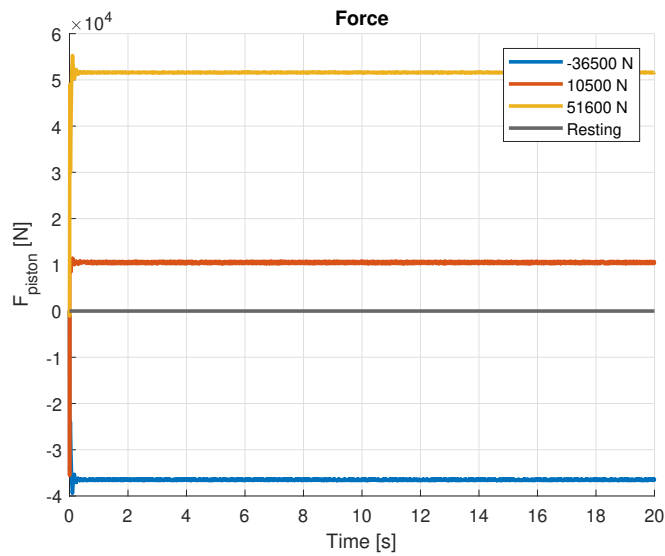


Figure 3.5. Piston's force, when given a reference of -36500 N, 10500 N, and 51600 N.

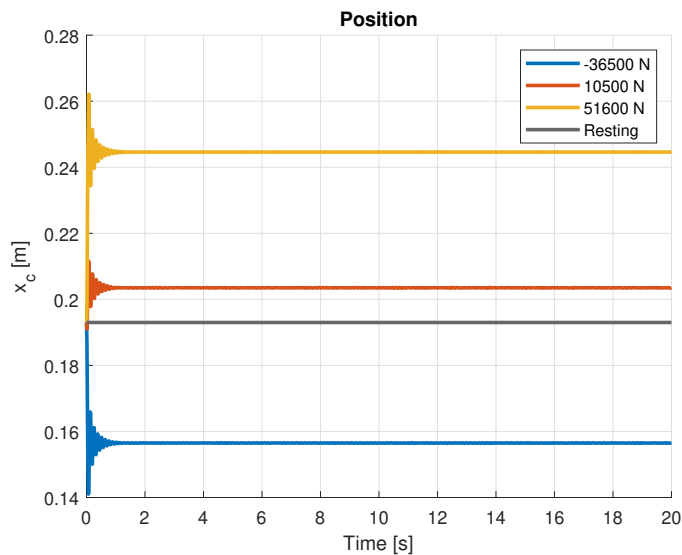


Figure 3.6. Piston's position, when exerting a force of -36500 N, 10500 N, and 51600 N.

With these results, the hydraulic model is considered to output an accurate force. The force from the cylinder will then be used as the force-input for the mechanical model.

3.2 Mechanical Model

3.2.1 Trigonometry

The system is a trigonometric system, i.e. it consists of three lengths, one of the lengths (L_c) being the hydraulic cylinder, which can be adjusted to change the angle ϕ_c , to move the arm of the excavator.

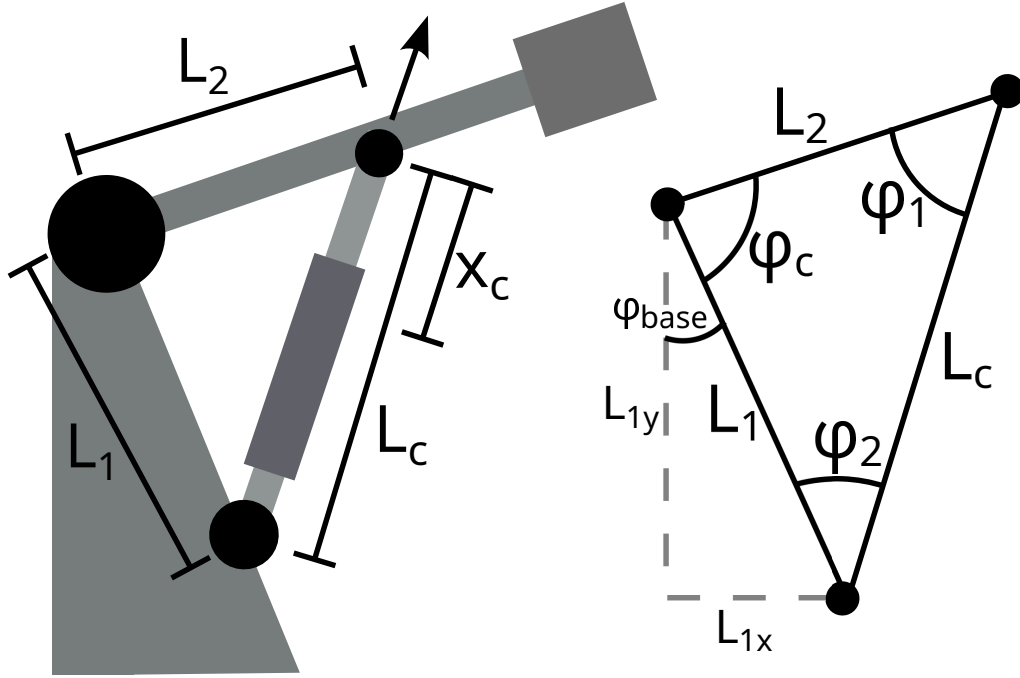


Figure 3.7. The setup of the excavator arm (left), reduced to a triangle (right). The cylinder length L_c can extend or contract to change the angles ϕ .

The angles of the triangle are given by the cosine relation:

$$\phi_1 = \text{acos} \left(\frac{L_1^2 - L_2^2 - L_c^2}{-2 \cdot L_2 \cdot L_c} \right) \quad (3.32)$$

$$\phi_2 = \text{acos} \left(\frac{L_2^2 - L_1^2 - L_c^2}{-2 \cdot L_1 \cdot L_c} \right) \quad (3.33)$$

$$\phi_c = \text{acos} \left(\frac{L_c^2 - L_1^2 - L_2^2}{-2 \cdot L_1 \cdot L_2} \right) \quad (3.34)$$

$$\phi_{\text{base}} = \text{acos} \left(\frac{L_{1x}^2 - L_{1y}^2 - L_1^2}{-2 \cdot L_{1y} \cdot L_1} \right) \quad (3.35)$$

The force from the hydraulic piston is exerted upon the excavator arm, which is translated into a rotational torque:

$$\tau = F \cdot r \cdot \sin(\theta) \quad (3.36)$$

Which for this hydraulic cylinder would be

$$\tau_{cyl} = F_{cyl} \cdot L_2 \cdot \sin(\phi_1) \quad (3.37)$$

In addition to the force from the piston, the arm is also being pulled on by gravity:

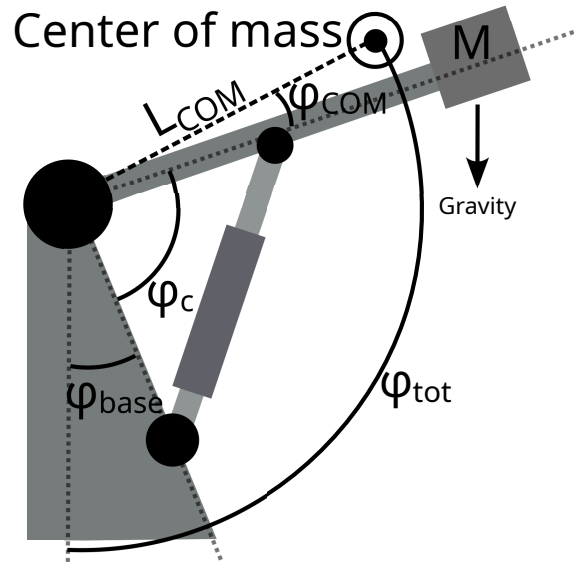


Figure 3.8. The gravity acting upon the center of mass of the arm. The second limb of the arm is assumed to remain at a constant angle, such that the center of mass would remain at a constant angle and distance, relative to the first limb L_2 .

$$\tau_{grav} = M \cdot g \cdot L_{COM} \cdot \sin(\phi_{tot}) \quad (3.38)$$

$$\phi_{tot} = \phi_{base} + \phi_c + \phi_{COM} \quad (3.39)$$

Where M is the mass of the rotating limb, g is the gravitational acceleration, L_{COM} is the distance from the rotating joint to the center of mass, ϕ_{COM} is the angle of the center of mass, relative to the angle of the arm, and ϕ_{base} is the slope of the base of the arm. This way the gravitational pull is greatest when the center of mass is horizontal from the rotating joint. The calculations are done assuming the cab of the excavator is perpendicular to the ground.

These torques are then translated into a rotational acceleration, dependent upon the arm's moment of inertia:

$$\dot{\omega} = \frac{\tau_{cyl} - \tau_{grav} - \omega \cdot B}{J} \quad (3.40)$$

$$\phi_c = \phi_{c0} + \int_0^t \int_0^t \dot{\omega} \, dt \, dt \quad (3.41)$$

Where ω is the system's angular velocity, B is the system's friction coefficient (Nm per rad/s), and J is the arm's moment of inertia.

The extension of the hydraulic cylinder is calculated based on the angle of the arm:

$$L_c^2 = L_1^2 + L_2^2 - 2 \cdot L_1 \cdot L_2 \cdot \cos(\phi_c) \quad (3.42)$$

$$x_c = L_c - L_{cmin} \quad (3.43)$$

The parameters used for the mechanical model can be found in table 3.5:

Length 1	L_1	1.1355	m
Length 1 x	L_{1x}	0.420	m
Length 1 y	L_{1y}	1.055	m
Length 2	L_2	0.5652	m
Minimum piston length	L_{cmin}	0.772	m
Total stroke length	L	0.386	m
Center of mass distance	L_{COM}	3.1397	m
Gravitational acceleration	g	9.82	m/s^2
Mass	M	402	kg
Linear Friction	B_{linear}	4000	[Ns/m]
Rotational Friction	B	2258	[Ns/rad]
Surface slope	ϕ_{base}	0.3789	rad
Center of mass offset angle	ϕ_{COM}	0.0204	rad
Total system moment of inertia	J	288.518	$kg * m^2$
Minimum Angle	ϕ_{cmin}	0.6615	rad
Maximum Angle	ϕ_{cmax}	1.3606	rad

Table 3.5. Mechanical system parameters

Note about the friction: To simplify calculations, the linear friction (Ns/m) of the piston is translated to a rotational friction (Ns/rad). By differentiating equation 3.43 with respect to ϕ_c , one can find a relation between the rotational speed of the arm, and the linear speed of the piston:

$$\frac{dx_c}{d\phi_c} = \frac{L_1 \cdot L_2 \cdot \sin(\phi_c)}{\sqrt{L_1^2 + L_2^2 - 2 \cdot L_1 \cdot L_2 \cdot \cos(\phi_c)}} \quad (3.44)$$

Since the system operates between the angles of $\phi_c = 0.6615$ rad and $\phi_c = 1.3606$ rad, the angle is assumed to be around 1 rad on average. At this angle, equation 3.44 yields a relation of $\frac{\dot{x}_c}{\dot{\phi}_c} = 0.5645 \frac{m}{rad}$. The friction would then have the same relation, therefore $B = B_{linear} \cdot 0.5645 = 2258 \frac{Ns}{rad}$.

3.2.2 Noise Model

In a practical application, control signals will have a high amount of noise, which can complicate the control of the system. This is especially prevalent on loud locations, such

as construction sites, in which an excavator may find itself. Therefore, any controller designed for this system must be able to handle some noise.

The audible spectrum spans the frequencies between 20 Hz and 20000 Hz [3]. Therefore, a 2000 Hz sinusoidal signal, ϕ_{noise} , is input into the angle of the system, ϕ_c . Assuming the mass at the end of the arm vibrates by $5.56 \cdot 10^{-6}$ radians.

In reality, the noise would be more complex and chaotic than a simple sinusoidal signal in an audible frequency. However, for this system, the sinusoidal frequency does an adequate job of introducing some chaotic behavior to the system.

3.2.3 Mechanical Model Validation

The mechanical model is validated through gravity. At a certain angle ϕ_{tot} , a certain amount of torque is produced by the gravity. Therefore, by inputting a certain amount of force, the angle should reach an equilibrium at an angle where $\tau_{cyl} = \tau_{grav}$.

The forces must match up with one of the configurations for force, or the system will not be able to output that force. The available forces are displayed on table 3.3

The forces should ideally be less than the force required to go above 90° , or it is possible that the angle will continue to climb until the cylinder is fully extended.

Therefore, the force required for an equilibrium at 90° must first be calculated:

$$\phi_{tot} = 90^\circ \quad (3.45)$$

$$\phi_{tot} = \phi_{COM} + \phi_c + \phi_{base} \quad (3.46)$$

$$\tau_{grav} = M \cdot g \cdot L_{COM} \cdot \sin(\phi_{tot}) \quad (3.47)$$

$$\tau_{grav} = 402 \cdot 9.82 \cdot 3.1397 \cdot \sin(90^\circ) = \underline{12394.2173Nm} \quad (3.48)$$

$$\phi_c = \phi_{tot} - \phi_{COM} - \phi_{base} \quad (3.49)$$

$$\phi_c = 90^\circ - 1.1680^\circ - 21.7083^\circ = 67.1237^\circ \quad (3.50)$$

$$L_c = \sqrt{L_1^2 + L_2^2 - 2 \cdot L_1 \cdot L_2 \cdot \cos(\phi_c)} \quad (3.51)$$

$$L_c = \sqrt{1.1355^2 + 0.5652^2 - 2 \cdot 1.1355 \cdot 0.5652 \cdot \cos(67.1237^\circ)} = 1.1098m \quad (3.52)$$

$$\phi_1 = \arccos\left(\frac{L_1^2 - L_2^2 - L_c^2}{-2 \cdot L_2 \cdot L_c}\right) \quad (3.53)$$

$$\phi_1 = \arccos\left(\frac{1.1355^2 - 0.5652^2 - 1.1098^2}{-2 \cdot 0.5652 \cdot 1.1098}\right) = 83.2523^\circ \quad (3.54)$$

$$\tau_{cyl} = F_{cyl} \cdot L_2 \cdot \sin(\phi_1) \quad (3.55)$$

$$F_{cyl} = \frac{\tau_{cyl}}{L_2 \cdot \sin(\phi_1)} \quad (3.56)$$

$$F_{cyl} = \frac{12394.2173Nm}{3.1397 \cdot \sin(83.2523^\circ)} = 22081.8636N \quad (3.57)$$

$$(3.58)$$

So 3 configurations were chosen, with a force smaller than 22081.8636 N:

- Configuration 14 = 10500 N
- Configuration 15 = 12000 N
- Configuration 16 = 17600 N

However, since a higher angle ϕ_c will also result in a lower angle ϕ_1 , which in turn reduces the torque that the cylinder exerts upon the arm, it is possible to reach an equilibrium above 90° . Thus three additional forces are chosen.

- Configuration 17 = 22400 N
- Configuration 18 = 23200 N
- Configuration 19 = 28500 N

Then the expected steady state angle must be calculated for these configurations. Since ϕ_1 is tied to ϕ_c , it would be advantageous to change it into an expression based on ϕ_c , so there is only one variable to isolate for. This is done with the sine relation:

$$\frac{\sin(\phi_c)}{L_c} = \frac{\sin(\phi_1)}{L_1} \quad \rightarrow \quad \frac{\sin(\phi_c)}{L_c} \cdot L_1 = \sin(\phi_1) \quad (3.59)$$

$$L_c^2 = L_1^2 + L_2^2 - 2 \cdot L_1 \cdot L_2 \cdot \cos(\phi_c) \quad (3.60)$$

$$\sin(\phi_1) = \frac{\sin(\phi_c) \cdot L_1}{\sqrt{L_1^2 + L_2^2 - 2 \cdot L_1 \cdot L_2 \cdot \cos(\phi_c)}} \quad (3.61)$$

This is then substituted into the equation for cylinder torque:

$$\tau_{cyl} = F_{cyl} \cdot L_2 \cdot \sin(\phi_1) \quad (3.62)$$

$$\tau_{cyl} = F_{cyl} \cdot L_2 \cdot \frac{\sin(\phi_c) \cdot L_1}{\sqrt{L_1^2 + L_2^2 - 2 \cdot L_1 \cdot L_2 \cdot \cos(\phi_c)}} \quad (3.63)$$

$$\tau_{grav} = M \cdot g \cdot L_{COM} \cdot \sin(\phi_{COM} + \phi_c + \phi_{base}) \quad (3.64)$$

$$\tau_{cyl} = \tau_{grav} \quad (3.65)$$

$$F_{cyl} \cdot L_2 \cdot \frac{\sin(\phi_c) \cdot L_1}{\sqrt{L_1^2 + L_2^2 - 2 \cdot L_1 \cdot L_2 \cdot \cos(\phi_c)}} = M \cdot g \cdot L_{COM} \cdot \sin(\phi_{COM} + \phi_c + \phi_{base}) \quad (3.66)$$

Inputting the values for F_{cyl} , and isolating for ϕ_c (for a range between 0.6615 and 1.3606 radians):

$$F_{cyl14} = 10500N \rightarrow \phi_c = -0.89 \ \& \ 2.56 \quad (3.67)$$

$$F_{cyl15} = 12000N \rightarrow \phi_c = -0.9765 \ \& \ 2.5173 \quad (3.68)$$

$$F_{cyl16} = 17600N \rightarrow \phi_c = -1.2960 \ \& \ 2.2886 \quad (3.69)$$

$$F_{cyl17} = 22400N \rightarrow \phi_c = 0.4529 \ \& \ 1.3224 \quad (3.70)$$

$$F_{cyl18} = 23200N \rightarrow \phi_c = 0.4010 \ \& \ -1.6047 \quad (3.71)$$

$$F_{cyl19} = 28500N \rightarrow \phi_c = 0.2503 \ \& \ -1.8775 \quad (3.72)$$

Since F_{cyl17} is the only force configuration with any steady-state positions for ϕ_c between 0.6615 and 1.3606 radians, this force is used for validation. If the model is built correctly, it should reach a steady state position at 1.3224 radians (or 75.7680°):

Configuration	Force	Expected Angle	Actual Angle
17	22400 N	1.3224 rad	1.3224 rad

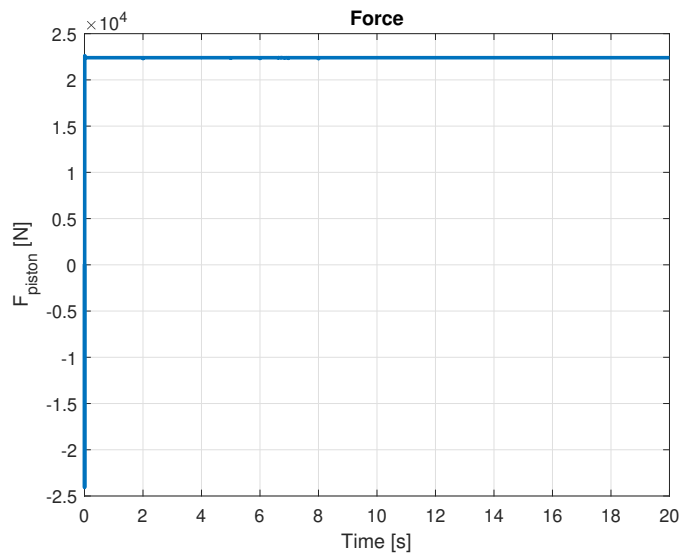


Figure 3.9. Piston's force, when given a reference of 22400 N

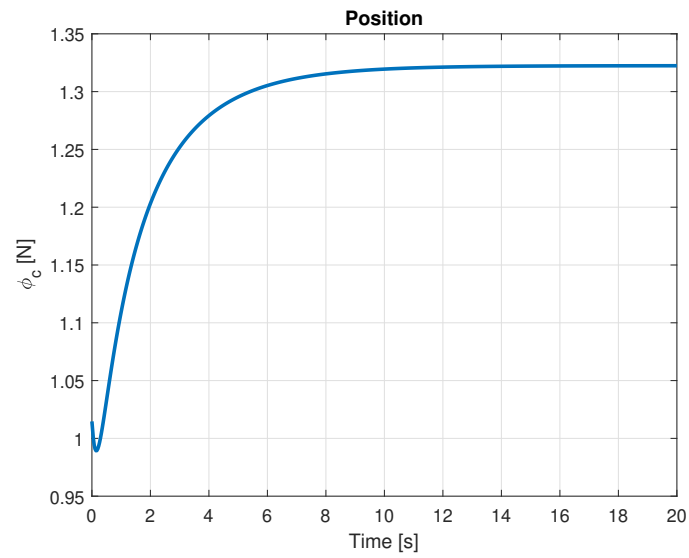


Figure 3.10. And ϕ_c , when receiving a force of 22400 N, settling on 1.3224 radians.

With this, the mechanical model is considered valid. It should be noted that for this test, the noise generator was disabled.

Control 4

After the mathematical model of the system has constructed, it needs a controller to control the output. Several PID-type controllers are tested, and then compared. However, before a controller can be designed, a transfer function is needed.

4.1 Mechanical Transfer Function And Linearisation

For the design of a linear controller for the system, a linear approximation of the system is required, in order to obtain a linear transfer function. Due to high amounts of non-linearity, the hydraulic part of the model is ignored for this section, and it is instead assumed that the hydraulic system will be able to provide the force that is requested by the controller. The input for this transfer function would be the force from the cylinder, F_{cyl} , while the output would be the angle, ϕ_c . Therefore, the transfer function would be based on the rotational acceleration in equation 3.40:

$$\ddot{\phi}_c = \frac{\tau_{cyl} - \tau_{grav} - B \cdot \dot{\phi}_c}{J} \quad (4.1)$$

This equation is then expanded, by inserting the equations for each component:

$$\ddot{\phi}_c = \frac{F_{cyl} \cdot L_2 \cdot \sin(\phi_1) - M \cdot g \cdot L_{COM} \cdot \sin(\phi_{base} + \phi_c + \phi_{COM}) - B \cdot \dot{\phi}_c}{J} \quad (4.2)$$

Since ϕ_1 is tied to ϕ_c , it would be advantageous to change it into an expression based on ϕ_c , as done in equation 3.61 from section 3.2.3.

$$\sin(\phi_1) = \frac{\sin(\phi_c) \cdot L_1}{\sqrt{L_1^2 + L_2^2 - 2 \cdot L_1 \cdot L_2 \cdot \cos(\phi_c)}} \quad (4.3)$$

$$\ddot{\phi}_c = \frac{F_{cyl} \cdot L_2 \cdot \frac{\sin(\phi_c) \cdot L_1}{\sqrt{L_1^2 + L_2^2 - 2 \cdot L_1 \cdot L_2 \cdot \cos(\phi_c)}} - M \cdot g \cdot L_{COM} \cdot \sin(\phi_{base} + \phi_c + \phi_{COM}) - B \cdot \dot{\phi}_c}{J} \quad (4.4)$$

This way, the transfer function only needs to be linearised with respect to three variables: ϕ_c , $\dot{\phi}_c$ and F_{cyl} .

The linearisation is done with a first-order Taylor approximation with three variables:

$$f(x, y, z) \approx f(x_0, y_0, z_0) + \left. \frac{df}{dx} \right|_{x_0, y_0, z_0} \cdot (x - x_0) + \left. \frac{df}{dy} \right|_{x_0, y_0, z_0} \cdot (y - y_0) + \left. \frac{df}{dz} \right|_{x_0, y_0, z_0} \cdot (z - z_0) \quad (4.5)$$

Before this can be done, some linearisation points need to be chosen for the system, based on which circumstances the system is expected to operate in the most, ideally far from the edges of the operating space. Therefore, for the position linearisation point, ϕ_{c0} , the cylinder is assumed to be half extended:

$$L_{c0} = L_{cmin} + \frac{L}{2} \quad (4.6)$$

$$\phi_{c0} = \arccos \left(\frac{\left(L_{cmin} + \frac{L}{2} \right)^2 - L_1^2 - L_2^2}{-2 \cdot L_1 \cdot L_2} \right) = 1.0147 \text{rad} \quad (4.7)$$

In this position, the force from the cylinder is assumed to be sufficient to counteract the gravity:

$$\tau_{cyl0} = \tau_{grav0} \quad (4.8)$$

$$F_{cyl0} \cdot L_2 \cdot \sin(\phi_{10}) = M \cdot g \cdot L_{COM} \cdot \sin(\phi_{base} + \phi_{c0} + \phi_{COM}) \quad (4.9)$$

$$F_{cyl0} = 21673.58 \text{N} \quad (4.10)$$

The system is assumed to be in steady-state, therefore the speed is assumed to be zero:

$$\dot{\phi}_{c0} = 0 \quad (4.11)$$

With this, the linear equation can be found (as all the other values are known constants):

$$\ddot{\phi}_c - \ddot{\phi}_{c0} \approx \left. \frac{d}{d\phi_c} \ddot{\phi}_c \right|_{\phi_{c0}, \dot{\phi}_c, F_{cyl0}} \cdot (\phi_c - \phi_{c0}) + \left. \frac{d}{d\dot{\phi}_c} \ddot{\phi}_c \right|_{\phi_{c0}, \dot{\phi}_c, F_{cyl0}} \cdot (\dot{\phi}_c - \dot{\phi}_{c0}) + \left. \frac{d}{dF_{cyl}} \ddot{\phi}_c \right|_{\phi_{c0}, \dot{\phi}_c, F_{cyl0}} \cdot (F_{cyl} - F_{cyl0}) \quad (4.12)$$

This is then rewritten in terms of change-variables:

$$\Delta \ddot{\phi}_c = K_1 \cdot \Delta \phi_c + K_2 \cdot \Delta \dot{\phi}_c + K_3 \cdot \Delta F_{cyl} \quad (4.13)$$

$$K_1 = \left. \frac{d\ddot{\phi}_c}{d\phi_c} \right|_{\phi_{c0}, \dot{\phi}_c, F_{cyl0}} = -5.1726 \quad (4.14)$$

$$K_2 = \left. \frac{d\ddot{\phi}_c}{d\dot{\phi}_c} \right|_{\phi_{c0}, \dot{\phi}_c, F_{cyl0}} = -7.8262 \quad (4.15)$$

$$K_3 = \left. \frac{d\ddot{\phi}_c}{dF_{cyl}} \right|_{\phi_{c0}, \dot{\phi}_c, F_{cyl0}} = 0.002029 \quad (4.16)$$

$$\ddot{\phi}_{c0} = 0 \quad (4.17)$$

Therefore the linear equation for the system can be expressed as

$$\ddot{\phi}_c = -5.1726 \cdot (\phi_c - 1.0147) - 7.8262 \cdot (\dot{\phi}_c - 0) + 0.001958 \cdot (F_{cyl} - 21673.58) \quad (4.18)$$

This equation then needs to be converted to the frequency domain, through a Laplace transformation:

$$\Phi_c(s) \cdot s^2 = -5.1726 \cdot \Phi_c(s) - 7.8262 \cdot \Phi_c(s) \cdot s + 0.001958 \cdot F_{cyl}(s) \quad (4.19)$$

Which can then be isolated to get an expression for $\frac{\Phi_c(s)}{F_{cyl}(s)}$:

$$\Phi_c(s) \cdot s^2 = -5.1726\Phi_c(s) - 7.8262\Phi_c(s) \cdot s + 0.001958F_{cyl}(s) \quad (4.20)$$

$$\Phi_c(s) \cdot s^2 + 5.1726\Phi_c(s) + 7.8262\Phi_c(s) \cdot s = 0.001958F_{cyl}(s) \quad (4.21)$$

$$\frac{\Phi_c(s)}{F_{cyl}(s)} = \frac{0.001958}{(s^2 + 7.8262s + 5.1726)} \quad (4.22)$$

This equation is then tested against the nonlinear mechanical model, to see if it gives results reasonably close to the real system:

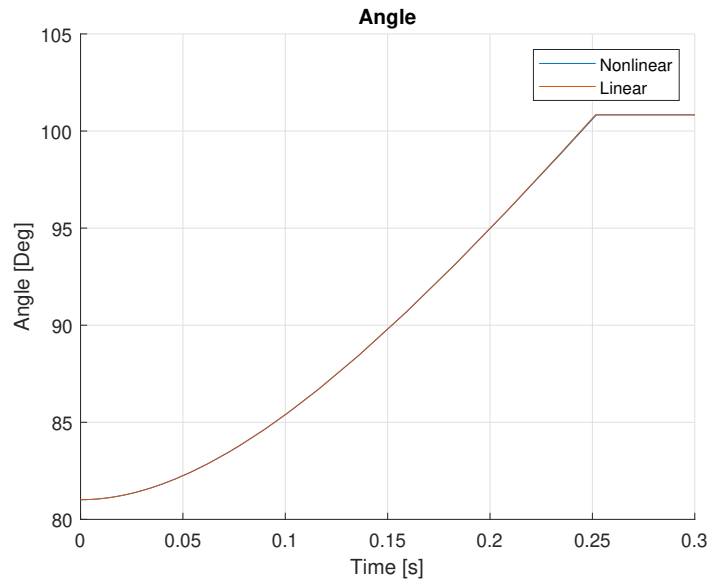


Figure 4.1. The response of the linear and nonlinear mechanical models, when given a constant force-input of 10000 N.

The linear model appears to be a very accurate approximation of the nonlinear mechanical model.

Two other linearisation points ($x_c = 0.25 L$ and $x_c = 0.75 L$) were also attempted, whose response can be seen in appendix A.

With this, the linear model is considered validated, and a linear controller can be designed based on this transfer function.

The transfer function has two poles at $s = -7.0974$ Hz and $s = 0.7288$ Hz, as can be seen on the root locus of the function. Complex roots means the system will oscillate if given an open-loop signal.

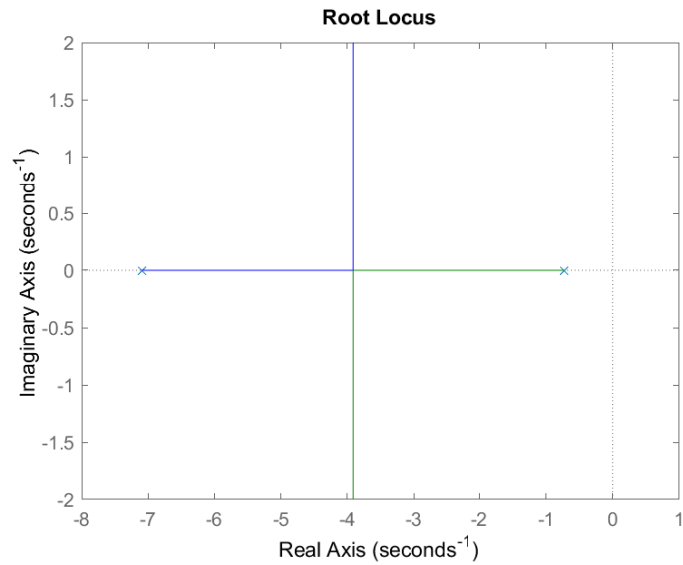


Figure 4.2. Root locus of the linear model.

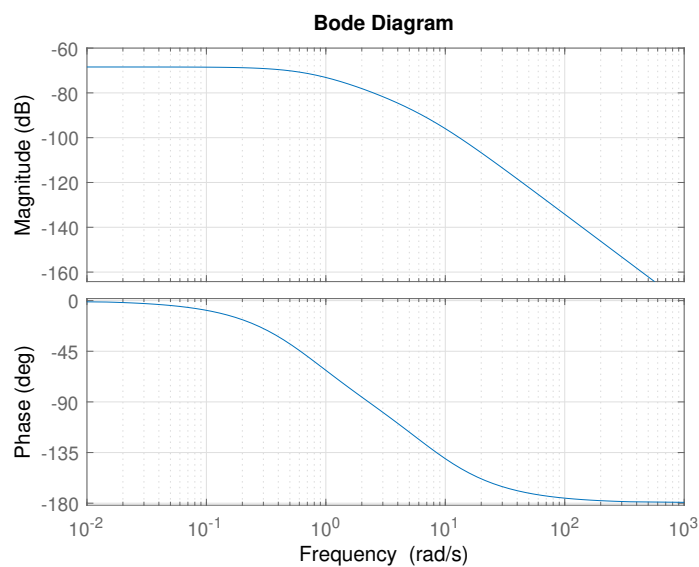


Figure 4.3. Frequency response of the linear model.

Since the system is constantly affected by gravity, it would be advantageous for the controller to have an integrator, to eliminate the steady state error that would occur if the controller were purely a gain. Therefore, a PI controller is designed for the system (which includes an integrator and a zero).

For a crane system, it would be ideal to have a rise time lower than 1 second, less than 5% overshoot, and 0% steady state error.

4.2 PI Controller

$$G_c(s) = \frac{K_p s + K_i}{s} \quad (4.23)$$

The initial K_p and K_i values for the PI controller were determined based on the following formulas: [4]

$$K_p = \frac{1}{|G_p(j\omega_1)H(j\omega_1)|} \quad (4.24)$$

$$K_i = 0.1 \cdot \omega_1 \cdot K_p \quad (4.25)$$

Where ω_1 is the frequency where the system has the desired phase angle, and $|G_p(j\omega_1)H(j\omega_1)|$ is the magnitude at that frequency.

For this controller, a phase margin of 70 degrees is desired. Therefore, the angle was chosen where the phase crosses 110° :

$$\omega_1 = 4.107 \text{ rad/s} \quad (4.26)$$

Which has the magnitude:

$$|G_p(j4.107)H(j4.107)| = -84.856 \text{ dB} = 0.00005717 \quad (4.27)$$

Therefore, the PI values were calculated as:

$$K_p = \frac{1}{0.00005717} = 17490 \quad (4.28)$$

$$K_i = 0.1 \cdot 4.107 \cdot 17490 = 7183 \quad (4.29)$$

Therefore, the PI controller would initially be set to:

$$G_c(s) = \frac{17490s + 7183}{s} \quad (4.30)$$

Which would result in the following closed-loop equation:

$$Y(s) = \frac{G_c(s)G(s)}{1 + G_c(s)G(s)} = \frac{34.24s^4 + 282s^3 + 287.2s^2 + 72.74s}{s^6 + 15.65s^5 + 105.8s^4 + 363s^3 + 313.9s^2 + 72.74s} \quad (4.31)$$

Which has the following step-response:

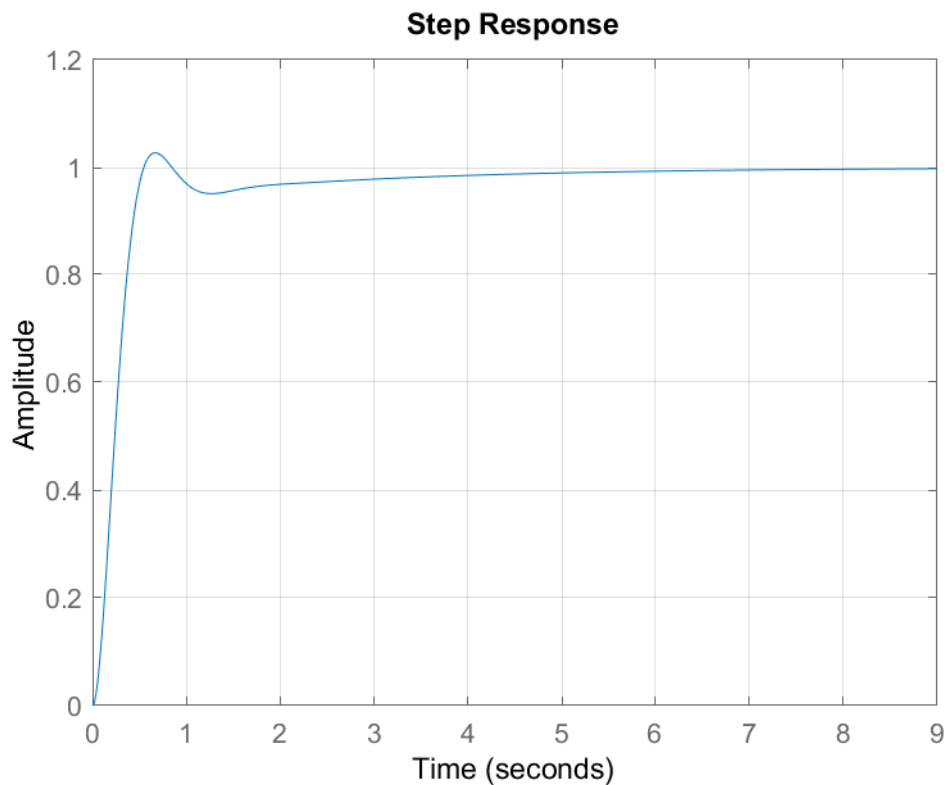


Figure 4.4. Closed-loop Step-response for the PI controller

Which is within the requirements for the system. However, it may be advantageous to attach a differentiator to the controller to reduce the overshoot, and potentially increase the speed.

4.3 PID Controller Design

$$G_c(s) = \frac{K_p s + K_i + K_d s^2}{s} \quad (4.32)$$

The K_p and K_i value calculations are identical to that of the PI controller:

$$K_p = \frac{1}{0.00005717} = 17490 \quad (4.33)$$

$$K_i = 0.1 \cdot 4.107 \cdot 17490 = 7183 \quad (4.34)$$

And the K_d value is calculated as:

$$K_d = \frac{\sin(\theta)}{\omega_1 \cdot |G_p(j\omega_1)H(j\omega_1)|} + \frac{K_i}{\omega_1^2} = 0.00143 \quad (4.35)$$

Where θ is the angle of the controller, $\angle G_c$, which should ideally be 0° [4].

$$K_d = \frac{\sin(0^\circ)}{4.107 \cdot 0.00005717} + \frac{7183}{4.107^2} = 426 \quad (4.36)$$

And the transfer function would be:

$$G_c(s) = \frac{K_p s + K_i + K_d s^2}{s} = \frac{17490s + 7183 + 426s^2}{s} \quad (4.37)$$

Closed loop:

$$Y(s) = \frac{G_c(s)G(s)}{1 + G_c(s)G(s)} = \frac{0.834s^5 + 40.77s^4 + 286.4s^3 + 287.2s^2 + 72.74s}{s^6 + 16.49s^5 + 112.4s^4 + 367.3s^3 + 313.9s^2 + 72.74s} \quad (4.38)$$

Which has the following step response:

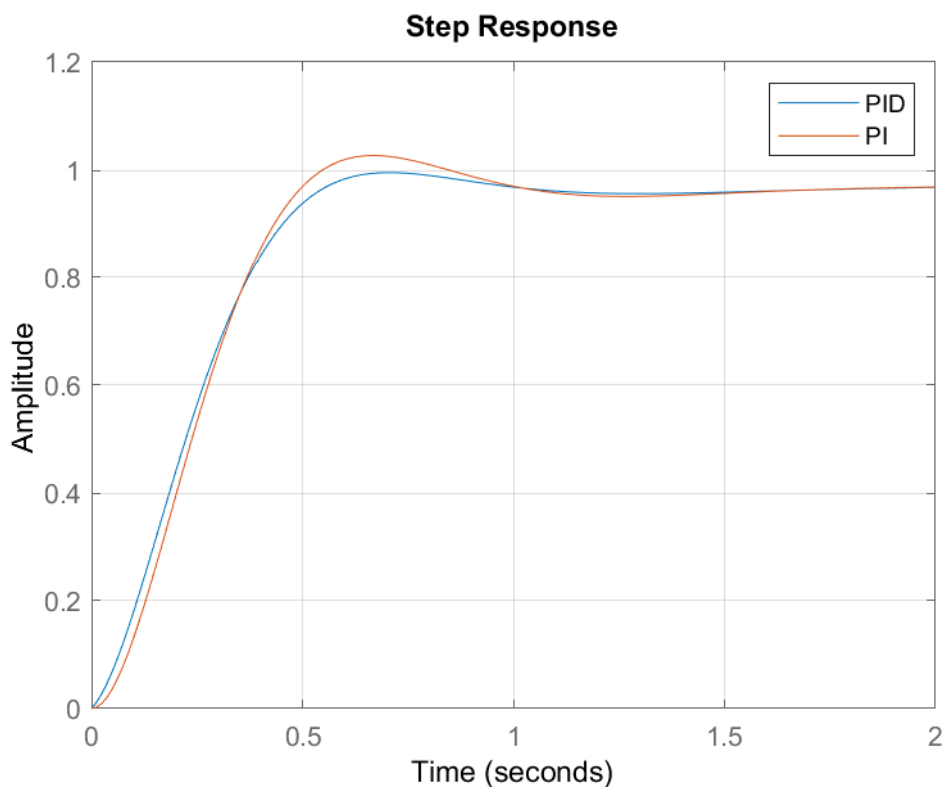


Figure 4.5. Closed-loop Step-response for the PID controller, compared to the PI controller

The PID controller's response is the same as the PI controller, except it rises slightly faster and has a lower overshoot. With this, it is concluded that a PID controller is better suited for controlling the system, based on purely accuracy-focused requirements.

Another PID controller is designed, tuned iteratively, using sisotool, with a final phase margin of 90 degrees. The resulting values were the following:

$$K_p = 608207 \quad (4.39)$$

$$K_i = 1188 \quad (4.40)$$

$$K_d = 74317 \quad (4.41)$$

Which had the following step-response:

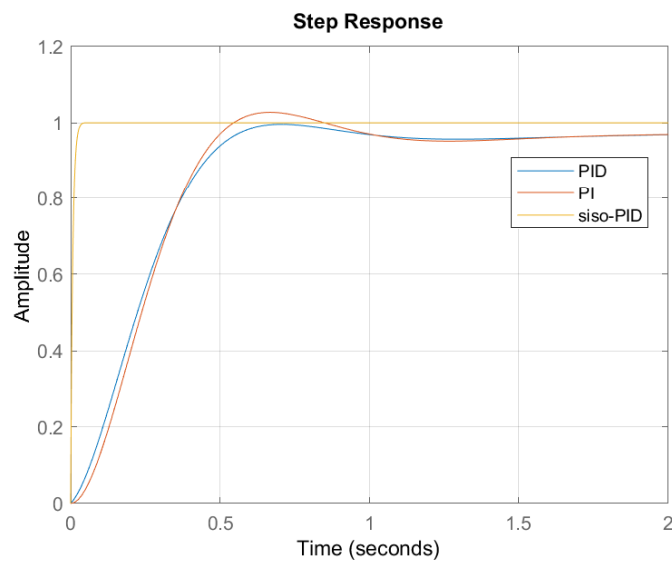


Figure 4.6. Closed-loop Step-response for the PID controller tuned with sisotool, compared to the two previous controllers derived via formulae.

For the PID controllers, a Lowpass-Filter was also designed:

4.3.1 Lowpass-Filter

When including the derivative component in a PID-controller, it will amplify high frequency waves, which includes background noise. This can lead to a lot of vibrations, since it is very rare to have a system without any background noise. Therefore, in order to have a derivative component, it is necessary to have a low-pass filter, to filter out all the high-frequency vibrations, such as sound, Wi-Fi, and background radiation.

For this system, a frequency of 100 rad/s (15.92 Hz) is chosen as the limit for the low-pass filter, as this is below the boundary for audible sound.[3]

$$H_{LPF}(s) = \frac{\omega_{LPF}}{s + \omega_{LPF}} \quad (4.42)$$

$$H_{LPF}(s) = \frac{100}{s + 100} \quad (4.43)$$

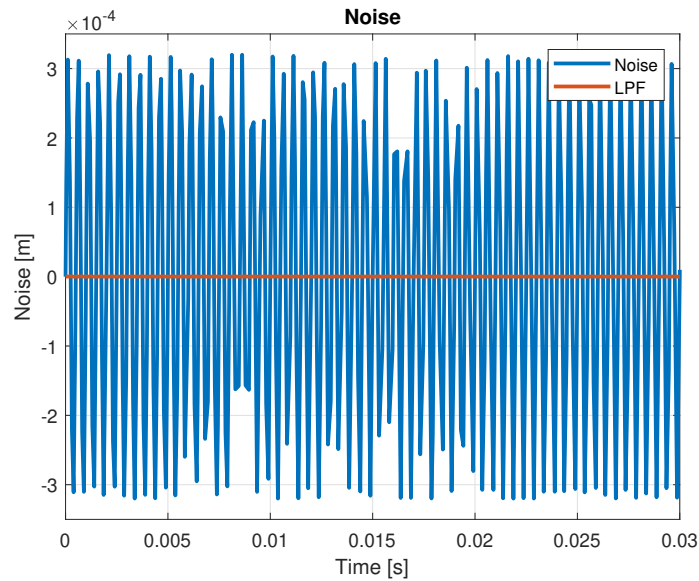


Figure 4.7. Noise input into the system, before and after passing through the LPF filter.

As seen on figure 4.7, the LPF almost completely nullifies the noise in the system, peaking at $3.08\text{e-}07$ m, reducing the noise by 99.9%.

4.3.2 Anti-Windup

When including the integrator component in a PI or PID controller, it will sum up the position error over time, and input it back as a reference to the system's actuator. This can backfire, because any actuator will have limits on how much force it can output (in this case, between -48400 N and 67600 N). This means that the integrator will continue to sum up the error for a long time while the actuator is in saturation, so when the system does reach the desired position, it will take a long time to undo the integrated error. This can lead to huge overshoot. Therefore, a saturation block is put into the force that the controller can output, and the force-overshoot is fed back and subtracted from the integrator's output:

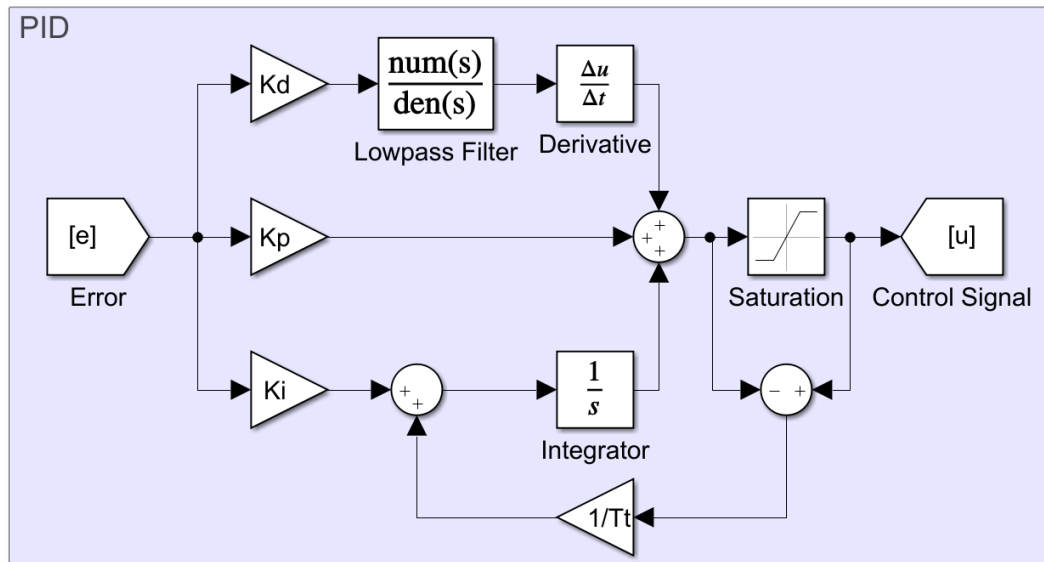


Figure 4.8. PID controller structure, with LPF and Anti-Windup implemented.

Where T_t is the tracking time constant, which determines how fast the integrator's out is reset after saturation:[4]

$$T_t = \sqrt{\frac{K_d}{K_i}} \quad (4.44)$$

This only holds when $K_d \neq 0$. Otherwise, $T_t = 1$.

4.3.3 PID validation

These three PI/PID controllers are then implemented into the full nonlinear model, including the discrete flow setup, the Force-Shifting-Algorithm, the Lowpass-Filter, and the Anti-Windup, to check if they use more force than the system is able to supply, if they are given a step-response of 19° (From 81° to 100° , bearing in mind that the system always starts at 81.01° , and the maximum possible angle of the system is $\phi_{tot} = 100.83^\circ$):

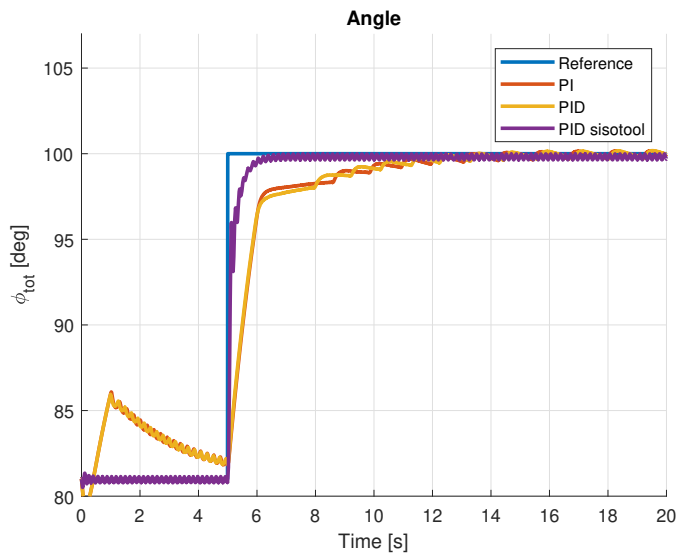


Figure 4.9. Angle of the arm, when given a 19° step-response from its resting position of 81° , using the 3 different controllers.

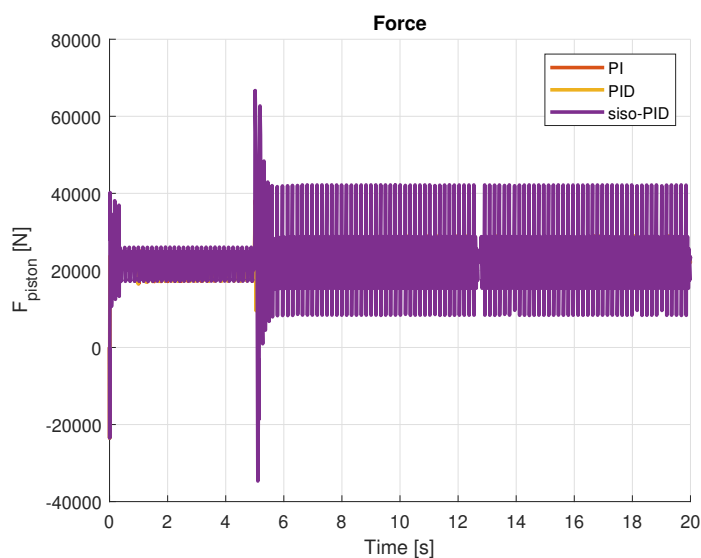


Figure 4.10. Force from the cylinder, when using the 3 different controllers.

It should be noted that, while the total angle of the system is measured in degrees, the controller still uses radians. It should also be noted that the integral component of all controllers has been set to start at 21673.58 N (The force required to counteract the gravity at the start position).

As can be seen on figure 4.10, , all three controllers stay within the range of force that the cylinder can output (-48400 to +67600 N), with the highest recorded force being +67064 N, and the lowest being -36420 N.

With this, it is concluded that all three of these controllers operate within the force restrictions of the system, even when given the most extreme step-response possible.

The performance of the controllers is then compared in terms of RMS Error and Maximum error:

$$\text{Error}(i) = \phi_{tot}(i) - \phi_{ref}(i) \quad (4.45)$$

$$\text{RMS Error} = \sqrt{\frac{\sum_{i=1}^N (\text{Error}(i))^2}{N}} \quad (4.46)$$

$$\text{Max Error} = \max(\text{Error}) \quad (4.47)$$

Where N is the number of entries in the Error vector.

Controller	RMS Error [deg]	Max Error [deg]
PI	2.0928	18.1134
PID	2.0980	18.1549
siso-PID	0.6696	18.9741

Table 4.2. Comparison of the accuracy of the controllers.

After these tests, the sisotool PID controller is henceforth chosen as the controller to be used going forward.

The next step is to calculate the energy-consumption of the system, and examine more energy-efficient methods of control.

Energy Efficiency 5

This project is mainly concerned with the energy consumption of the hydraulic system. The following equations are used to calculate the energy-consumption of the hydraulic system:

$$\mathcal{P}_{hyd} = Q \cdot p = (Q_{p1} \cdot p_1) + (Q_{p2} \cdot p_2) + (Q_{p3} \cdot p_3) \quad (5.1)$$

$$E_{hyd} = \int_0^t \mathcal{P}_{hyd} \quad (5.2)$$

Where Q_{ps1} is the flow from pressure source 1, Q_{ps2} is the flow from pressure source 2, Q_{ps3} is the flow from pressure source 3. It should be noted that the energy is only counted when there is a positive flow into the each chamber of the hydraulic cylinder.

5.1 Trajectory

The energy consumption will be analyzed for a double trapezoidal trajectory, consisting of four ramp inputs, such as one might expect for the movement of an excavator arm while it is moving up and down:

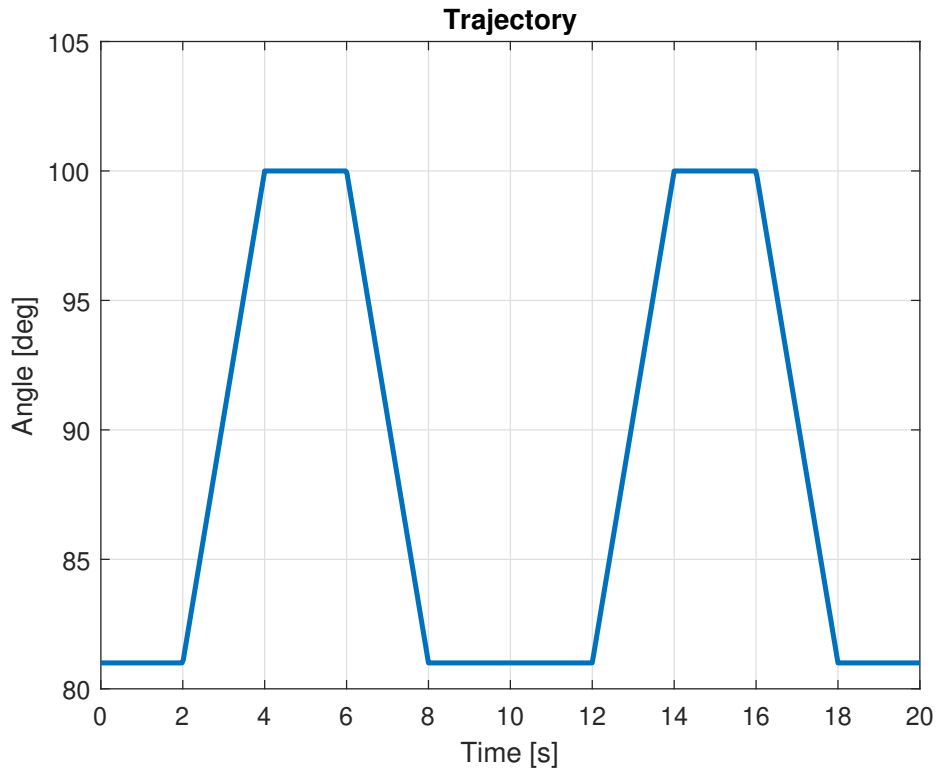


Figure 5.1. Double trapezoidal trajectory for the system

During this trajectory, the RMS error, maximum error, and energy consumption will be monitored, and compared between the energy-saving methods.

The energy saving methods are focused on the force-shifting algorithm, rather than varying the control methods. Two main methods for energy savings are examined:

5.2 FSA Sampling Time Variation Experiment

First, the sampling time for the FSA is examined. The default setting is a sampling time of 1 ms, or 1000 Hz. In this section, various other sampling times are examined, while using the PID controller designed in section 4.3. This will make it so the valves don't change position as often, which could potentially save energy as the system will not change directions as often.

5.2.1 1 ms Sampling Time

First, the standard sampling time of 1 ms is tested.

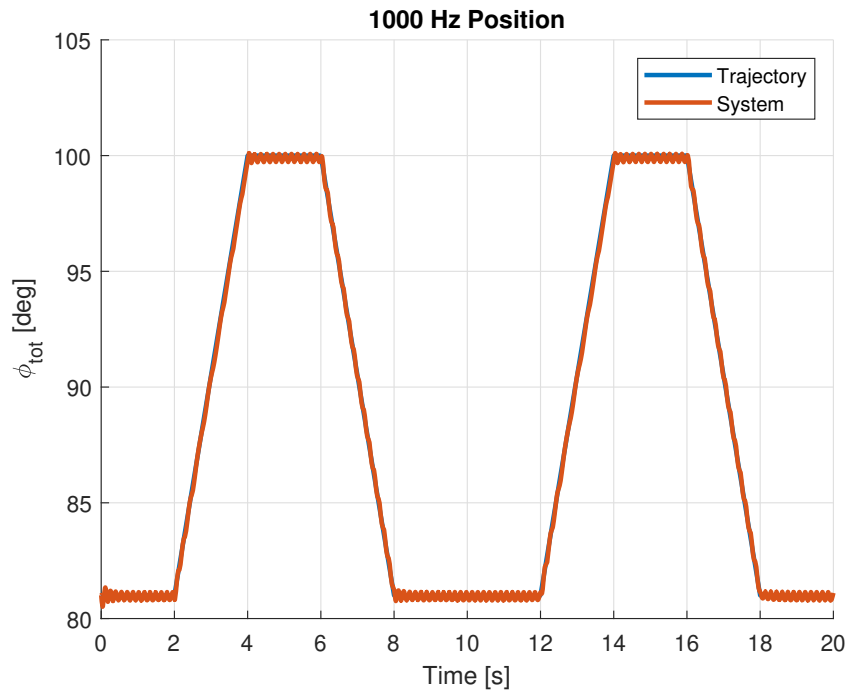


Figure 5.2. Position tracking for a 1 ms sampling time controller.

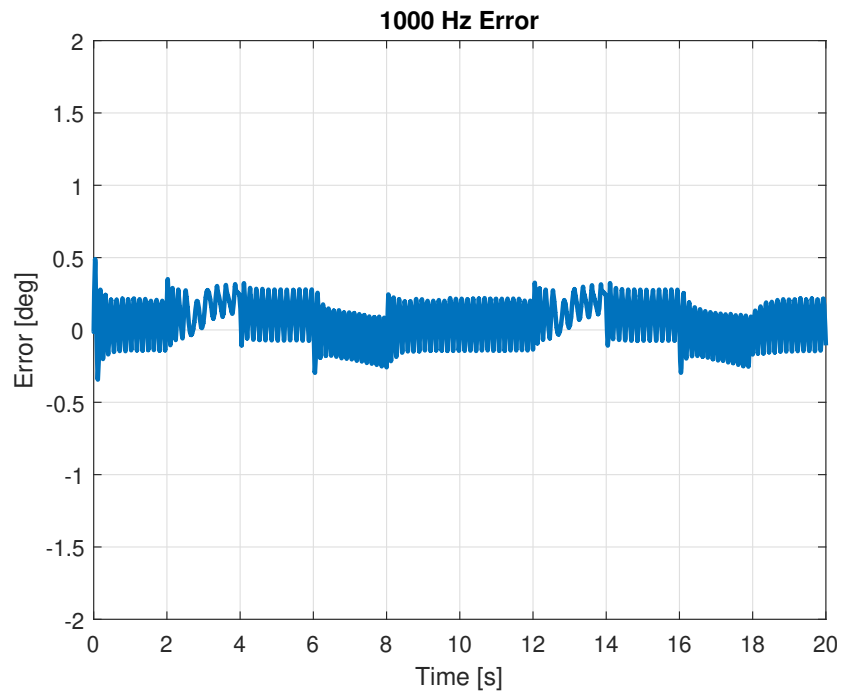


Figure 5.3. Error for a 1 ms sampling time controller.

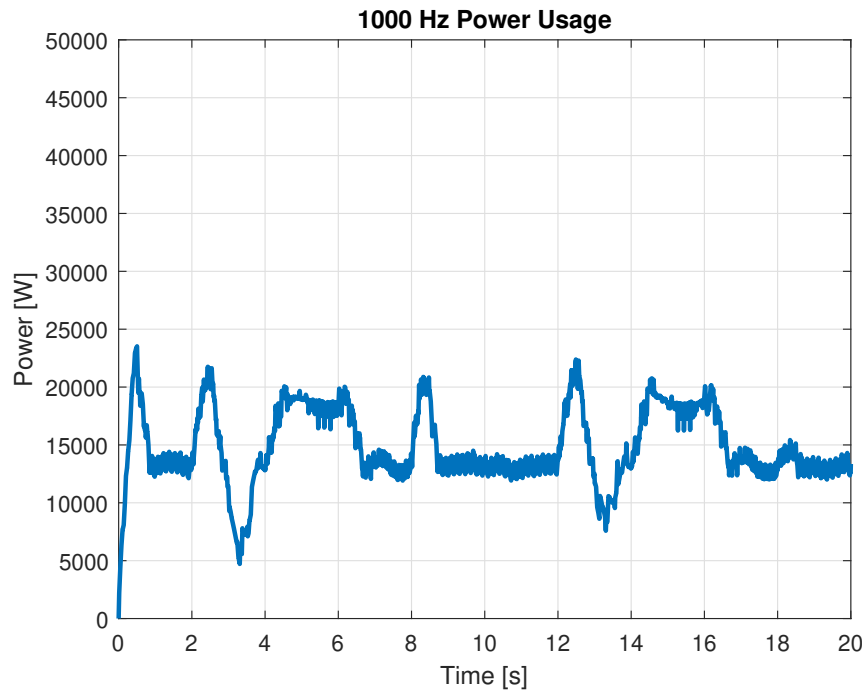


Figure 5.4. Power usage for a 1 ms sampling time controller, with a 500 ms moving average.

As expected, the PID with a 1000 Hz controller is very precise, despite the considerable noise in the system.

5.2.2 10 ms Sampling Time

The sampling time is raised to 10ms:

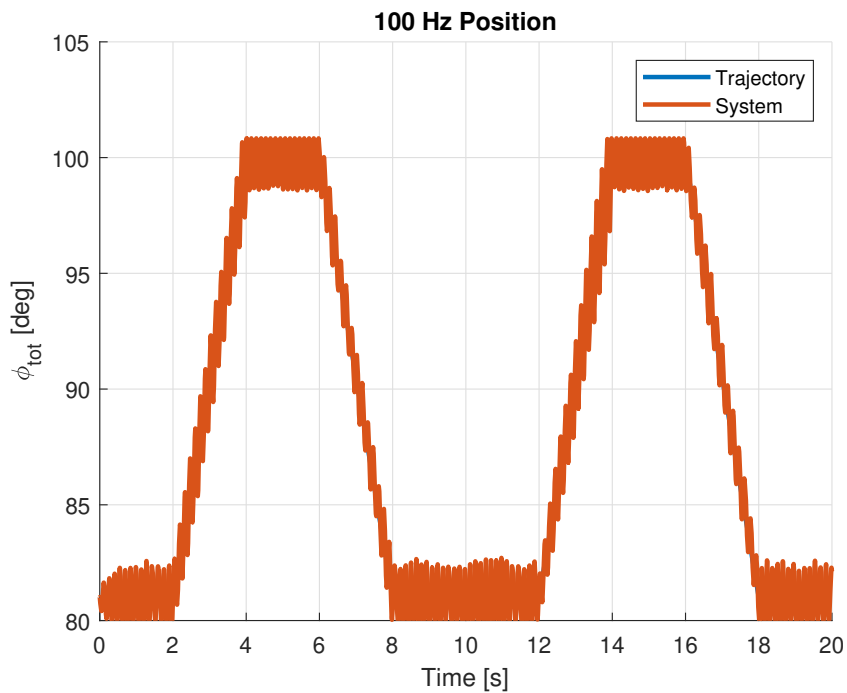


Figure 5.5. Position tracking for a 10 ms sampling time controller.

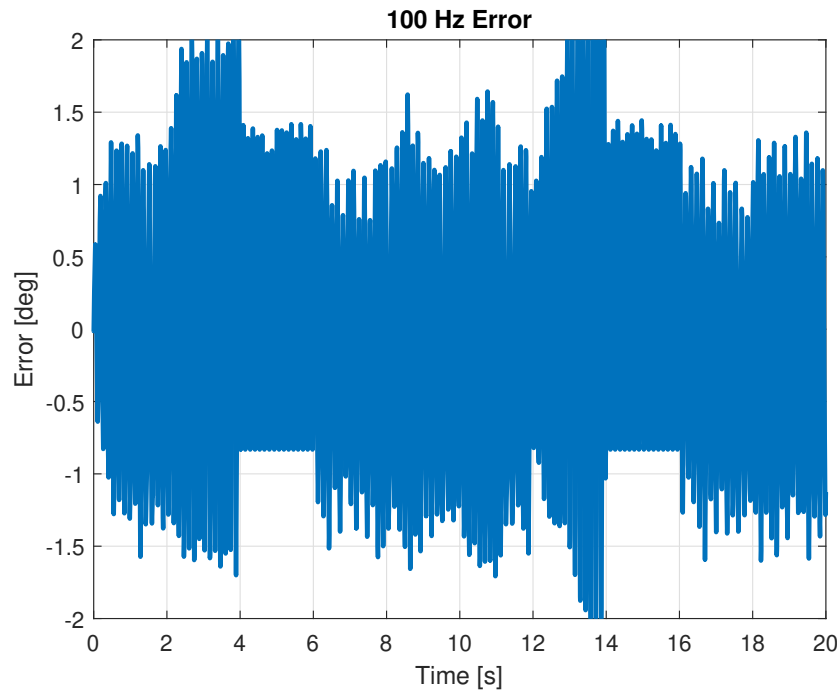


Figure 5.6. Error for a 10 ms sampling time controller.

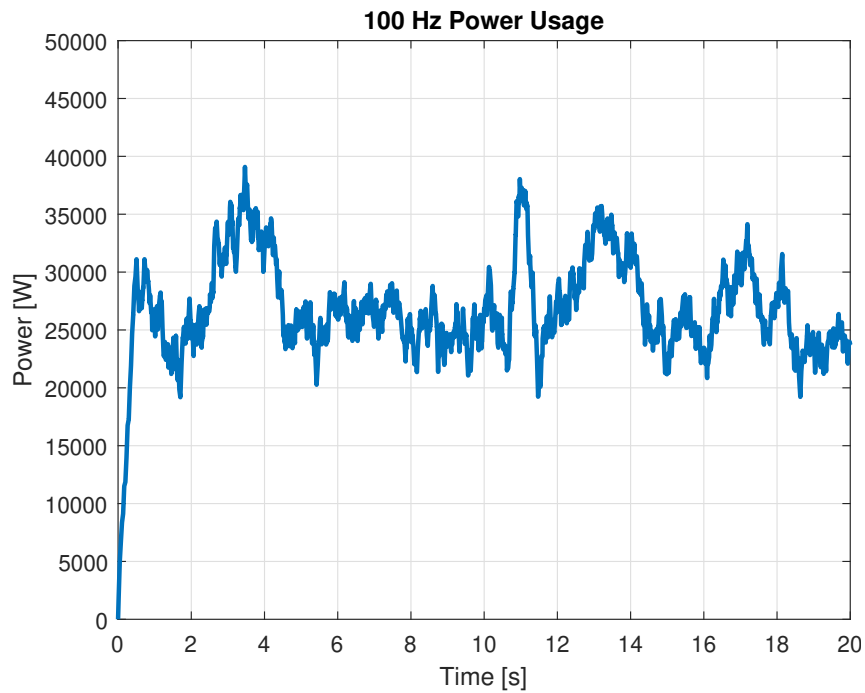


Figure 5.7. Power usage for a 10 ms sampling time controller, with a 500 ms moving average.

On the position graph, the error appears to have increased, but on the error graph it can be seen that the error is within roughly the same boundaries as with the 1 ms sampling time. However, it now has considerably more vibrations.

5.2.3 100 ms Sampling Time

The sampling time is then raised to 100 ms.

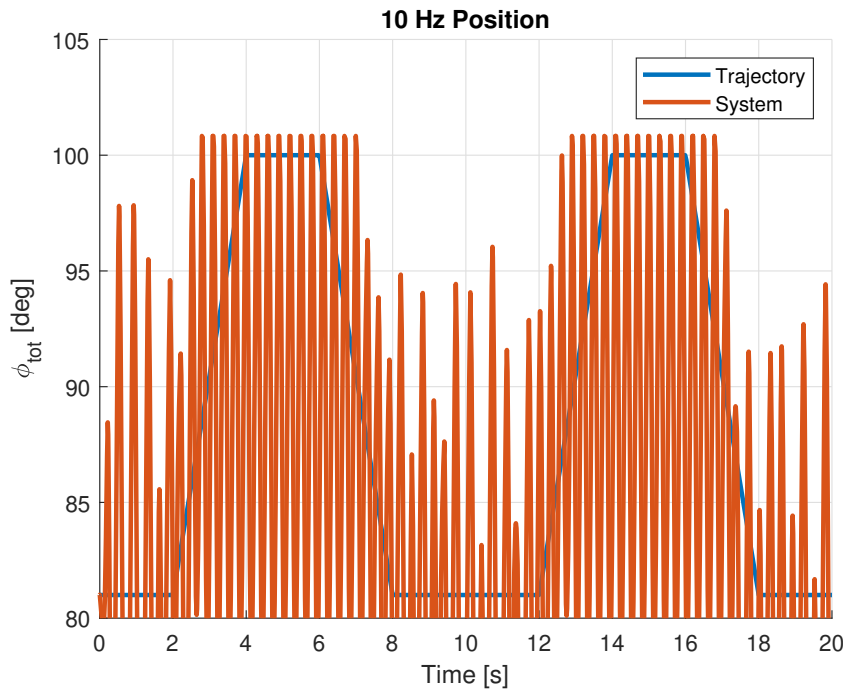


Figure 5.8. Position tracking for a 100 ms sampling time controller.

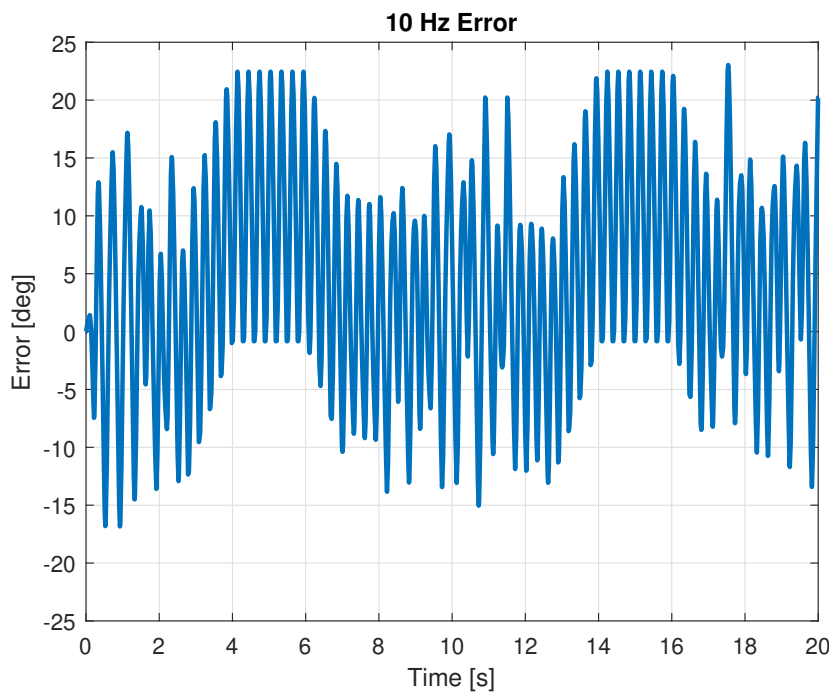


Figure 5.9. Error for a 100 ms sampling time controller.

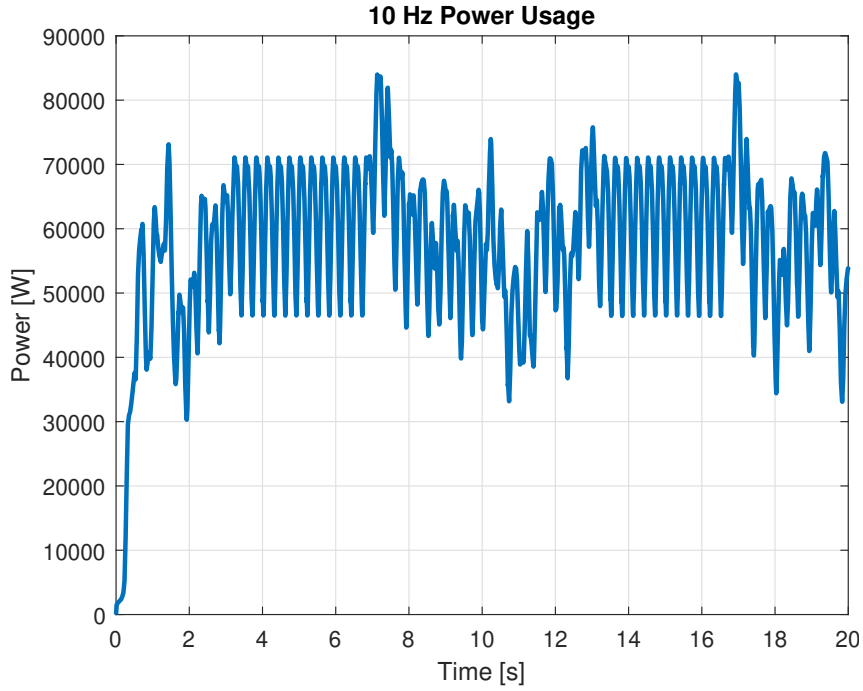


Figure 5.10. Power usage for a 100 ms sampling time controller, with a 500 ms moving average.

These figures show that 10 Hz (or 100 ms sampling) is completely unable to control the system.

A total of 11 different sampling times were tested. Only 3 graphs are shown in this section to avoid cluttering, but the position, error, and power graphs for the other sampling times can be found in Appendix B.

Table 5.2 shows the results with the different sampling times:

Sampling Time	RMS Error [deg]	Max Error [deg]	E_{hyd} [J]
0.1 ms	0.1518	0.4852	285270
0.3 ms	0.1542	0.4862	286486
0.7 ms	0.1578	0.4899	302305
1 ms	0.1572	0.4898	300184
3 ms	0.1515	0.5097	353635
7 ms	0.1721	0.5112	417292
10 ms	0.9441	2.5924	542101
13 ms	1.7569	3.8939	586460
17 ms	2.4477	5.6621	604981
20 ms	3.1968	7.0438	687654
100 ms	9.9462	23.0339	1170376

Table 5.2. Comparison of the accuracy and energy consumption of the different switching times.

Increasing the sampling time does not seem to have an effect on the error, until the sampling time goes above 7 ms, which roughly coincides with the 8 ms switch-time for the valve discussed in section 3.1.2. After 8 ms, the error increases dramatically with each increase

in sample time.

Notably, the faster sampling times seem to use *less* energy than the slower sampling times.

5.3 Locking Mechanism

The second energy-saving method examined in this chapter is a locking mechanism.

As mentioned in section 3.1.1, the system has 28 different configurations for force, and the 10th configuration has all valves closed, but still allows flow between the chambers, or the piston would be unable to move.

This section will investigate a special setting for the 10th configuration, where the channels are closed, to *deliberately* lock the piston in place, when it has reached a desired position. As observed in section 5.2, the position tends to oscillate around the desired position, as the piston is unable to lock itself in place perfectly, due to the system only having discrete forces. This up and down movement wastes energy from the pressure sources.

With this setting, the system will be able to freeze itself, such that no energy is wasted while the arm is at a desired angle.

There are three conditions that must all be satisfied for the locking mechanism to activate:

5.3.1 Error Margin

The first condition is that the arm's angle must be within a certain distance of the reference. The margin is somewhat arbitrary, but must be wide enough that the system can stay within that margin for long enough that the FSA can detect it, depending on what the sampling time of the FSA is set to. A slow sampling may require a wider margin of error. The wider the margin, the easier it is for the system to lock itself.

For this test, the margin is set to 0.1 degrees, i.e. the error must be less than 0.1° for this condition to be satisfied:

$$IF(|\phi_{tot} - \phi_{ref}| < 0.1^\circ) \quad \text{then} \quad Condition_1 = TRUE \quad (5.3)$$

5.3.2 Stationary Reference

The second condition is that the locking mechanism can only activate while the reference position is stationary, or moving very slowly.

If the arm locks itself in place while the reference trajectory is moving (such as during a ramp-input), it could lead to awkward jerky motion. Therefore, the second condition checks the derivative of the reference.

For this test, the reference must move at a rate of less than 1° per second for condition 2 to be satisfied:

$$IF\left(\left|\frac{d}{dt}\phi_{ref}\right| < 1^\circ\right) \text{ then } Condition_2 = TRUE \quad (5.4)$$

5.3.3 Arm Rotational Velocity

The third worry is that, while the arm is in motion, it carries a certain amount of kinetic energy. If the arm is suddenly stopped, that energy is turned into pressure, and subsequently heat. Therefore, the system must ensure that it does not lock the arm while it is moving too fast, or there is a chance it could damage the system.

Pressure Check

Assuming the kinetic energy is turned into pressure at a 1-to-1 ratio, it should follow the equation for potential energy in a pressure chamber:

$$E = P \cdot V \quad (5.5)$$

The volume in this case, is the volume of the innermost chamber of the cylinder, V_1 , plus the dead volume at the end, V_{d1} .

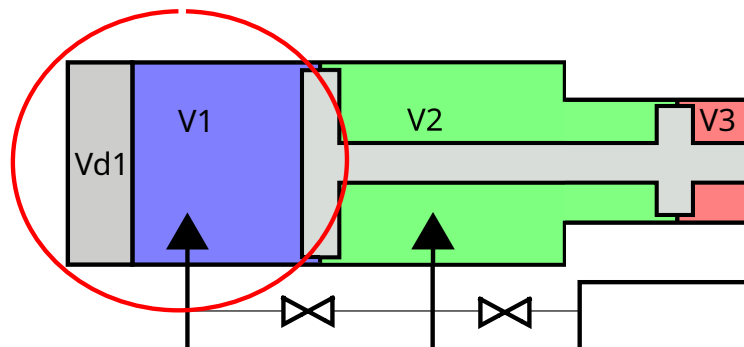


Figure 5.11. The area where the pressure would build from stopping the motion of the arm.

For a conservative estimate, it is assumed that the cylinder is completely retracted, such that the volume is at its smallest point:

$$V_1 = A_1 \cdot x_c \quad (5.6)$$

$$x_c = 0 \rightarrow V_1 = 0 \quad (5.7)$$

Therefore, only the dead volume is accounted for:

$$V = V_{d1} = 0.0017241m^3 \quad (5.8)$$

So each joule of kinetic energy would raise the pressure of the chamber by $1 / 0.0017241 = 580$ Pa.

Therefore, to keep the pressure-increase below 1 bar, the kinetic energy would have to be below $100000 / 580 = 172.4$ J.

$$E_{kin} = \frac{1}{2} J \omega^2 \quad (5.9)$$

$$172.4 = \frac{1}{2} 288.518 \omega^2 \quad (5.10)$$

$$\omega = \sqrt{\frac{172.4 \cdot 2}{288.518}} = 1.0932 \quad (5.11)$$

Therefore, in order for the third condition to be satisfied, the rotational velocity of the arm must be less than 1.0932 rad/s, or 62.64 deg/s:

$$IF(|\frac{d}{dt}\phi_{tot}| < 1.0932 rad/s) \text{ then } Condition_3 = TRUE \quad (5.12)$$

Temperature Check

After the kinetic energy has been turned into pressure, it may afterward turn into thermal energy. Assuming the system is using mineral oil 46 as its hydraulic fluid, it would have a specific heat capacity of $1.67 \frac{kJ}{kg}$ [5], and a density of $879 \frac{kg}{m^3}$ [6]. Therefore, it would take 1468 J to heat the oil by 1°C.

Using a Cat 313 GC Excavator as reference, its hydraulic system has a total hydraulic fluid volume of 85 liters [7]. So it would take $1468 \cdot 85 = 124780$ J to raise the temperature of the hydraulic fluid by 1°C.

Therefore, it is determined that temperature would not be an issue for the locking mechanism.

5.3.4 Test

The locking mechanism is then tested, with the 3 conditions for activation:

- Error less than 0.1 deg
- Ref changing less than 1 deg/s
- Arm moving less than 62.64 deg/s

Along with the sisotool PID, running with a sampling time of 1 ms:

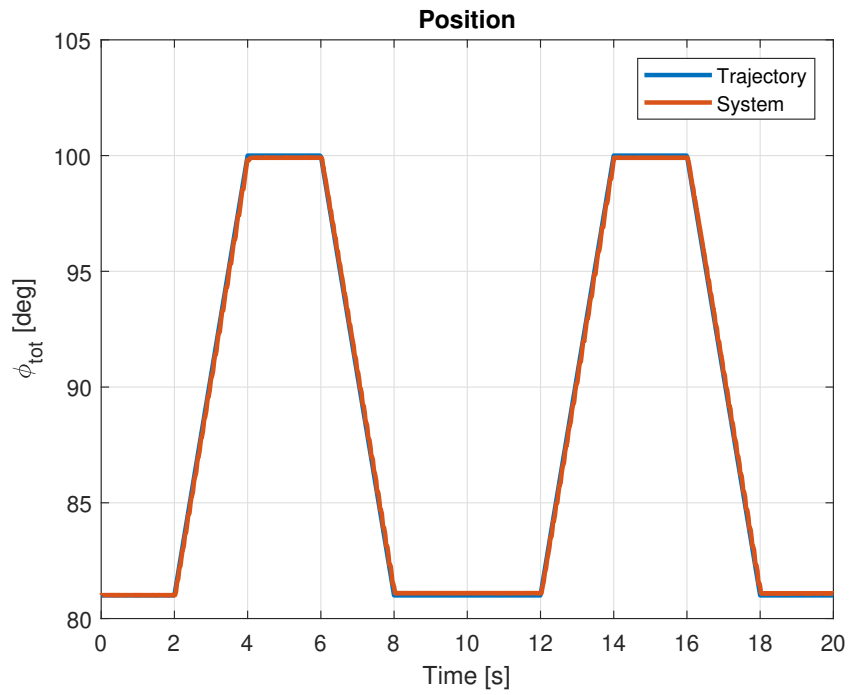


Figure 5.12. Position tracking with the locking mechanism enabled.

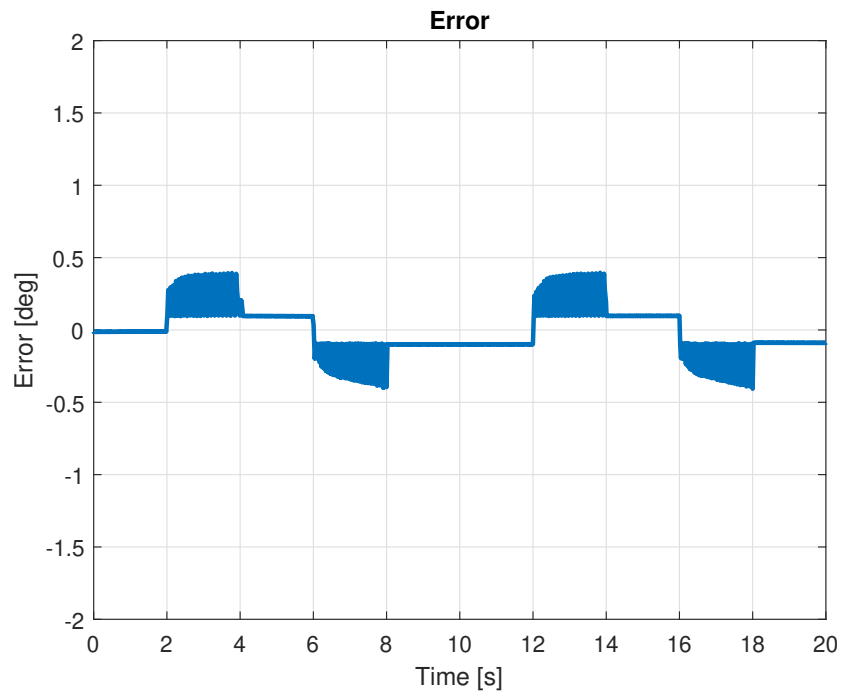


Figure 5.13. Error with the locking mechanism enabled.

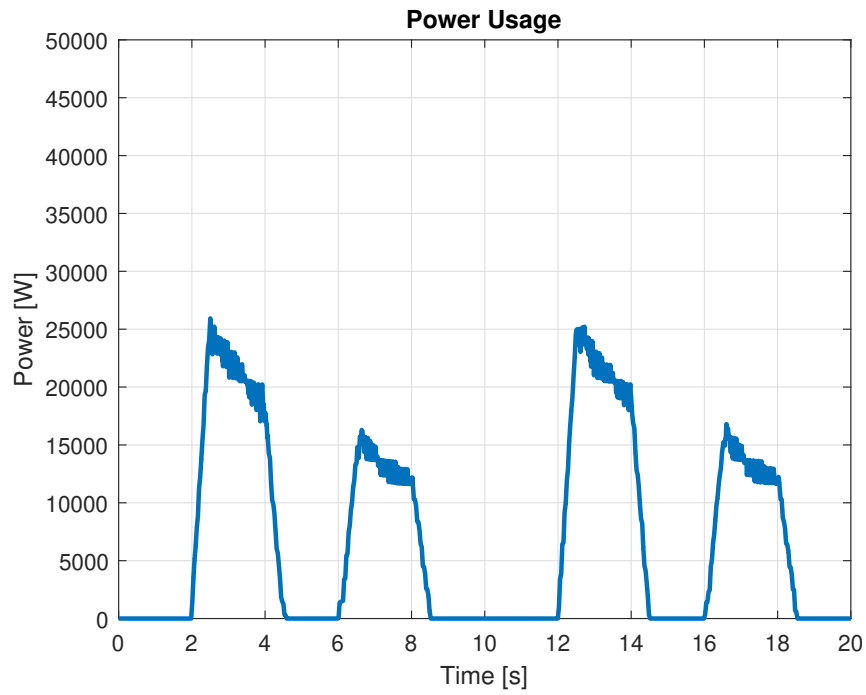


Figure 5.14. Power usage with the locking mechanism enabled, with a 500 ms moving average.

Another experiment is performed, this time with a tighter error margin (0.01 deg instead of 0.1 deg):

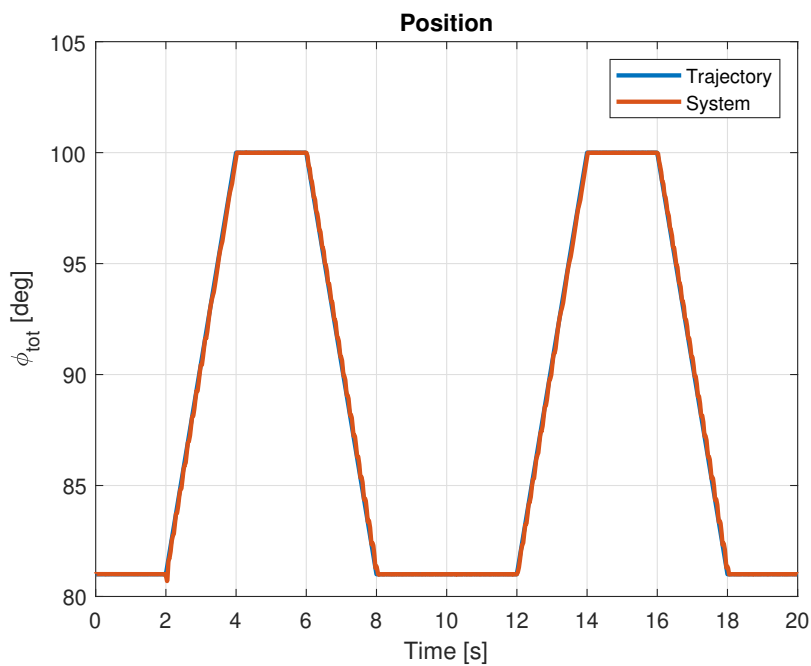


Figure 5.15. Position tracking with a tighter margin of error.

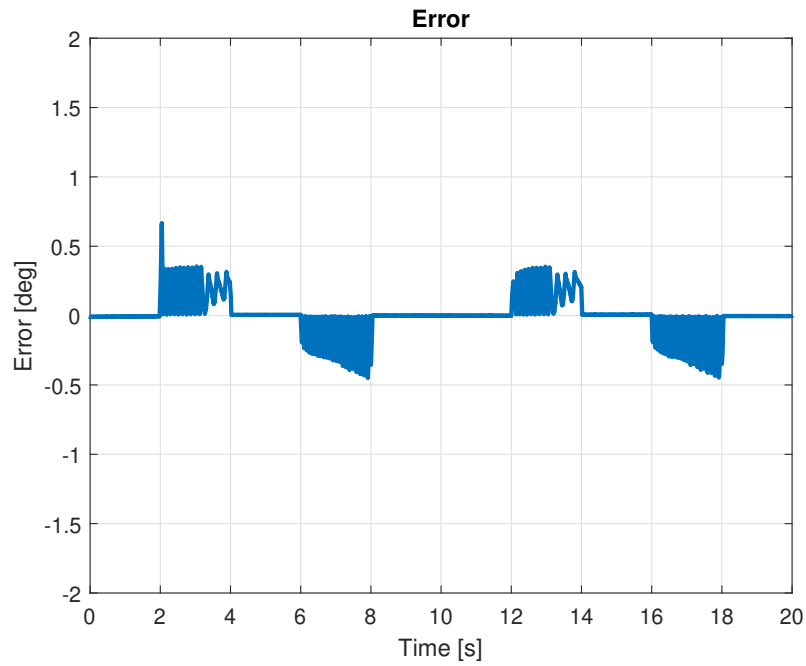


Figure 5.16. Error with a tighter margin of error.

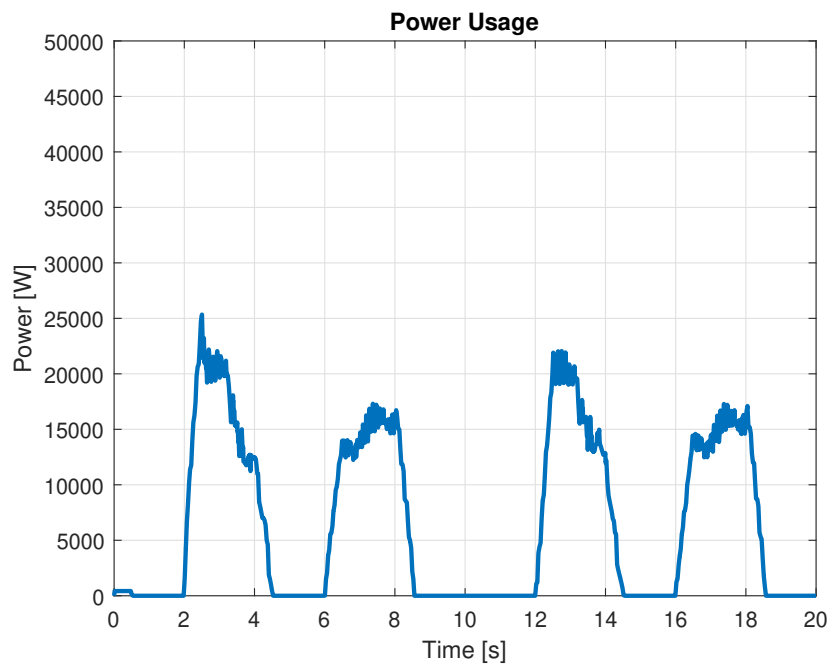


Figure 5.17. Power usage with a tighter margin of error, with a 500 ms moving average.

Lock	RMS Error [deg]	Max Error [deg]	E_{hyd} [J]
OFF	0.1572	0.4898	300184
0.1°	0.1636	0.4064	140236
0.01°	0.0282	0.6650	133933

Table 5.3. Comparison of the accuracy and energy consumption with and without the locking mechanism enabled.

As seen in table 5.3, the basic locking mechanism allows the system to use 53.28% less energy, while getting roughly the same error. Tightening the error margin to 0.01 deg significantly reduces the RMS error, but only has a small effect on the energy usage.

It should be noted that the energy saved via the locking mechanism depends largely on how much time the trajectory spends in a constant position. The 53.28% energy savings from these tests is because the arm spends 12 of the 20 seconds (60%) of the trajectory with a constant reference position.

With a step-input trajectory, the energy savings would be significantly higher. With a sinusoidal trajectory, the energy savings would be significantly lower.

Conclusion 6

The goal of this project was to investigate ways that the energy efficiency of a digital hydraulic multi-chambered cylinder could be improved.

Two main methods of saving energy were tested: Varying sample times, and a locking mechanism.

Sampling Time	RMS Error [deg]	Max Error [deg]	E_{hyd} [J]
1 ms (0.01° Lockon)	0.0282	0.6650	133933
1 ms (0.1° Lockon)	0.1636	0.4064	140236
0.1 ms	0.1518	0.4852	285270
0.3 ms	0.1542	0.4862	286486
0.7 ms	0.1578	0.4899	302305
1 ms	0.1572	0.4898	300184
3 ms	0.1515	0.5097	353635
7 ms	0.1721	0.5112	417292
10 ms	0.9441	2.5924	542101
13 ms	1.7569	3.8939	586460
17 ms	2.4477	5.6621	604981
20 ms	3.1968	7.0438	687654
100 ms	9.9462	23.0339	1170376

Table 6.2. Combination of tables 5.2 and 5.3 from chapter 5, showing the collective results of all the energy consumption tests.

From table 6.2, the following conclusions are made:

- The sampling frequency has little effect on the error, below 7 ms. Which roughly coincides with the 8 ms delay on the valves; Even if the controller is faster, the valves are not fast enough to act on it.
- Having a slow sampling time does not save energy. On the contrary, a slower sampling time will *increase* energy consumption. A faster sampling frequency will generally save more energy than it uses. Therefore, the choice of controller frequency would primarily be a financial decision. However, below 1 ms, the energy savings become small.
- A locking mechanism is an effective way of both reducing error and saving energy, especially for trajectories that involve long periods of holding the same position.

Discussion and Future

Work 7

7.1 Energy Efficiency of PI and PID Controllers

After the energy consumption analysis of the various sampling times, the PI and PID controllers derived via formulae were once again tested to compare their energy efficiencies versus the sisotool PID controller (though using the trapezoidal trajectory rather than a step-input), and the test showed the following results:

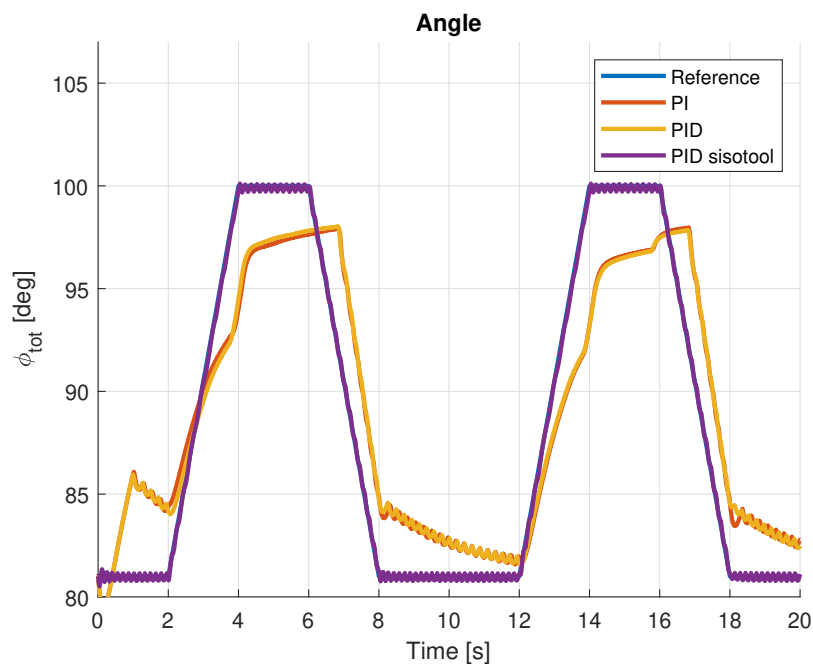


Figure 7.1. Trajectory tracking of the 3 controllers.

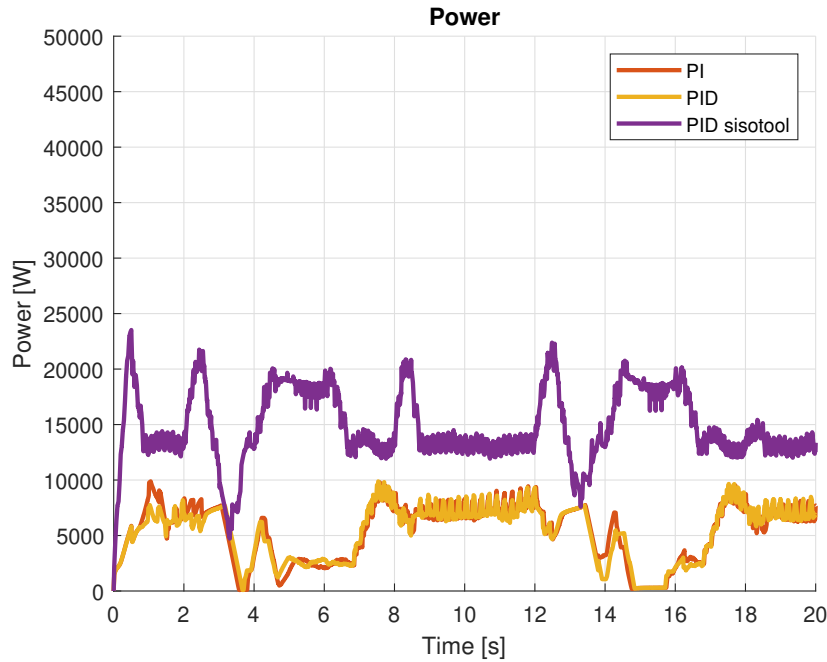


Figure 7.2. Power usage of the 3 controllers.

Controller	RMS Error [deg]	Max Error [deg]	E_{hyd} [J]
PI	3.2908	6.8222	113158
PID	3.2600	6.8120	115140
siso-PID	0.1572	0.4898	300184
1 ms (0.01° Lockon)	0.0282	0.6650	133933
1 ms (0.1° Lockon)	0.1636	0.4064	140236

Table 7.2. Comparison of the accuracy of the controllers.

So, although the formulae-designed controllers were slower and less accurate, they also used less energy, compared to the sisotool PID.

However, with the locking mechanism designed in section 5.3 enabled, the sisotool PID controller only uses 16.3% more energy than the formulae PID.

Due to their slow speed, the formulae PI & PID never manage to reach the reference angle of the trajectory, so they are incompatible with the locking mechanism; It would never activate (for this particular trajectory).

In most cases, a 1892.7% increase in RMS error would not be worth it for a 14.0% decrease in energy consumption.

7.2 Valve Energy Usage

For this project, the energy consumption of the valves themselves was not included in the energy consumption calculations. Assuming that each valve requires 16 W to stay open, even if they were active for the entire 20-second trajectory, it would only be a 320 J energy

consumption per valve, 960 J for 3 valves (since there are never more than 3 valves active at the same time). The lowest recorded energy usage of the system (excluding the formulae PI & PID tested after the fact) was 133933 J. Therefore, the valve energy consumption can be considered insignificant.

Additionally, the energy requirements of the electronics were also not accounted for. According to the user manual of an NI myRIO 1900, it requires up to 14 W of power[8], which would be 280 J for the 20 second trajectory, which would also be insignificant.

7.3 PID Activity During Lock

While the locking mechanism is engaged, the PID controller was still active, which meant that the integral component was still summing up error over time while the arm was frozen. This can lead to large spikes of movement when the locking mechanism is released after a long period of holding the arm in place.

If this project were revisited in the future, the locking mechanism would have to be designed such that the integrator is paused while the lock is active.

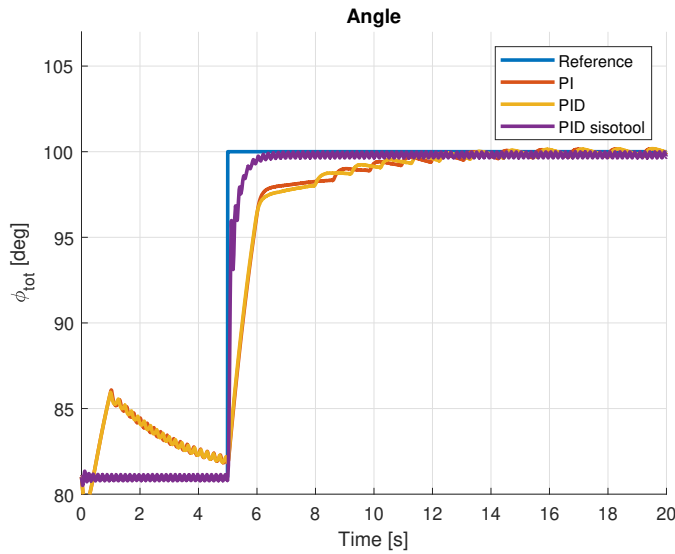
7.4 Alternate Types of Controllers

For this project, only PID-type controllers were investigated. Other SISO controllers such as Lag-Lead-type controllers were not investigated, as it was deemed unlikely that they would improve the energy consumption of the system in any way that the PID-type controllers were not already capable of, since the main energy-drain comes from the movement of the arm, and the flow which drives that movement. SISO controllers focus on moving the system's position to reduce error, regardless of which SISO control method is used.

However, it is possible that MIMO control methods, such as Linear Quadratic Control, or Model Predictive Control, could improve the energy efficiency of the system, as they are able to account for both the accuracy and power usage simultaneously. Therefore, these could be interesting to examine in a future project.

7.5 Improving PID efficiency

As stated in section 7.1, the formulae-designed controllers used less energy than the siso-PID. This is likely because they are less aggressive, which leads to fewer unnecessary oscillations (as can be seen in e.g. the step-response in figure 4.9, where the siso-PID can be seen to move back and forth several times, which wastes unnecessary energy).



The PID controller could be tuned to be more efficient. Partially by tuning it according to its response in the nonlinear model, rather than through the simplified linear model, to get a fast low-oscillation response. It could also be tuned with the locking mechanism in mind, i.e. a fast rise time to get to the reference point, then slowing down so the locking mechanism can take over.

7.6 Water Hammering

Since the hydraulic fluid itself has a mass, it therefore also has a momentum. In hydraulic systems, when a valve is suddenly closed, while hydraulic fluid is flowing through it, it causes the fluid to hammer into the valve, significantly increasing the pressure. This is known as water hammering, or hydraulic shock.

The pressure rise from changing the velocity of a fluid can be calculated with the Joukowski equation:

$$\Delta P = -\rho c \Delta v \quad (7.1)$$

Where ρ is the density of the fluid, c is the speed of sound in the fluid, and Δv is the change in velocity of the fluid. In the case of a valve being shut, the velocity would go down to zero. In some cases, it can even rupture holes in a pipe system[9].

This can be avoided by designing the hydraulic trajectories to be smooth (e.g. by using a quintic polynomial matrix, to get a finite acceleration derivative).

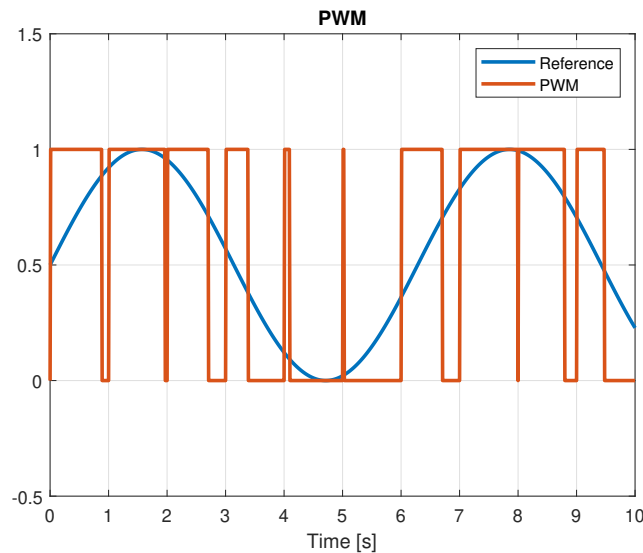
However by nature of being a digital hydraulic system, transitions are *always* sudden for this type of system, regardless of how slight the adjustments are, since every change in configuration means fully opening and fully closing a set of valves.

This can be alleviated via safety valves, to redirect flow back into the tank, and prevent the pressure from climbing to dangerous levels. However, the presence of the water hammering effect means that every switch in configurations means a small amount of fluid is redirected through the safety valves, which wastes a small amount of energy for each switch (Since $\mathcal{P} = Q \cdot P_s$).

Therefore, it could be interesting to include this effect in the energy consumption of the system, as it would disincentivize frequent switching between configurations.

7.7 Pulse Width Modulation

PWM was not investigated in this project. A major limitation of a discrete-input system such as this is that it becomes hard to control when the system requires an input that is between two of the discrete values. Therefore, PWM could be used to give the system an approximation of these inbetween values, thereby potentially reducing error.



However, this method of control would also involve frequent switching between configurations (depending on the frequency of the PWM's duty-cycle), which may use a lot extra energy. Therefore, it could be interesting to investigate the energy savings while the system is using PWM.

7.8 Granularity

Another way of making the system both more precise and more energy efficient is to make the discrete input-values more granular, i.e. giving the system more precise values to choose between.

For a discrete hydraulic system such as this, it can be done by increasing the number of on/off valves, e.g. a 4x4 system of valves rather than 3x3, thereby having 257 different

configurations to choose between, rather than 28.

It can also be done by lowering the supply pressures, so the force-configurations are moved closer together, so there is a smaller gap between each configuration. Especially considering that, as can be seen on figure 4.10, the force-requirement stays between 28651 N and 15355 N for 97.86% of the trajectory (the majority of this force is just to counteract the gravity), so the force range of -48400 to +67600 N may be excessive.

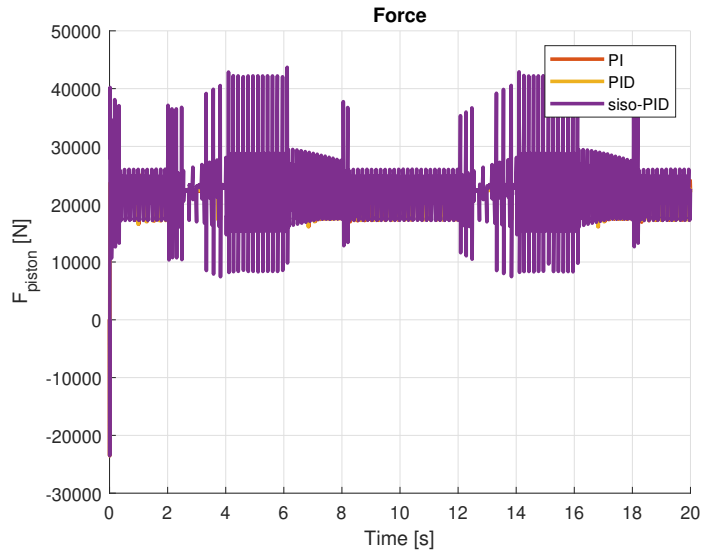


Figure 7.3. Force from the cylinder, when using the 3 different controllers for the trapezoidal trajectory.

Bibliography

- [1] Cat. https://www.cat.com/en_GB.html.
- [2] Matti Linjama. Digital Fluid Power – State Of The Art. 2011.
- [3] National Library of Medicine: The Audible Spectrum.
<https://www.ncbi.nlm.nih.gov/books/NBK10924/>.
- [4] Charles Phillips and John Parr. *Feedback Control Systems, 5th ed.* 2010.
- [5] Engineering Toolbox.
https://www.engineeringtoolbox.com/specific-heat-fluids-d_151.html.
- [6] Anders Hedegaard Hansen. *Fluid Power Systems v0.4.* 2019.
- [7] Caterpillar Inc: Cat 313 GC Excavator Data Sheet.
<https://s7d2.scene7.com/is/content/Caterpillar/CM20200508-0f77e-21265>.
- [8] NI myRIO-1900 User Guide and Specifications.
<https://www.ni.com/docs/en-US/bundle/myrio-1900-getting-started>.
- [9] Hydrodynamic Design, Part 11: The Water Hammer. <https://wcponline.com/2013/12/06/hydrodynamic-design-part-11-water-hammer/>.

Appendix

App: Linearisation Points A

Three linearisation points were investigated for the linear model in section 4.1:

- $x_c = 0.25 \cdot L$
- $x_c = 0.50 \cdot L$
- $x_c = 0.75 \cdot L$

These gave the following transfer functions:

$$x_c = 0.25 \cdot L \quad \rightarrow \quad \frac{\Phi(s)}{F(s)} = \frac{0.001911}{s^2 + 7.8262 \cdot s + 3.4271} \quad (\text{A.1})$$

$$x_c = 0.50 \cdot L \quad \rightarrow \quad \frac{\Phi(s)}{F(s)} = \frac{0.001958}{s^2 + 7.8262 \cdot s + 5.1726} \quad (\text{A.2})$$

$$x_c = 0.75 \cdot L \quad \rightarrow \quad \frac{\Phi(s)}{F(s)} = \frac{0.001942}{s^2 + 7.8262 \cdot s + 4.6559} \quad (\text{A.3})$$

These gave the following step-responses in comparison to the nonlinear model:

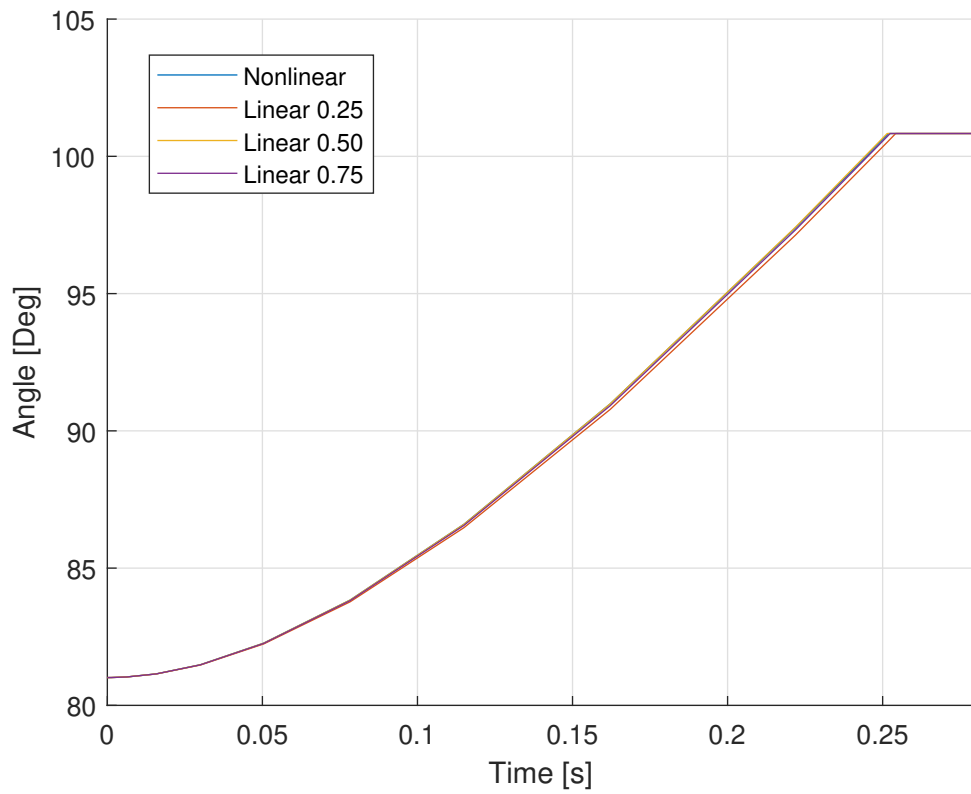


Figure A.1. Comparison of the step-response of the 3 linearisation points.

They all have very similar responses. But overall, the linearisation point of $x_c = 0.5 \cdot L$ was determined to be the most accurate representation of the nonlinear system.

App: Sampling Times B

In order to reduce clutter, only 3 sampling times were highlighted in section 5.2. The graphs for the other 8 sampling times are displayed below:

0.1 ms

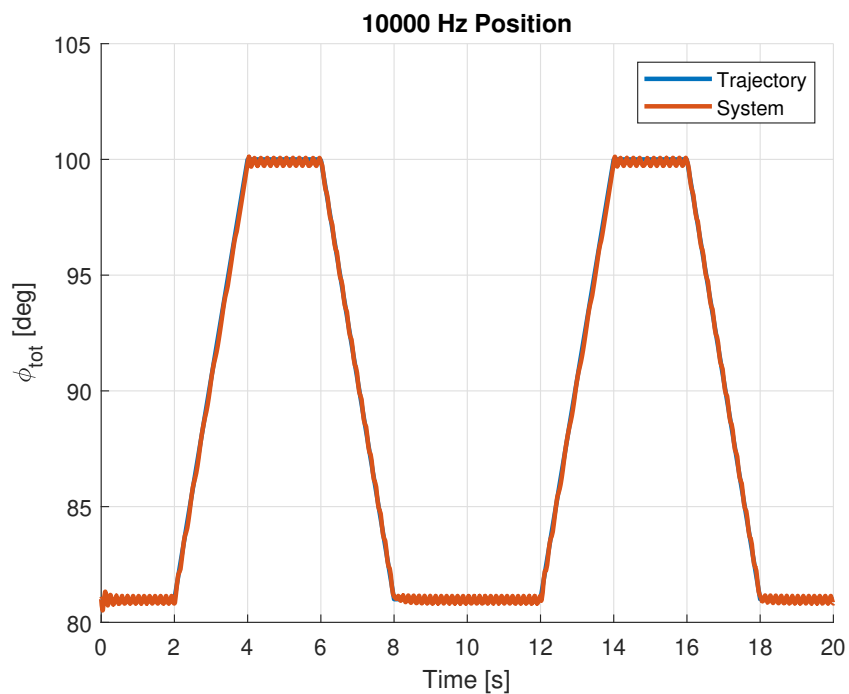


Figure B.1. Position tracking for a 0.1 ms sampling time controller.

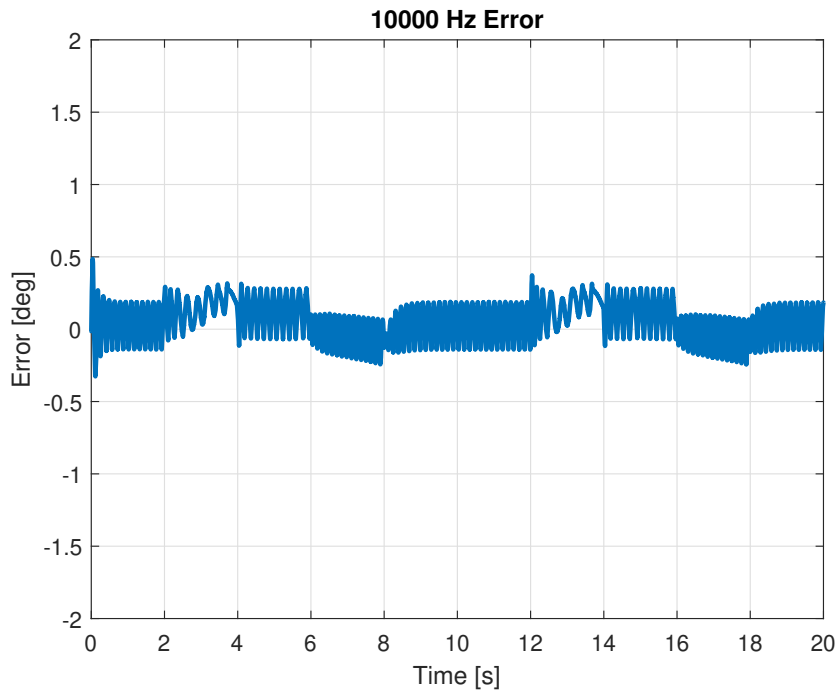


Figure B.2. Error for a 0.1 ms sampling time controller.

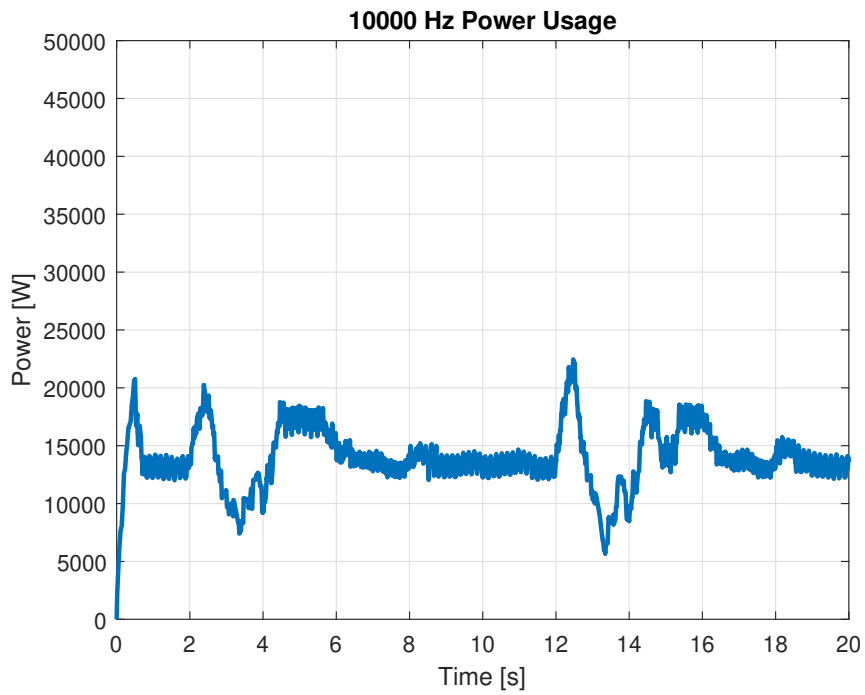


Figure B.3. Power usage for a 0.1 ms sampling time controller, with a 500 ms moving average.

0.3 ms

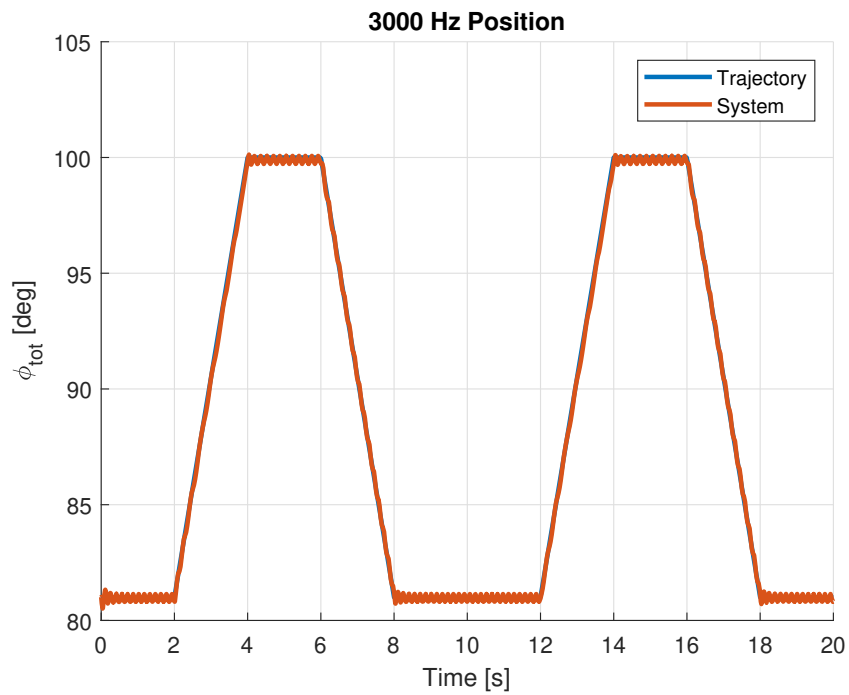


Figure B.4. Position tracking for a 0.3 ms sampling time controller.

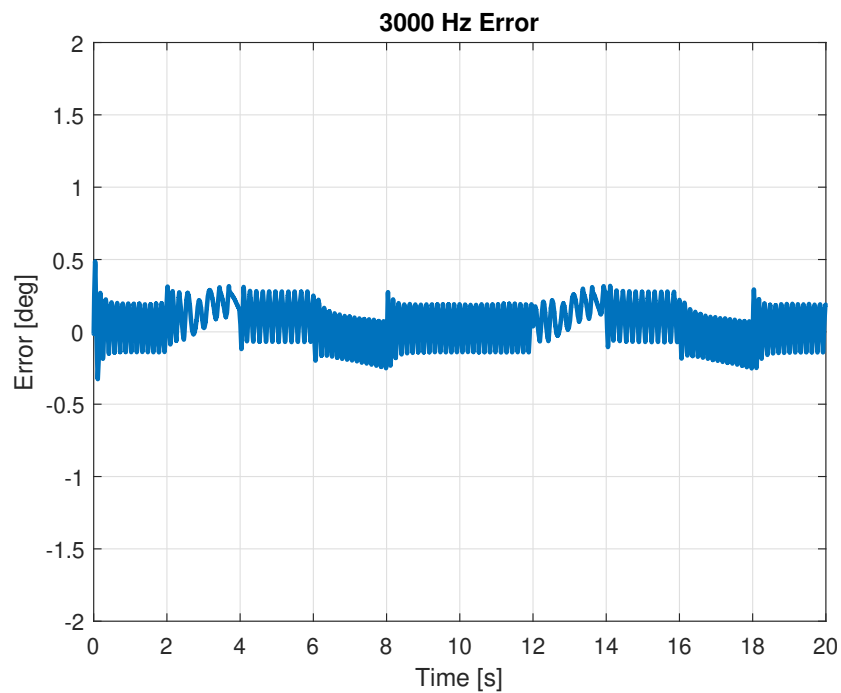


Figure B.5. Error for a 0.3 ms sampling time controller.

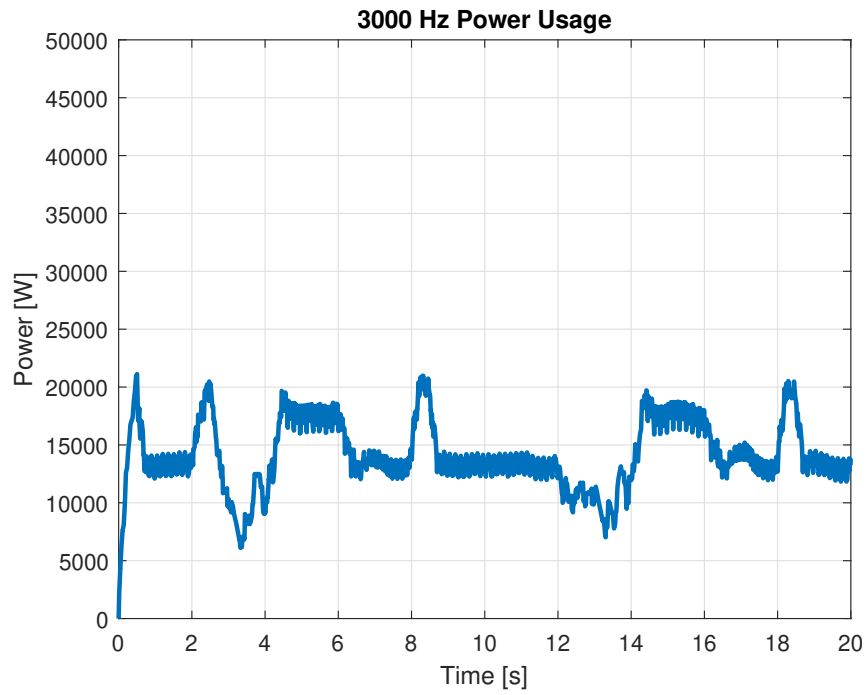


Figure B.6. Power usage for a 0.3 ms sampling time controller, with a 500 ms moving average.

0.7 ms

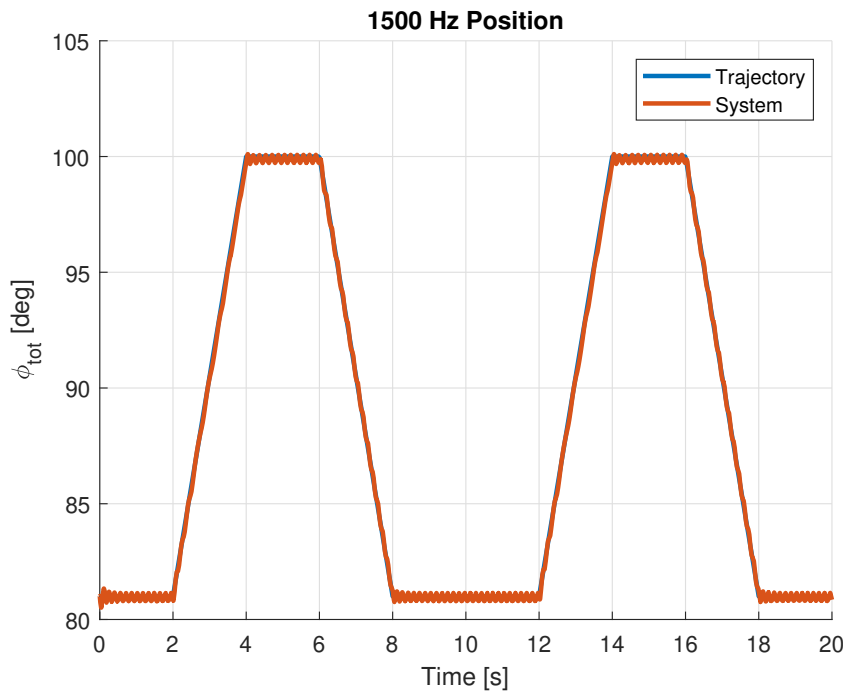


Figure B.7. Position tracking for a 0.7 ms sampling time controller.

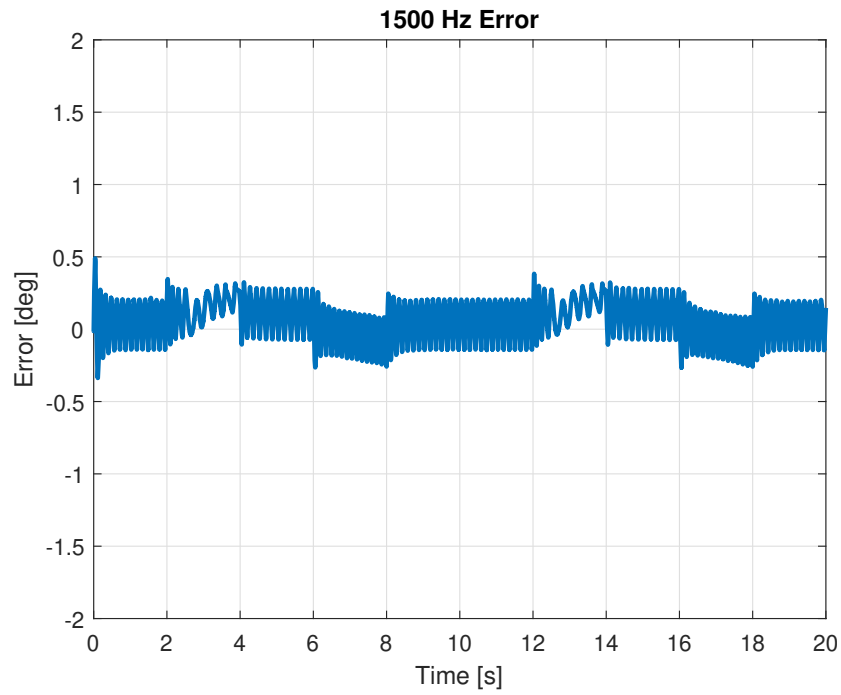


Figure B.8. Error for a 0.7 ms sampling time controller.

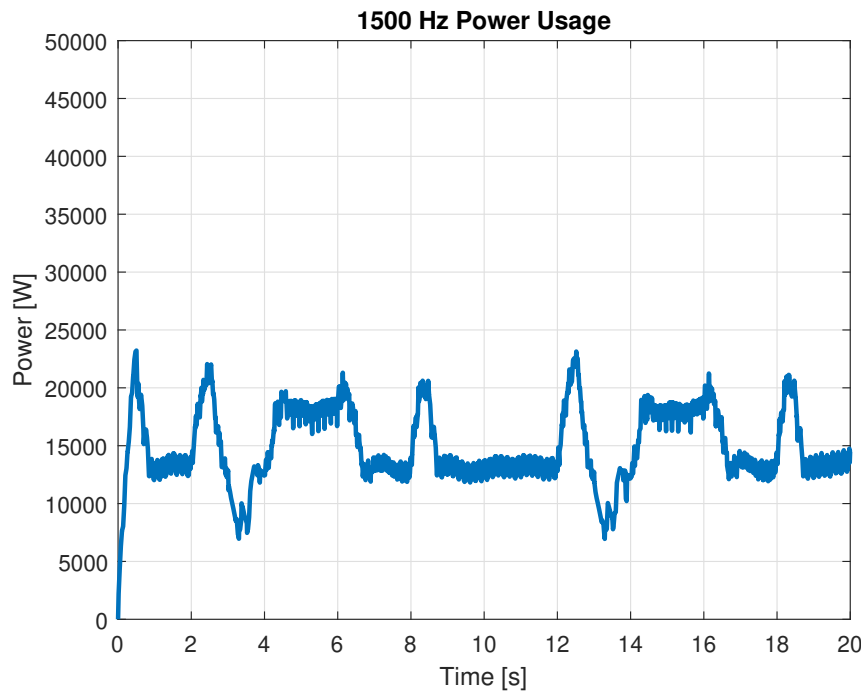


Figure B.9. Power usage for a 0.7 ms sampling time controller, with a 500 ms moving average.

1 ms

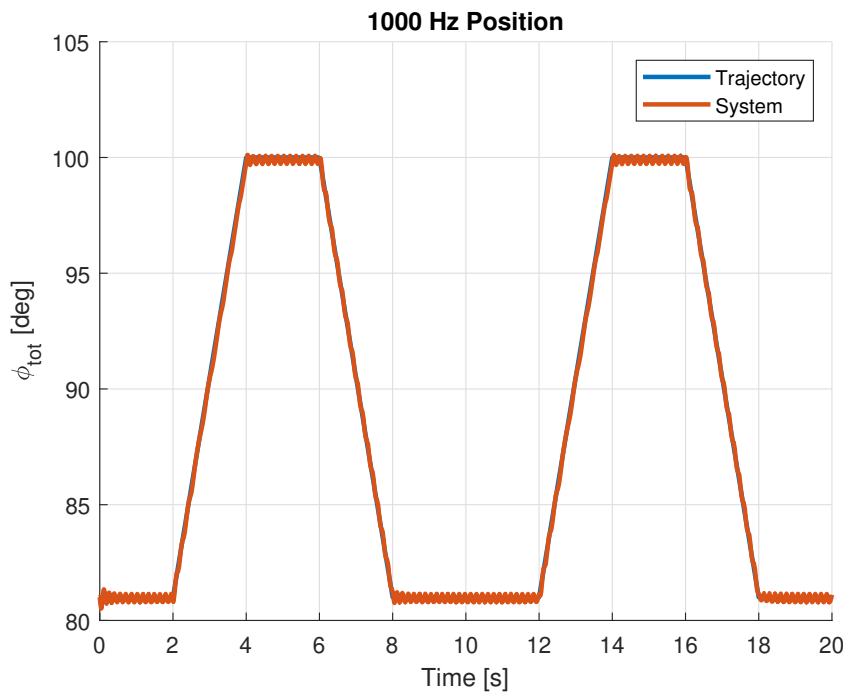


Figure B.10. Position tracking for a 1 ms sampling time controller.

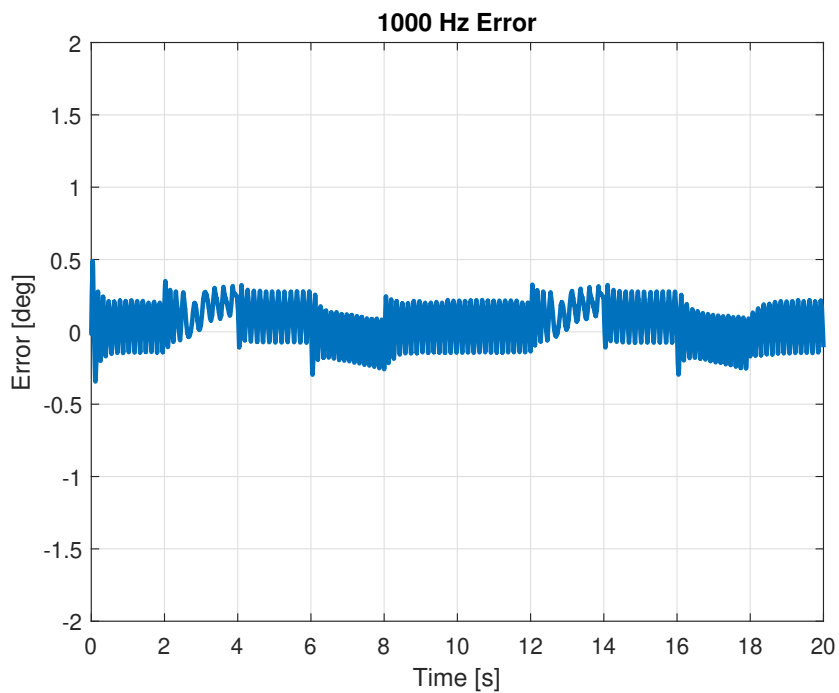


Figure B.11. Error for a 1 ms sampling time controller.

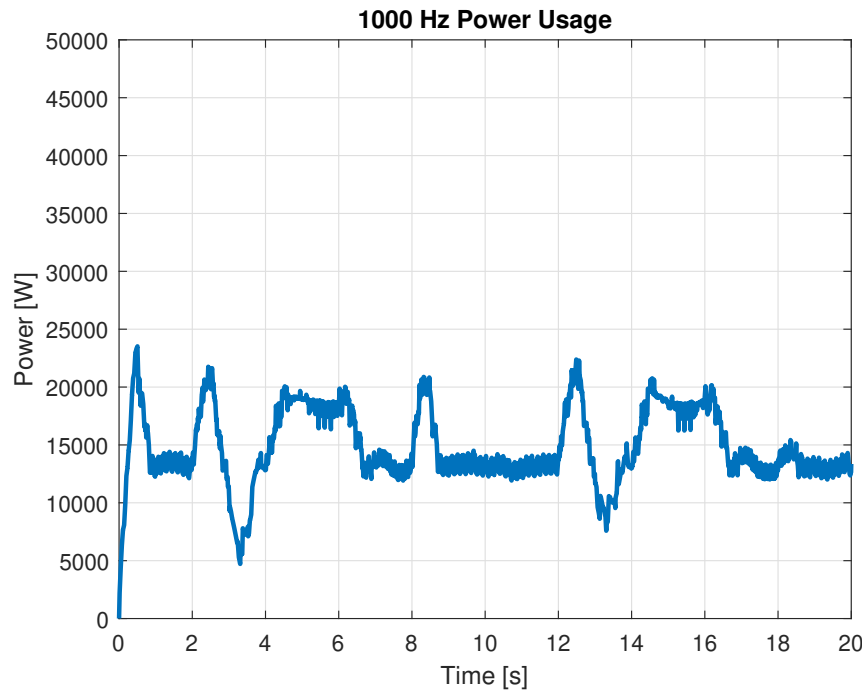


Figure B.12. Power usage for a 1 ms sampling time controller, with a 500 ms moving average.

3 ms

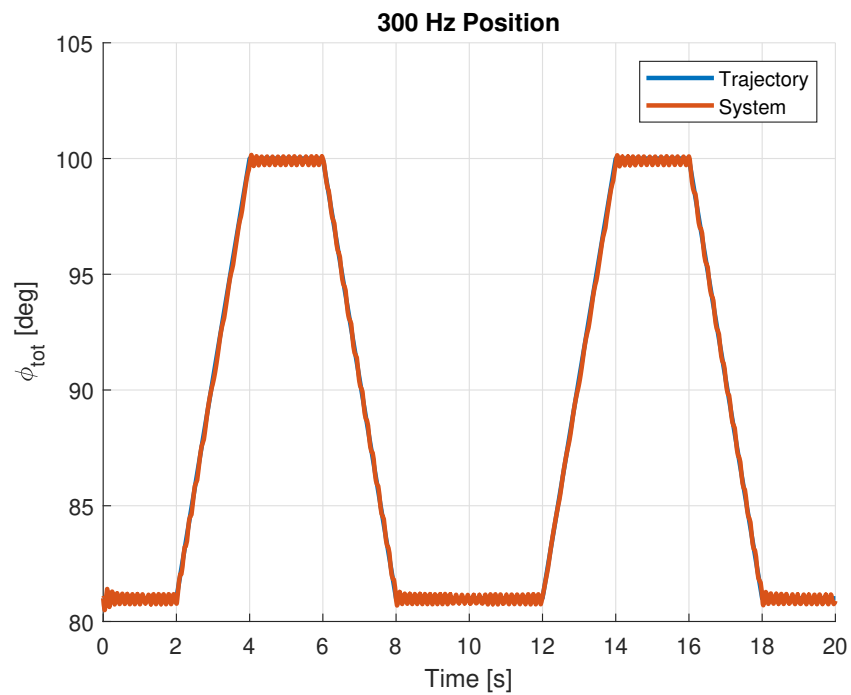


Figure B.13. Position tracking for a 3 ms sampling time controller.

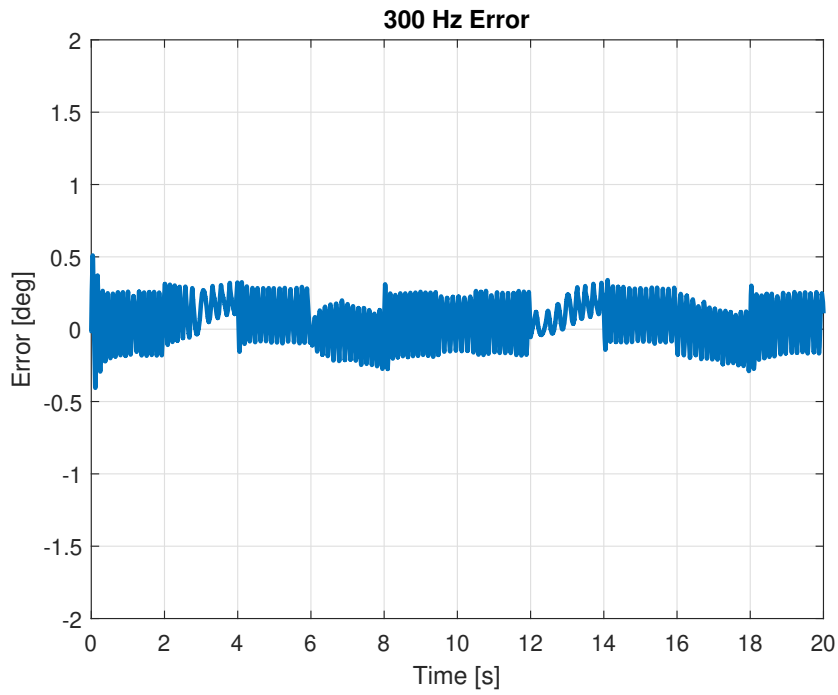


Figure B.14. Error for a 3 ms sampling time controller.

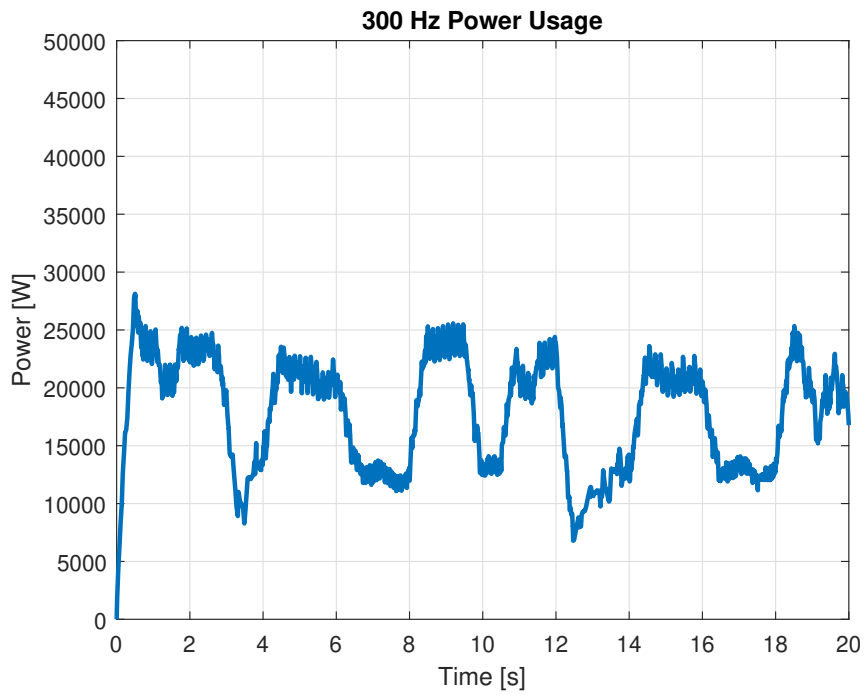


Figure B.15. Power usage for a 3 ms sampling time controller, with a 500 ms moving average.

7 ms

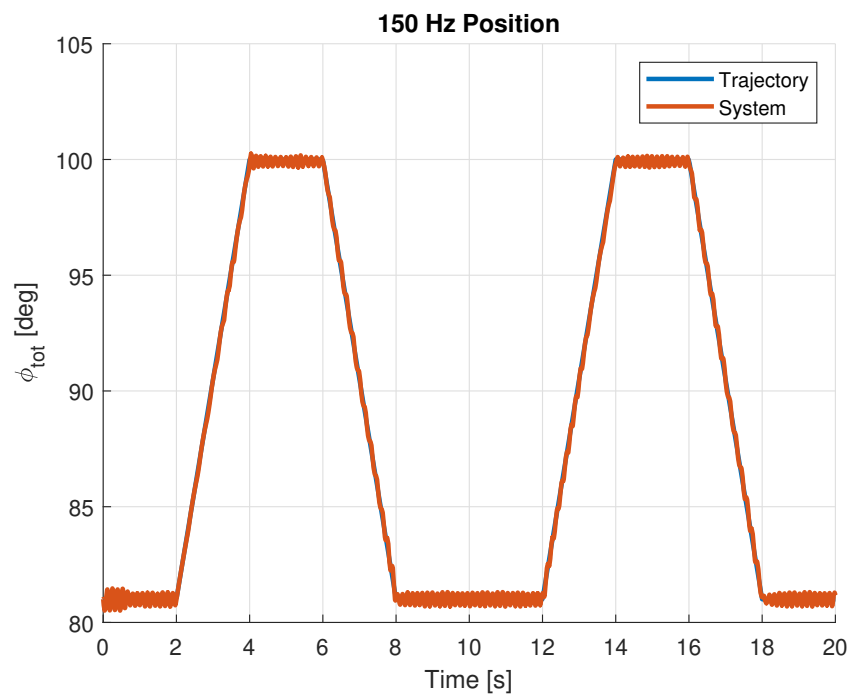


Figure B.16. Position tracking for a 7 ms sampling time controller.

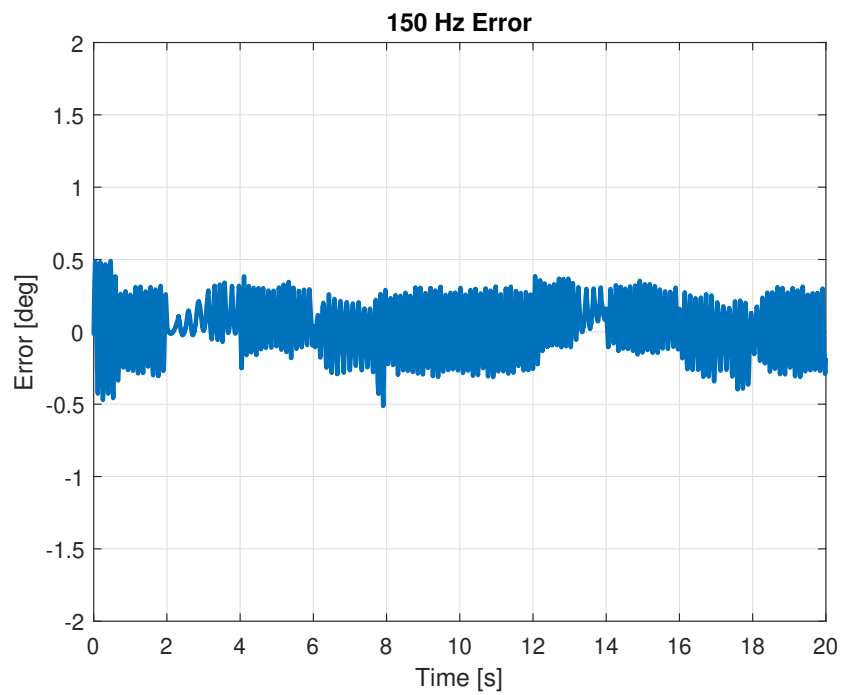


Figure B.17. Error for a 7 ms sampling time controller.

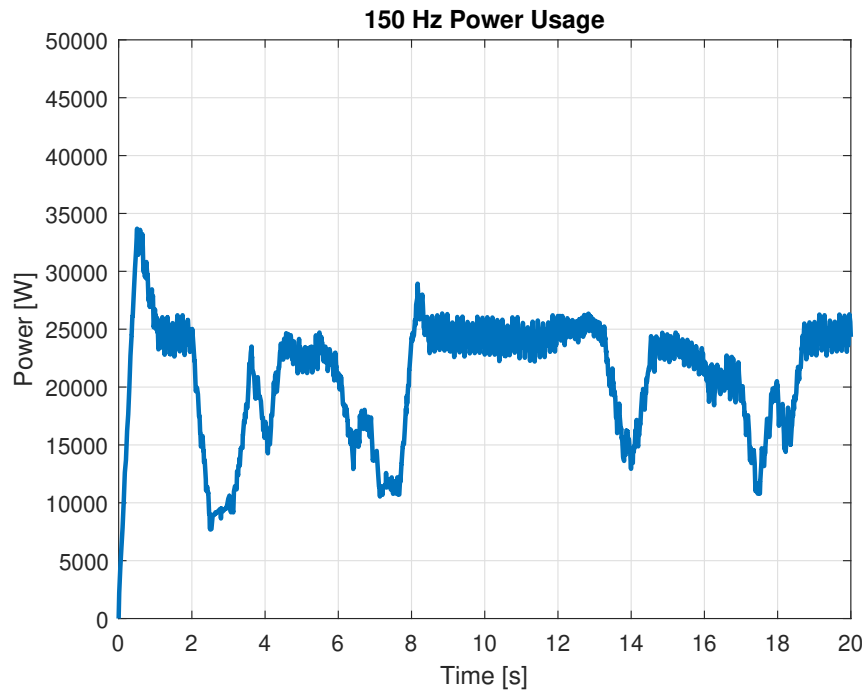


Figure B.18. Power usage for a 7 ms sampling time controller, with a 500 ms moving average.

10 ms

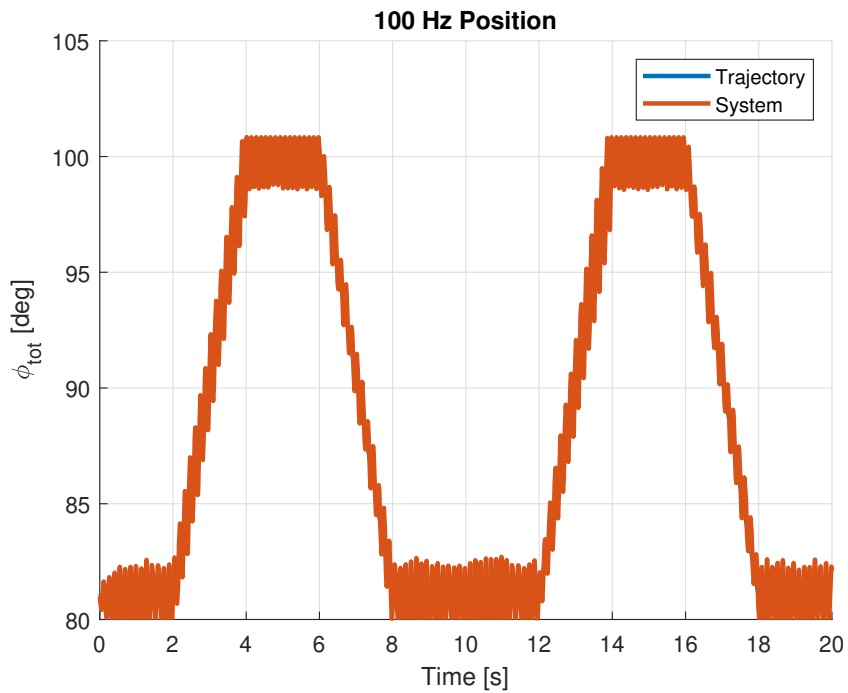


Figure B.19. Position tracking for a 10 ms sampling time controller.

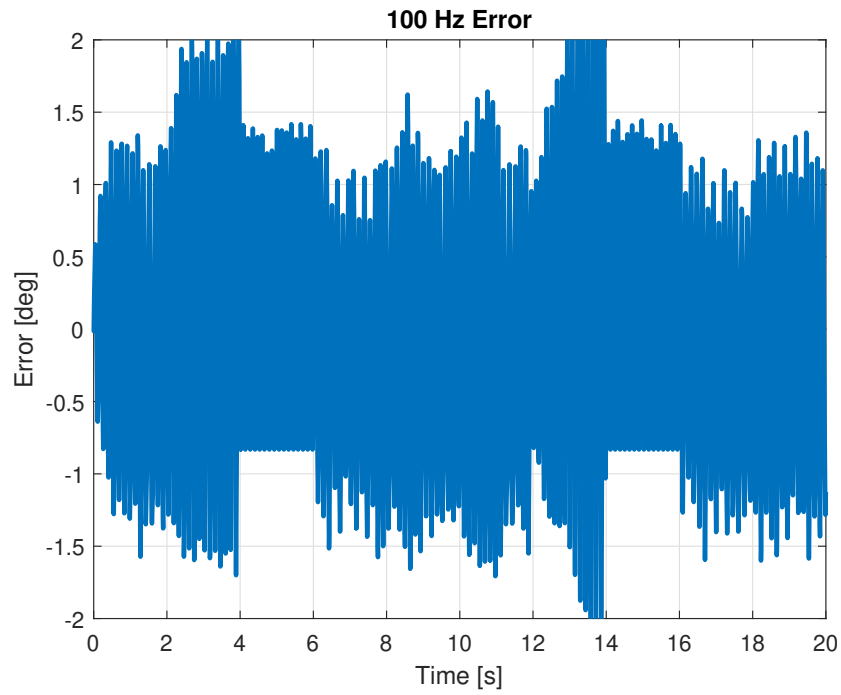


Figure B.20. Error for a 10 ms sampling time controller.

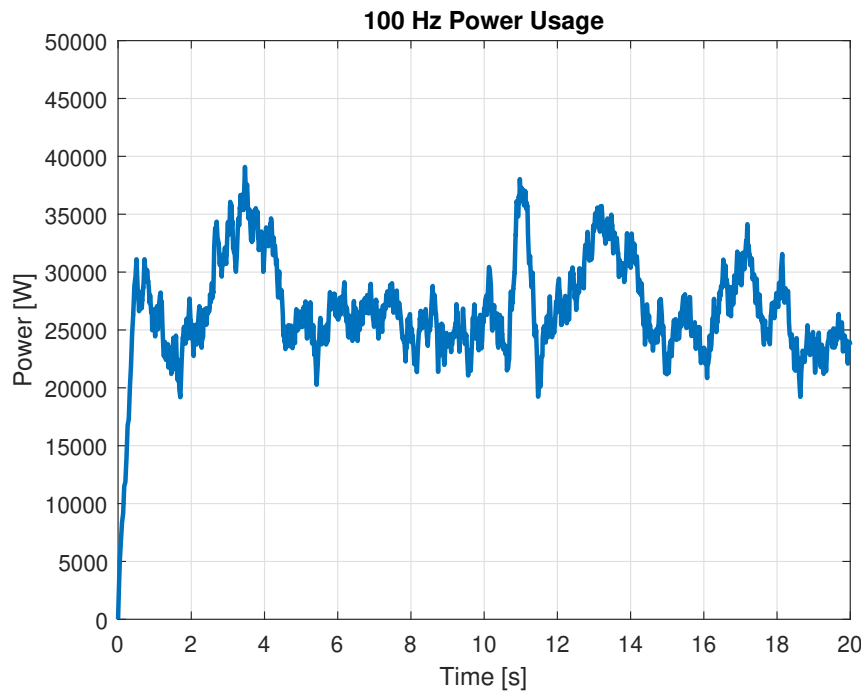


Figure B.21. Power usage for a 10 ms sampling time controller, with a 500 ms moving average.

13 ms

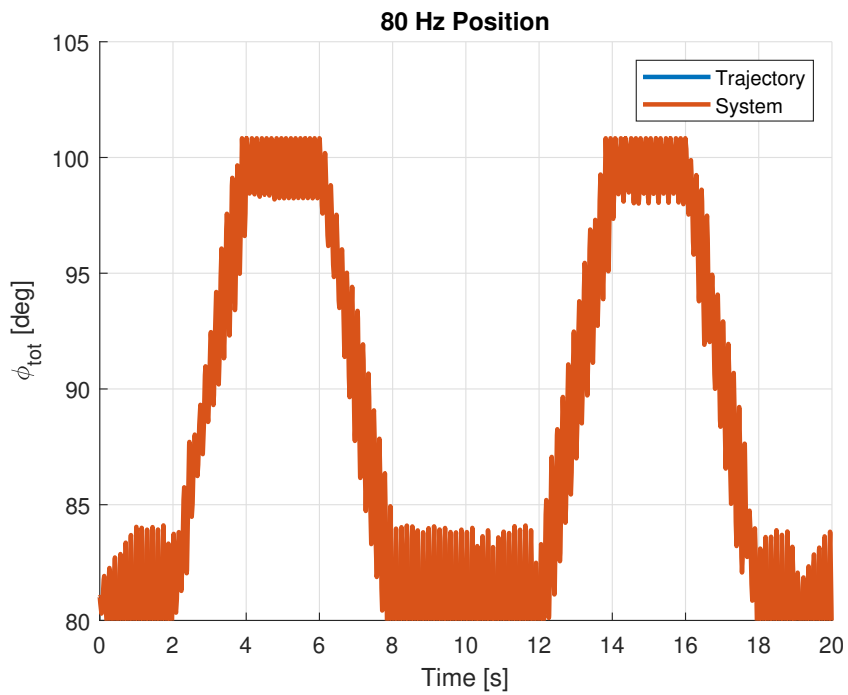


Figure B.22. Position tracking for a 13 ms sampling time controller.

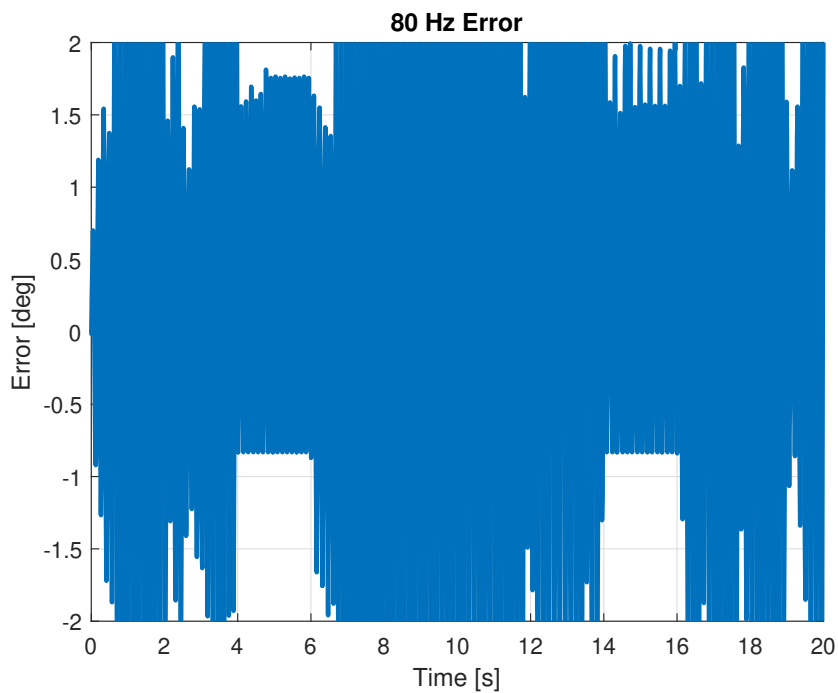


Figure B.23. Error for a 13 ms sampling time controller.

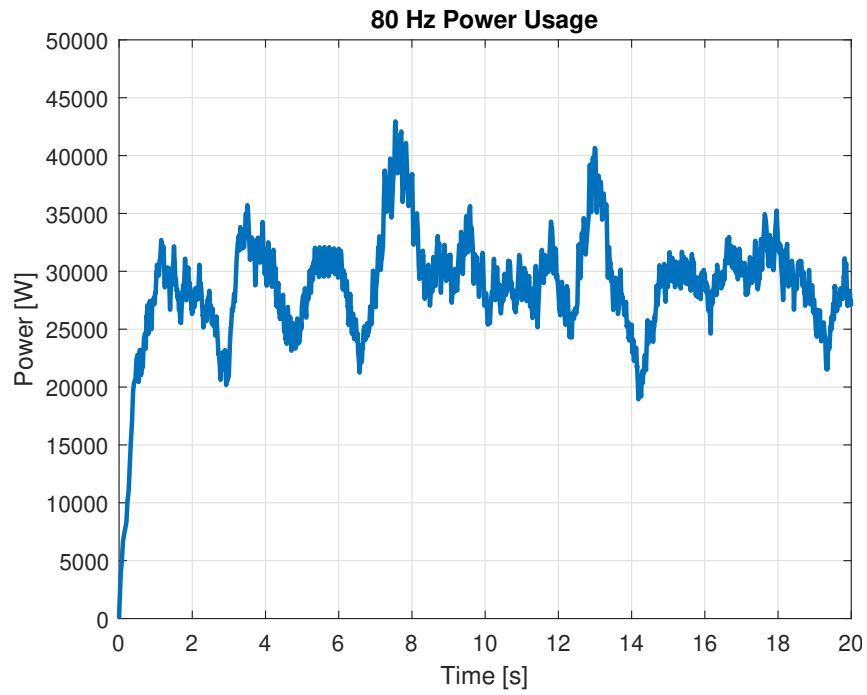


Figure B.24. Power usage for a 13 ms sampling time controller, with a 500 ms moving average.

17 ms

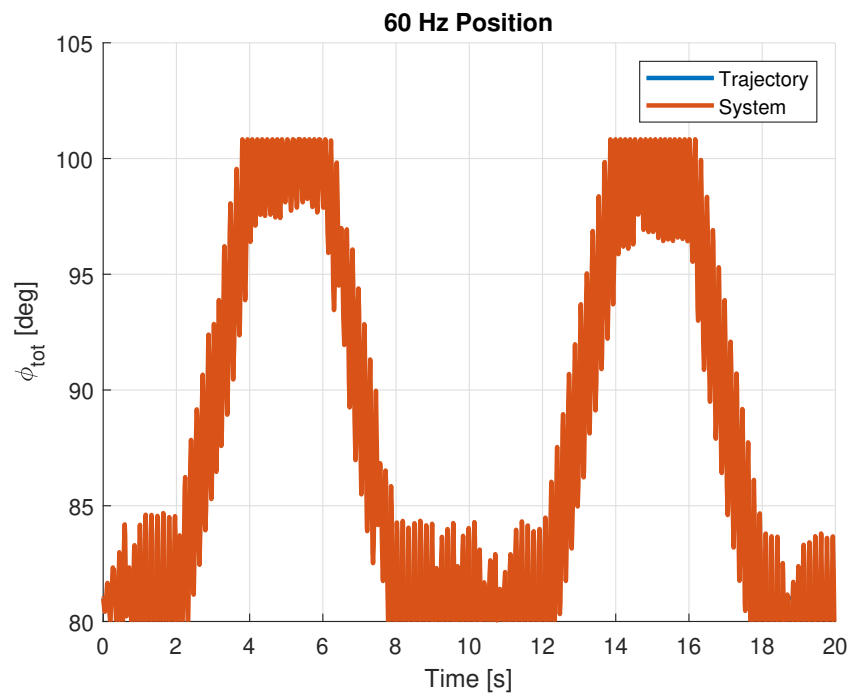


Figure B.25. Position tracking for a 17 ms sampling time controller.

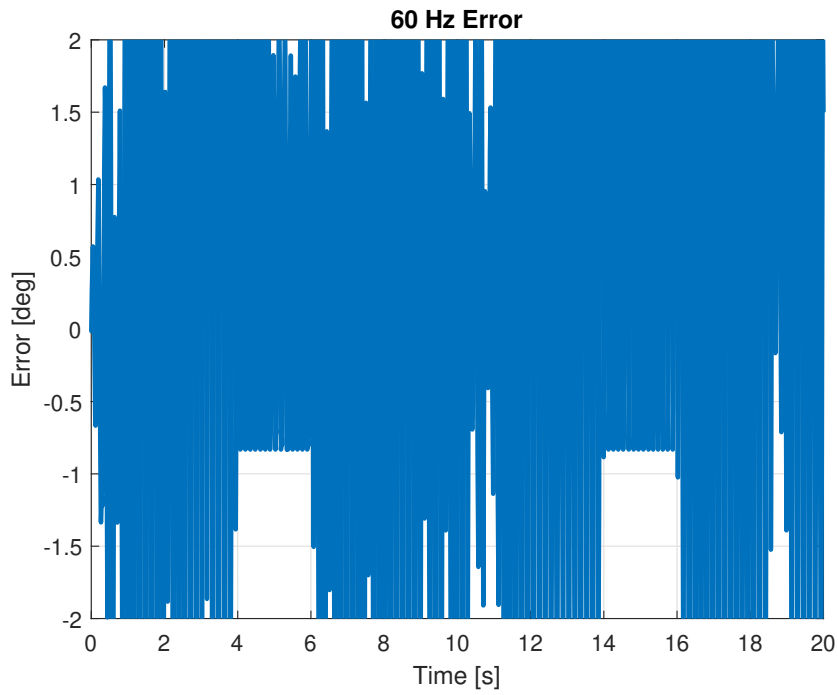


Figure B.26. Error for a 17 ms sampling time controller.

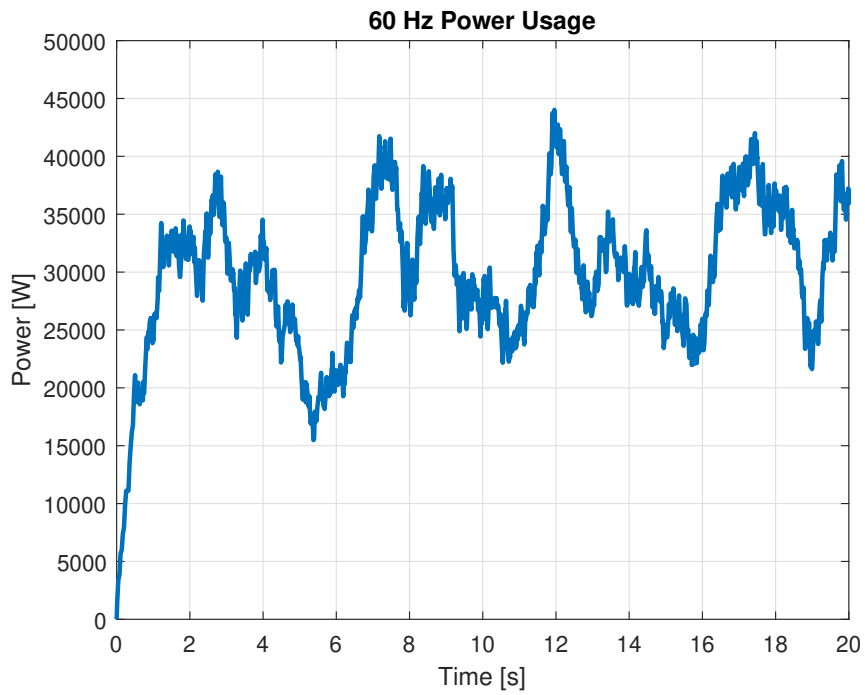


Figure B.27. Power usage for a 17 ms sampling time controller, with a 500 ms moving average.

20 ms

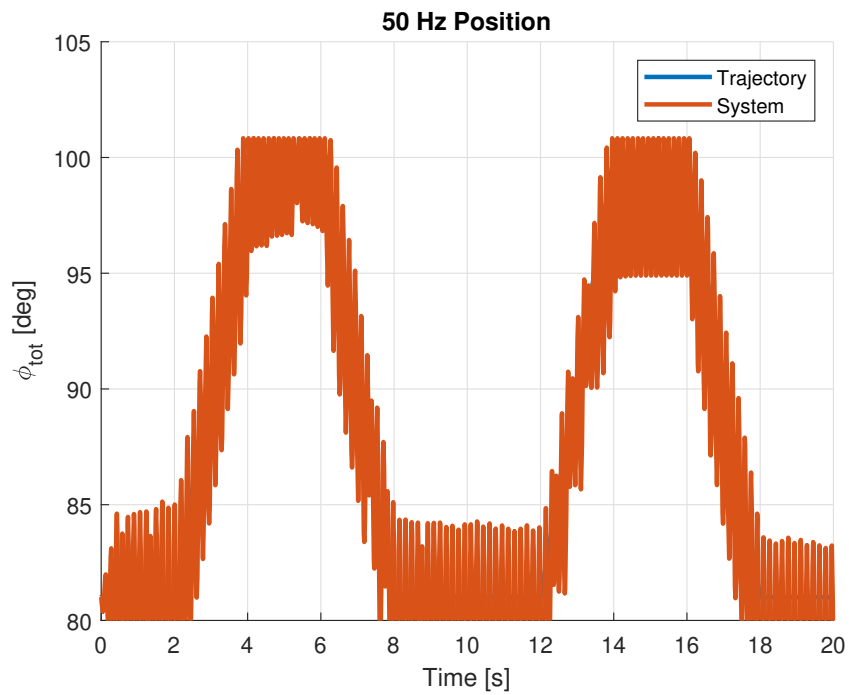


Figure B.28. Position tracking for a 20 ms sampling time controller.

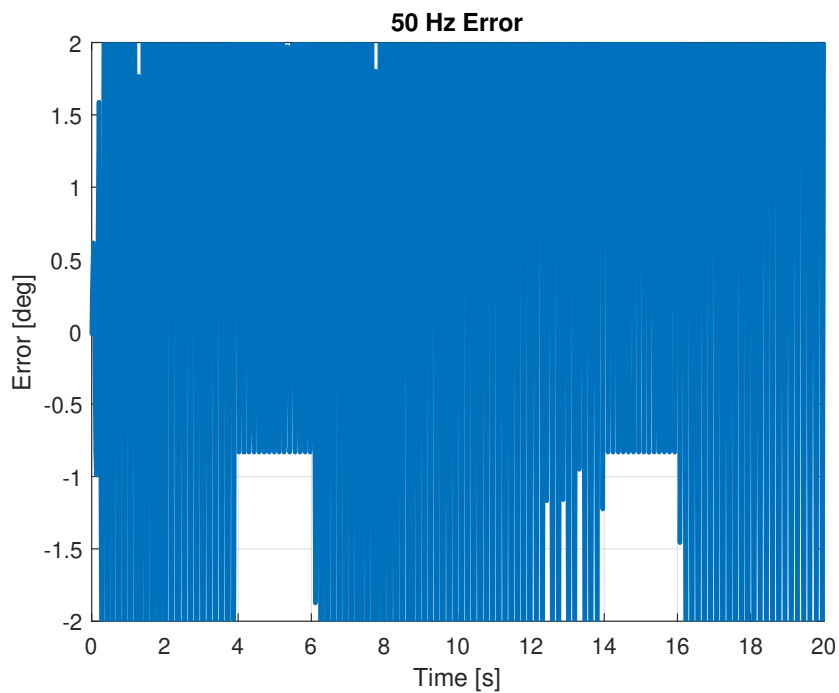


Figure B.29. Error for a 20 ms sampling time controller.

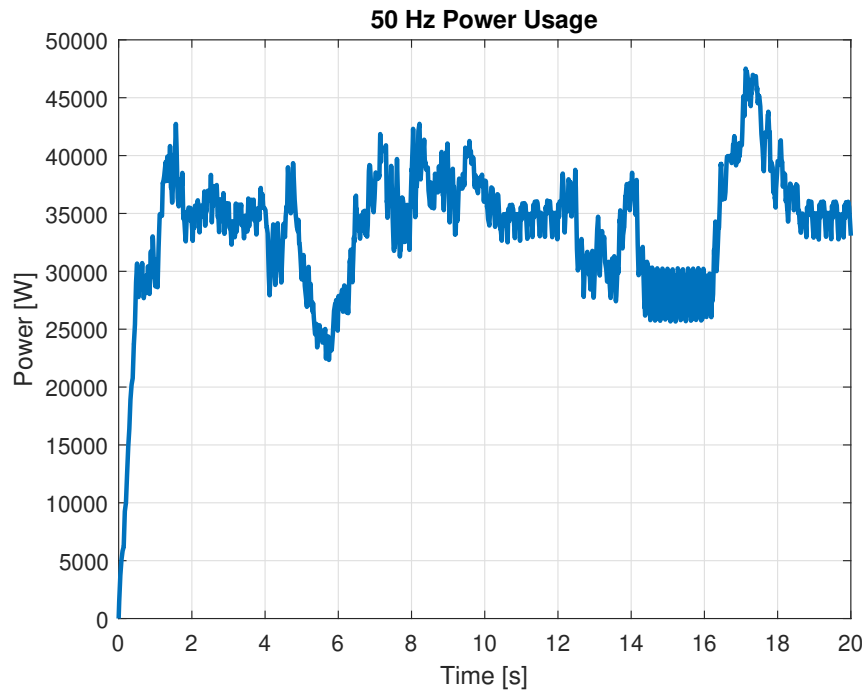


Figure B.30. Power usage for a 20 ms sampling time controller, with a 500 ms moving average.

100 ms

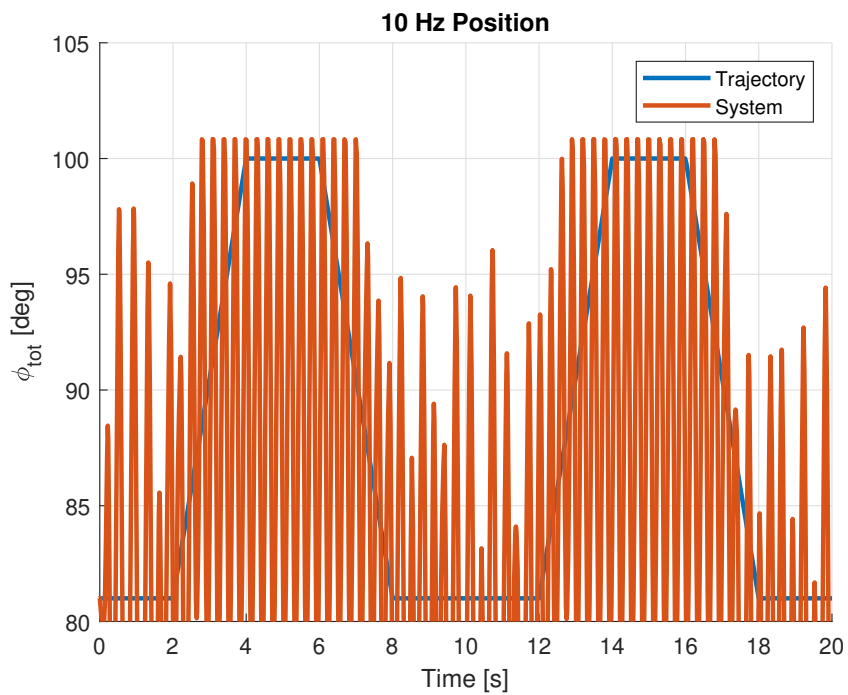


Figure B.31. Position tracking for a 100 ms sampling time controller.

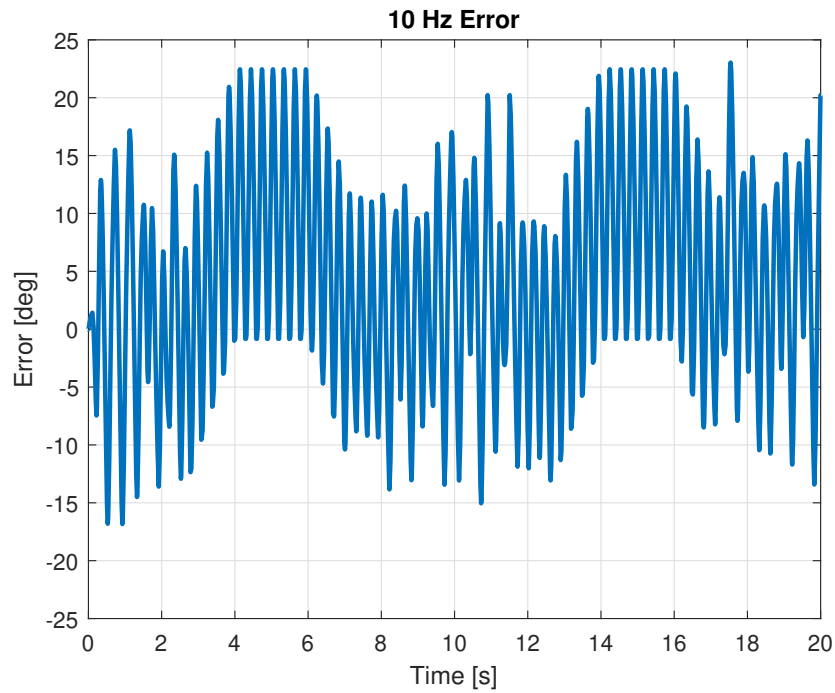


Figure B.32. Error for a 100 ms sampling time controller. NB: The Y-axis for error has been widened; It does not have less error than the previous graphs.

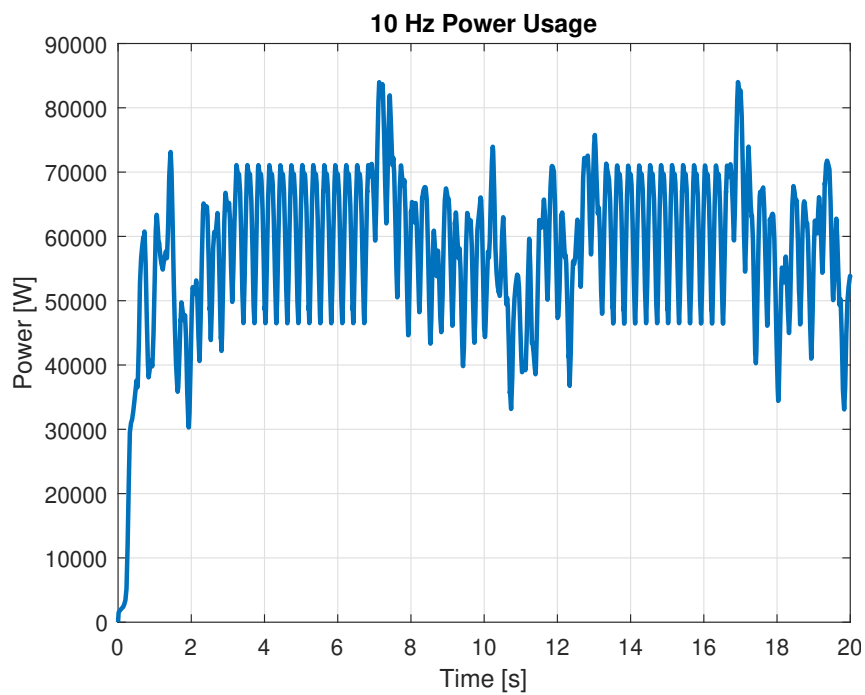


Figure B.33. Power usage for a 100 ms sampling time controller, with a 500 ms moving average.

Error Comparison

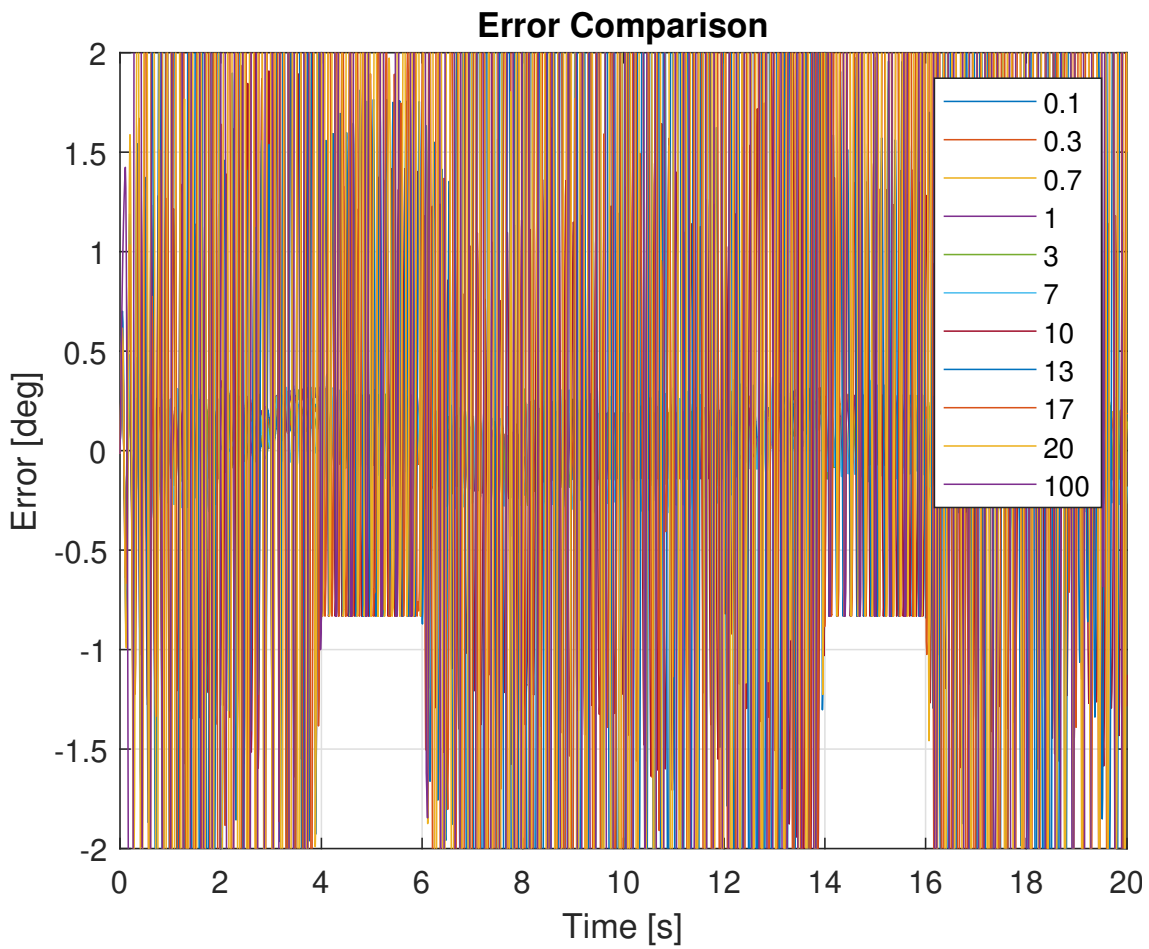


Figure B.34. Error for all frequencies.

It is difficult to see what is happening, due to the massive oscillations from the lines above 10 ms sampling time. Below is a graph with the 5 slowest sampling times removed:

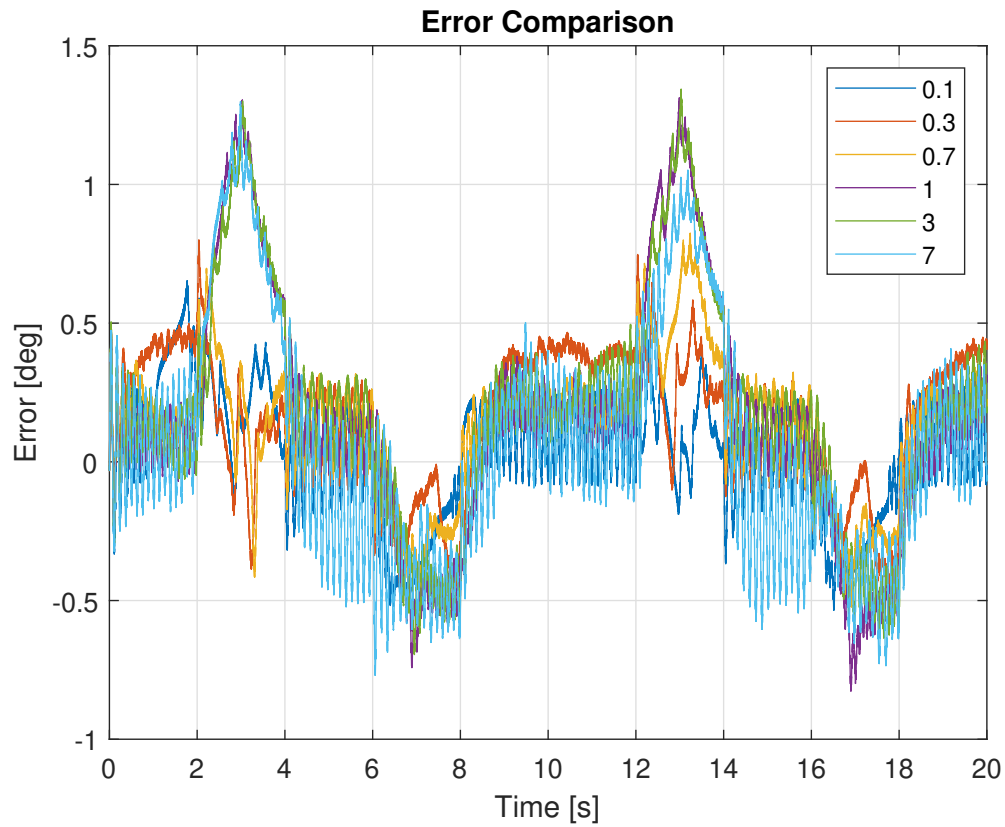


Figure B.35. Error for all frequencies up to 7 ms

Higher sampling times have a higher error in the points where the trajectory is ramping (2 to 4 sec, 6 to 8 sec, 12 to 14 sec, 16 to 18 sec), but they all seem to have roughly the same average error during the steady parts of the trajectory (0 to 2 sec, 4 to 6 sec, 8 to 12 sec, 18 to 20 sec).

Power Comparison

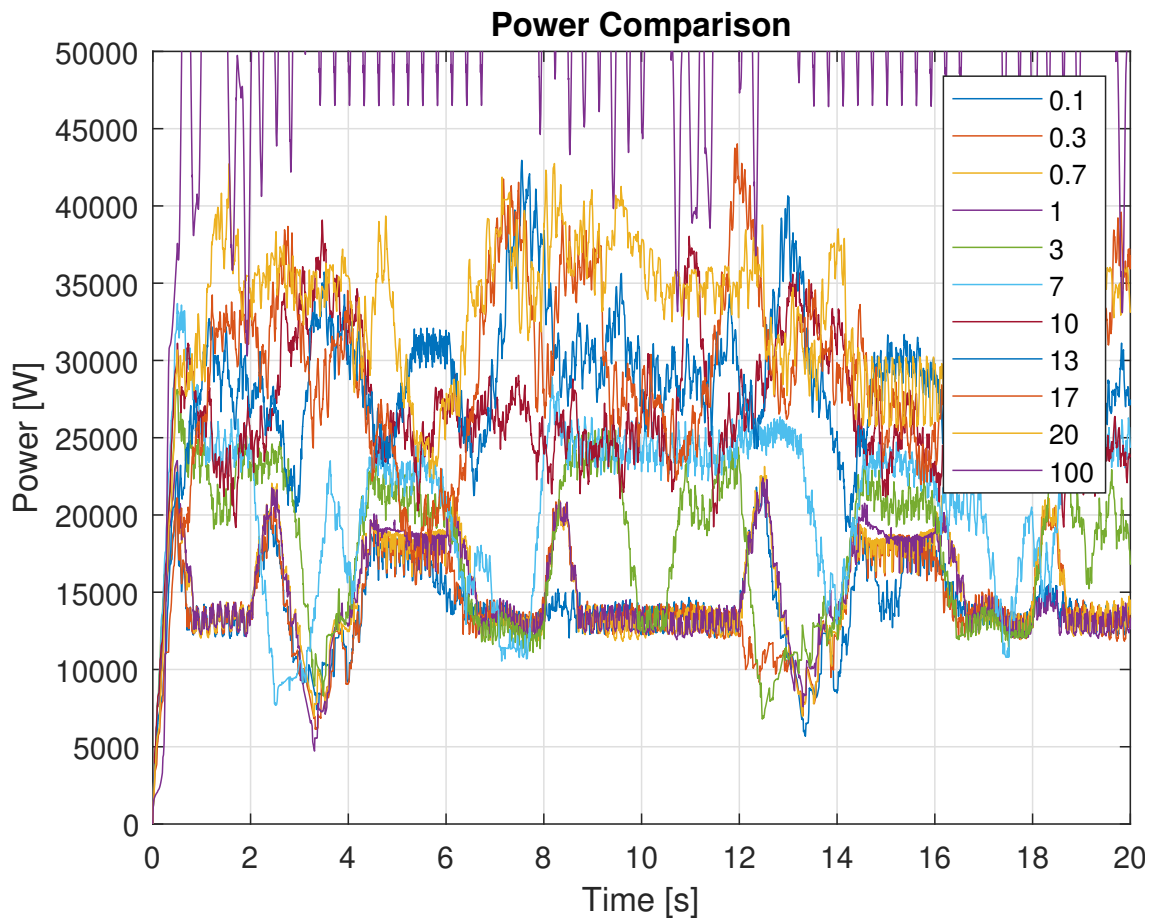


Figure B.36. Power for all frequencies, with a 500 ms moving average.

The general power usage seems to go down until 1 ms (100, 20, 17 and 13 are the lines with the highest power usage, apologies for repetition of colors), after which it goes up again, with 100 ms using the most power for most of the trajectory.